MASTERARBEIT | MASTER'S THESIS

Titel | Title

Synthesis of Halogenated Rubrolide Analogues

verfasst von | submitted by

Gloria Elisa Krappinger BSc

angestrebter akademischer Grad | in partial fulfilment of the requirements for the degree of

Magistra pharmaciae (Mag. pharm.)

Wien | Vienna, 2024

Studienkennzahl lt. Studienblatt | Degree programme code as it appears on the student record sheet:	UA 066 605
Studienrichtung lt. Studienblatt | Degree programme as it appears on the student record sheet:	Masterstudium Pharmazie
Betreut von | Supervisor:	Ass.-Prof. Dipl.-Chem. Dr. Nina Schützenmeister

Zusammenfassung

Der Anstieg von bakteriellen Resistenzen, Überpopulation und der Klimawandel sind nur ein paar wenige der Herausforderungen, mit welchen unser Gesundheitssystem in der heutigen Zeit konfrontiert ist. Dementsprechend sind Ausbrüche von infektiösen Krankheiten in den letzten Jahrzenten spürbar angestiegen. Daher ist es essenziell, nach neuen antiviralen und antibakteriellen Medikamenten zu forschen, vor allem, um vulnerable PatientInnengruppen zu schützen. Großes Potential für neue Wirkstoffe für die Medikamentenentwicklung liegt in marinen Organismen. Zu diesen zählt unter anderem die Seescheide *Ritterella rubra*, aus welcher die ersten Rubrolide isoliert wurden. Neben diesen marinen Organismen, produziert auch der Pilz *Aspergillus terreus* Rubrolide. Je nach Substitutionsmuster zeigen Rubrolide antivirale und/oder antibakterielle Eigenschaften, Zytotoxizität, Inhibition von Aldose-Reduktase, entzündungshemmende Aktivität und selektive Inhibition von Phosphatase 1 und 2A. Der Fokus dieser Arbeit liegt auf der Synthese von 3-Iod-Rubrolid C und 3-Brom-Rubrolid R, zwei Derivate von Rubrolid C und R, um sie darauffolgend Bioaktivitätstests zu unterziehen. 3-Iod-Rubrolid C wurde über sieben Schritte synthetisiert, inklusive literaturbekannter Methoden, wie der Suzuki-Miyaura Kreuzkupplungsreaktion, der Tsuji-Trost Allylierung und der vinylogen Aldolkondensation. Die Verbindung in *Z*-Konfiguration wurde erfolgreich hergestellt, mit einer Ausbeute von 12%. Das zweite Naturstoffanalogon, 3-Brom-Rubrolid R, wurde über vier Schritte hergestellt. Die Suzuki-Miyaura Reaktion und die vinyloge Aldolkondensation wurden auch hier durchgeführt. Das finale Produkt in *Z*-Konfiguration wurde mit einer Ausbeute von 15% erfolgreich synthetisiert.

Abstract

The rise of antimicrobial resistances, overpopulation and climate change are only a few of the challenges that recent times pose to our public health system. Accordingly, over the last few decades, emergences of infectious diseases have perceptibly increased. Therefore, research for possible new antiviral and antibacterial drugs is essential, especially for the protection of more vulnerable population groups. In marine organisms, there lies huge potential for discovering new active agents for drug development. Among these, there is the marine ascidian *Ritterella rubra*, from which the first rubrolides were isolated. Besides these marine organisms, the fungus *Aspergillus terreus* produces rubrolides as well. Rubrolides hold antiviral and/or antibacterial activity, cytotoxicity, inhibition of aldose reductase, anti-inflammatory activity and selective inhibition of phosphatases 1 and 2A. This work focuses on the synthesis of 3-iodo-rubrolide C and 3-bromo-rubrolide R, two derivatives of rubrolides C and R, for the purpose of implementing further biological activity tests. 3-iodo-rubrolide C was obtained by a seven-step synthesis, including literature known procedures like the Suzuki-Miyaura cross-coupling reaction, the Tsuji-Trost allylation and vinylogous aldol condensation. The compound was successfully synthesized in *Z*-configuration in 12% yield. The second natural product, 3-bromo-rubrolide R, was attained in four steps. Suzuki-Miyaura cross-coupling and vinylogous aldol condensation had to be performed here as well. The final product was also successfully obtained in *Z*-configuration in 15% yield.

Table of contents

Table of figures

Abbreviations

µ	micro
Å	Ångstrom (1 Å = $1 \cdot 10^{-10}$ m)
ABTS	2,2'-azino-di-(3-ethylbenzthiazoline-6-sulfonic acid)
Ac	acetyl
aq.	aqueous
ATR	attenuated total reflectance
Boc	*tert*-butyloxycarbonyl
calcd.	calculated
cat.	catalytic
conc.	concentrated
COSY	correlated spectroscopy
δ	chemical shift
d	doublet
DBU	1,8-diazabicycloundecen-7-ene
DCM	dichlormethane
DIPEA	*N*,*N*-diisopropylethylamine
DMF	dimethylformamide
DPPH	1,1-diphenyl-2-picrylhydrazyl
EI	electron ionisation
equiv.	equivalent
ESI	electron spray ionisation
Et	ethyl
EtOAc	ethylacetate
g	gram
h	hour
HCl	hydrochloric acid
HPLC	high pressure liquid chromatography
HRMS	high resolution mass spectrometry
Hz	hertz
IC_{50}	half maximal inhibitory concentration

IR	infrared spectroscopy
J	coupling constant
lit.	literature
λ	wave length
m	multiplet (NMR)
M	molar concentration
m/z	mass per charge
me	methyl
MeCN	acetonitril
MeOH	methanol
MHz	mega hertz
min	minute
mL	milliliter
mmol	milli molar
mol-%	molar fraction
Mp	melting point
MS	molecular sieve
n-BuLi	*n*-butyllithium
nm	nanometer
NMR	nuclear magnetic resonance
NOESY	nuclear overhauser effect spectroscopy
PE	petroleum ether
Ph	phenyl
ppm	parts per million
PTC	phase transfer catalyst
Rf	retention factor
r.t.	room temperature
s	singlet (NMR)
sat.	saturated
t	triplet (NMR)
TBS	*tert*-butyldimethylsilyl
TFA	trifluoro-acetate
Tf	triflate
THF	tetrahydrofuran

Ts	tosylate
TLC	thin layer chromatography
UV	ultraviolet
~	wavenumber
v/v	volume per volume
Vis	visible

1. Introduction

From 1940 to 2004, 335 emergences of known or new infections were recorded globally.[1] 54% of them were caused by bacteria and 25% by viruses or prions.[2] Possible reasons for these developments are the rise in population, the development of drug resistances, aging population, increased international travel and in particular the consequences of climate change.[1] Due to global warming and more frequent precipitation, pathogens and also their vectors, like mosquitos, are changing their transmission patterns and are more likely to spread. This is, among other factors, because of the climate's direct influence on their growth, virulence and survival.[3] For example, the occurrence of Dengue fever, which is transmitted by mosquitos and is one of the fastest spreading diseases worldwide, rose by 30 times, considering the last 50 years. Every year there are 100-390 million new Dengue infections recorded globally.[4] As these changes are very likely to persist and even be amplified in the future, it is of great urgency to find new active ingredients for the development of new antibacterial and antiviral drugs.[2]

1.1. Rubrolides

Rubrolides are natural products that have been isolated from the marine ascidian *Ritterella rubra* and from *Aspergillus terreus*.[5] These marine natural products were isolated for the first time by Miao *et al.* in 1991.[6] The ascidian *Ritterella rubra* belongs to the family of *Ritterellidae* and is part of the sub-phylum *Tunicata.*[7] It is a filter-feeding invertebrate that can be found in various oceans, especially in the southwestern Pacific Ocean.[8] On the other hand, *Aspergillus terreus* belongs to the genus *Aspergillus*, which is a group of sapotrophic fungi, found particularly in dust, soil and compost heaps but also in stored rice, corn and barley.[9] Rubrolides potentially hold antibacterial and antiviral effects, cytotoxicity, inhibition of aldose reductase, anti-inflammatory activity and selective inhibition of phosphatases 1 and 2A.[10, 11]

1.2. Chemical structures and biological activities of rubrolides

1.2.1. General chemical structure of rubrolides

Rubrolides incorporate isolated, polysubstituted butenolides. Most rubrolides contain phenolic, brominated substituents and some are chlorinated in position 3 of the furanone framework. The

basic chemical structure of rubrolides, in which R' typically stands for a hydrogen atom or a methyl group, R'' represents a hydrogen atom, a bromine atom or alkyl chains and R''' mostly happens to be a hydrogen or a chlorine atom, is shown in figure 1.[12]

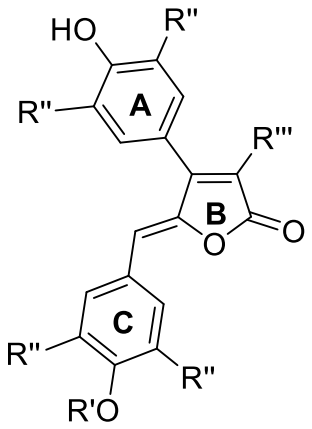

1

Figure 1: General chemical structure of rubrolides.

1.2.2. Rubrolide C 2

Rubrolide C **2** is substituted with two bromine substituents in positions 3'' and 5'' (Figure 2). It occurs as a red amorphous solid.[6]

In 2024, Wu and co-workers reported that rubrolide C **2** exhibits some herbicidal inhibitory effect against rapeseed.[13] Additionally, it showed inhibitory activity against *S. aureus* and *Bacillus subtilis* growth with a minimal inhibitory concentration of 2-11 μg/disc.[14]

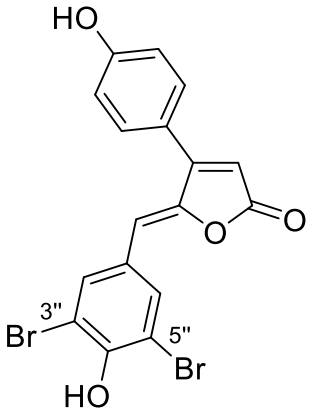

2

Figure 2: Chemical structure of rubrolide C **2**.

1.2.3. Rubrolide R 3

Rubrolide R **3** was isolated in 2014 from *Aspergillus terreus.*[15] It is not halogenated and is substituted with a prenyl group at the aromatic C-ring. In biological activity tests, rubrolide R **3** displayed an effect on Influenza A virus (H1N1) with an IC_{50} value of 221.6 μM.[15] It demonstrated a slight antioxidant effect against DPPH and a strong antioxidant effect against ABTS as well.[16] Moreover, it showcased antiviral activity against *p*H1N1 (pandemic swine flu) and H3N2 (seasonal flu).[17]

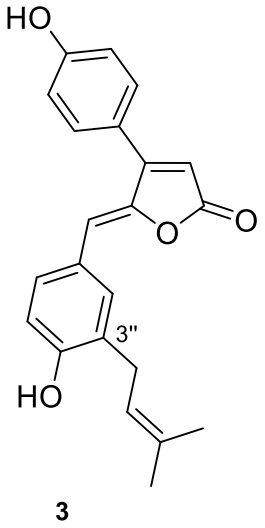

3

Figure 3: Chemical structure of rubrolide R **3**.

Rubrolide R **3** was synthesized for the first time by M. Schacht in 2017 [17, 18] and by K. Damodar in 2017 as well.[19]

1.3. Suzuki-Miyaura cross-coupling reaction

In 2010, R. Heck, E. Negishi and A. Suzuki were awarded the Nobel prize for their work on palladium catalyzed cross-couplings in organic synthesis.[20] The Pd-catalyzed cross-coupling reaction, which uses boronic acids or boronic esters as coupling partners, is named Suzuki-Miyaura reaction and was developed by *Suzuki* and *Miyaura* in 1979.[21] For the synthesis of rubrolides, a Suzuki-Miyaura cross-coupling reaction has often been employed.[17, 22] The Suzuki-Miyaura reaction involves organic halides or pseudohalides (**4**) and organoboron compounds (**5**), which form, in presence of a palladium catalyst, a new carbon-carbon bond (**6**)

and **7** (Scheme 1).[21] Additionally to Pd-catalysts, the sufficient catalytic activity of gold [23] or nickel [24] has been proven as well.

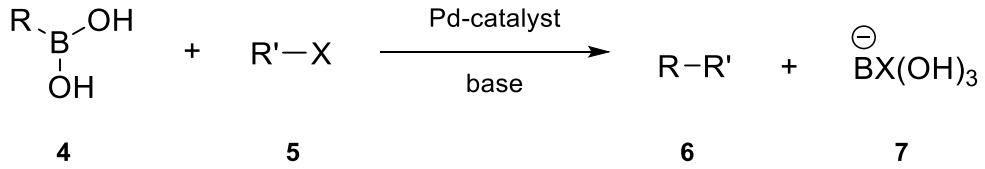

Scheme 1: Suzuki-Miyaura cross-coupling reaction.

During the reaction, an organic rest R is transferred from the boron atom to the organic rest R' of the halide or triflate **5**. In this manner, a new C-C bond is formed, which results in R-R' **6**. The exact mechanism behind this was unknown for decades. In 2016, Thomas and Denmark proposed two possible explanations for the reaction mechanism. They discovered the three intermediate structures right before the carbon transfer via low-temperature nuclear magnetic resonance spectroscopy and the nuclear Overhauser effect.[25]

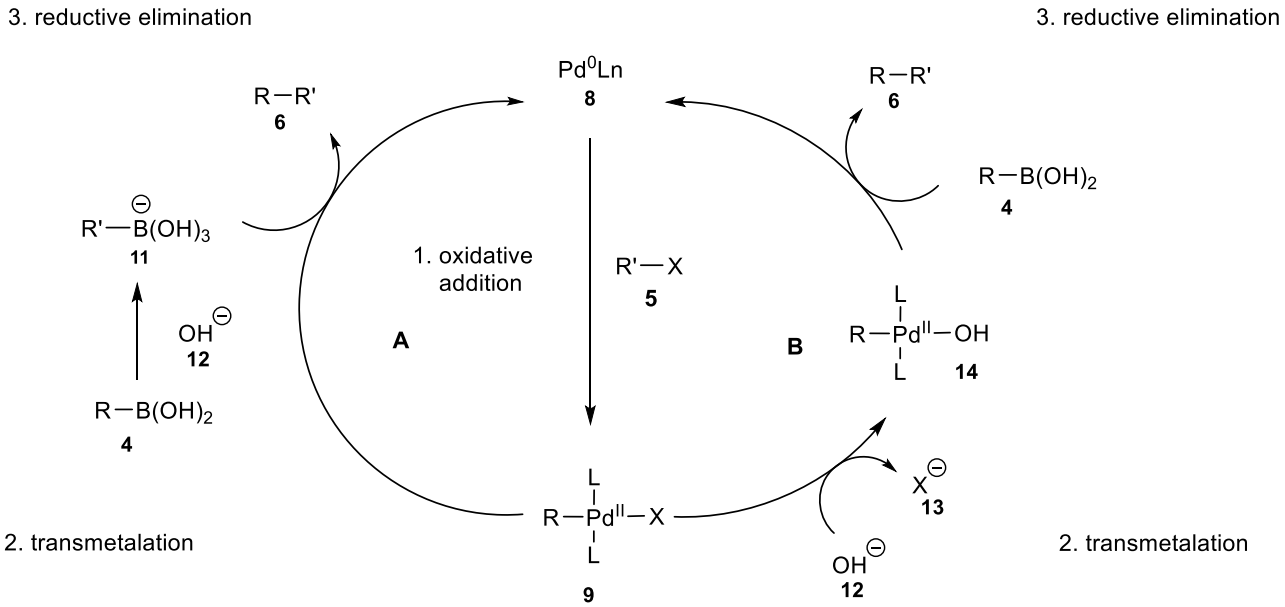

Scheme 2: Catalytic cycle of the Suzuki-Miyaura cross-coupling reaction (scheme adapted from Thomas and Denmark).[25]

Three steps are involved in the proposed mechanism. It starts with oxidative addition, in which a halide or pseudohalide **5** is added to the Pd^0 complex **8**. Thereby, Pd^0 is oxidized to Pd^{II}, consequently forming a stable *trans*-σ-Pd^0 complex **9**. This step is the rate determining step of this cycle and is the same for both pathways.[26] The second step is the transmetalation. In this

step, a ligand exchange between the boronic acid **4** and the palladium complex **9** takes place. At this stage, two mechanistically different pathways are described. In *pathway A*, base **12** coordinates to the boronic acid **4** to form boronate **11**. Whereas in *pathway B*, activation of the palladium complex **9** by base **12** leads to complex **14**. Until now, it is still not completely discovered how exactly these pathways take place. In literature, both pathways were described. NOE studies of three palladium complexes, which were formed during the transmetalation process, demystified the mechanism of the Suzuki-Miyaura cross coupling reaction.[25]

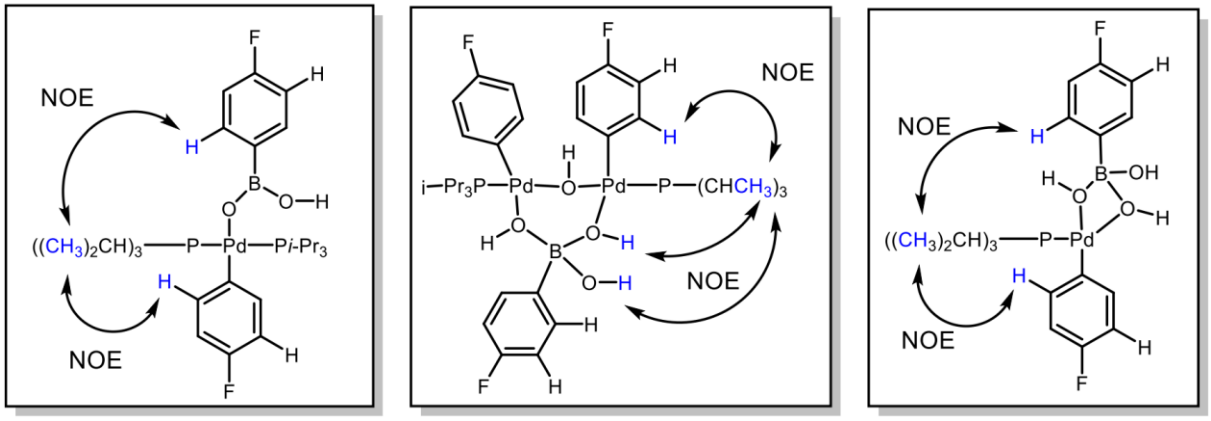

Figure 4: Palladium complexes, which can be formed during transmetalation in the Suzuki-Miyaura reaction.[25]

The last step, reductive elimination, decreases the coordination and oxidation state of the palladium.[27] Hence, the palladium catalyst **8** is recovered and can enter the catalytic cycle again. The desired cross-coupling product **6** is formed. Reductive elimination is the same for *pathway A* and *pathway B*.[28]

1.4. Tsuji-Trost allylation

The Tsuji-Trost allylation is another key step in the synthesis of rubrolide R **3** and a very relevant reaction to build up C-C, C-N or C-O bonds. The Tsuji-Trost reaction generally proceeds with high regio- stereo- and chemoselectivity.[29] During the reaction, allylic reagent **16** with a good leaving group, for example carbonates, esters or halogens, is formally attacked by nucleophile **15**, for example amines, carbanions, sulphides or sulphinates.[29] The palladium catalyst inserts into the C-X bond of the allylic compound **16** to create a π-allyl complex. The nucleophile **15** can then attack the complex in two possible positions. Hard nucleophiles first

attack the Pd, which give the allylation product after reductive elimination. Soft nucleophiles directly add to the allyl moiety to form product **17**.[30]

Generally, the reaction takes place in organic solvents like toluene, THF or dioxane and a palladium catalyst (such as Pd_2dba_3 or $Pd(PPh_3)_4$) is added to the dissolved starting materials. More recently, the use of Pd(0) in water has also been reported.[29]

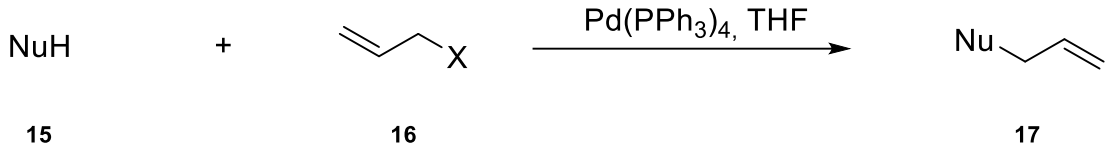

Scheme 3: Tsuji-Trost allylation.

1.5. Vinylogous aldol condensation

The aldol reaction is a very common method in organic synthesis for C-C bond formation. Two carbonyl compounds are involved. One carbonyl reacts as *C*-nucleophile and the other one acts as electrophile. The reaction proceeds in two steps. The first one is aldol addition, during which either a β-hydroxyaldehyde or a β-hydroxyketone forms. Depending on the substrates and the reaction conditions, a condensation step can take place, which eliminates water to form an α,β-unsaturated carbonyl compound.[31]

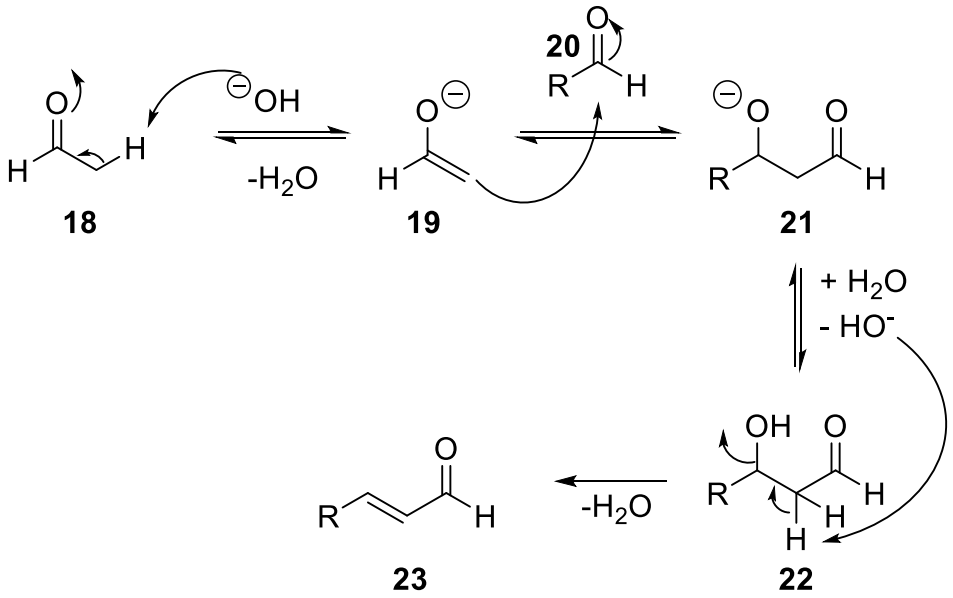

Scheme 4: Reaction mechanism of the base catalyzed aldol condensation.

The vinylogous aldol condensation is a special form of aldol condensation. In this case, nucleophile **25** attacks in the vinylogous position of the electrophilic carbonyl **24**. That is, because in α,β-unsaturated carbonyl compounds, the effect of functional groups expands to the double bond.[32] In rubrolide syntheses, the vinylogous aldol reaction is applied to create a new double bond between furanone **24** and aldehyde **25**. [33, 34]

Scheme 5: Reaction overview of the vinylogous aldol condensation reaction.

Formation of the desired product takes place after the addition of a base. In the case of rubrolide R derivatives, DIPEA (Hünig's base) is used and in the case of rubrolide C derivatives, Et_3N is added as base. The optimal base for the reaction needs to be optimized depending on the substitution pattern of the rubrolide.[33] Furthermore, DBU is added in the third step to successfully remove the intermediate TBS-ether, which might have been formed, and to form the desired double bond by elimination of water. This approach can be implemented via one-pot reaction with no purification of the intermediate products (Scheme 5). [34]

2. Aim of the project

The aim of the project is the synthesis of two rubrolide analogues: rubrolide C 2 and R 3. Both compounds are required for antibacterial and antibiofilm (*Stenotrophomonas maltophilia*) testing.[35] The required compounds are 3-iodo rubrolide C **27** and 3-bromo rubrolide R **28** (Figure 5).

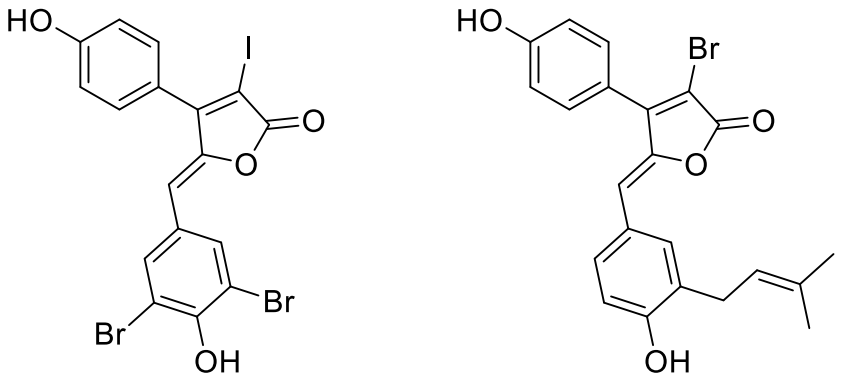

27 **28**

Figure 5: Chemical structures of 3-iodo-rubrolide C **27** and 3-bromo-rubrolide R **28**.

2.1. Retrosyntheses of rubrolide derivatives C 27 and R 28

For the synthesis of rubrolide C derivative **27,** three commercially available building blocks are required.

The desired rubrolide C analogue **27** can be synthesized in four steps starting from tetronic acid **34**. Derivative **27** might be obtained via vinylogous aldol condensation of aldehyde **29** with butenolide **30**. Butenolide **30** was obtained by iodination of the Suzuki-Miyaura product **31**, which can be obtained by cross-coupling of the triflate **33** and the commercially available boronic acid **32**.

The triflate **33** can be obtained from tetronic acid **34** after treatment with triflic anhydride and triethylamine (Scheme 6).

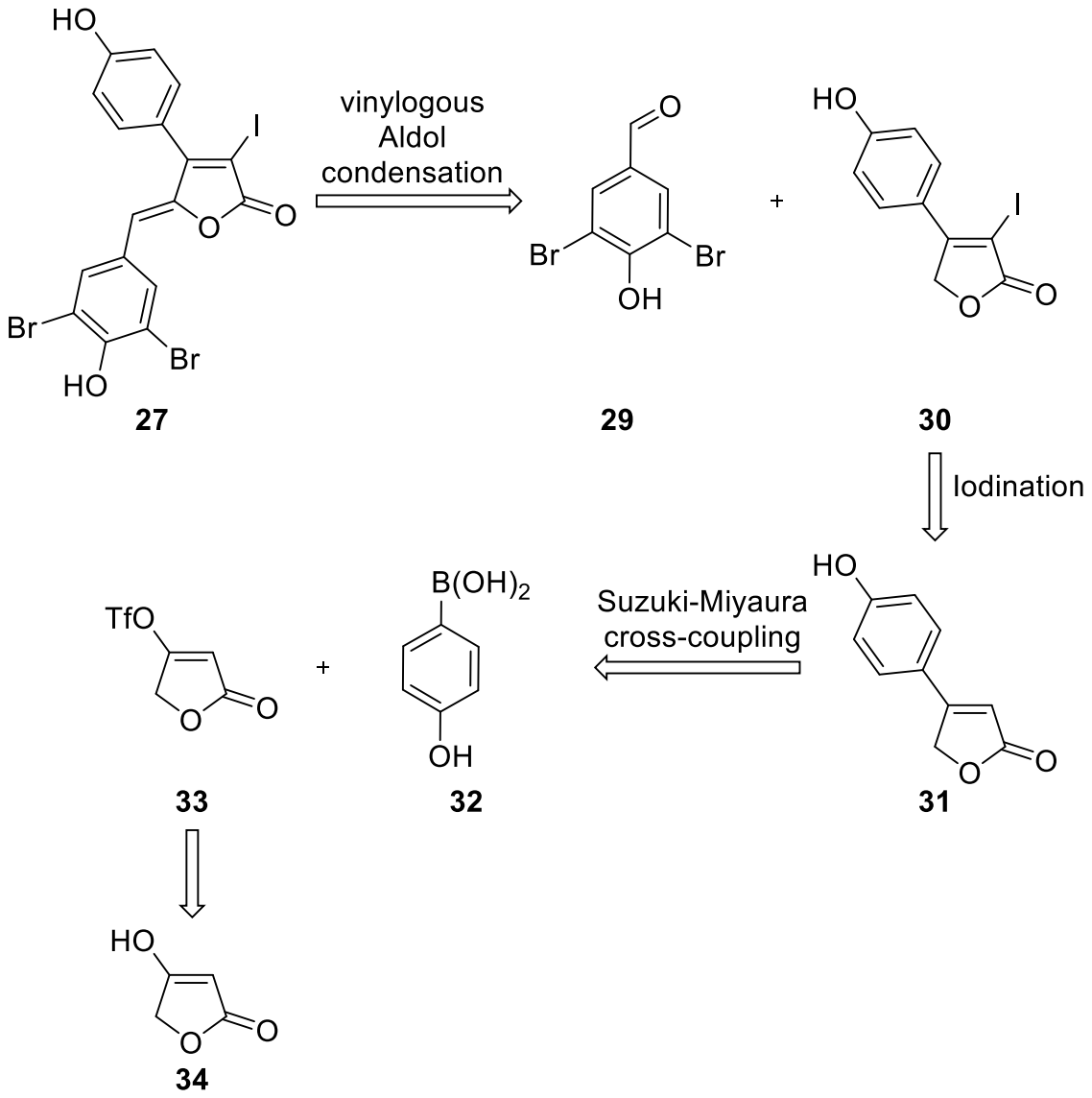

Scheme 6: Retrosynthesis of 3-iodo-rubrolide C **27**.

For the synthesis of rubrolide R derivative **28**, four commercially available building blocks are required. Starting from tetronic acid **34,** rubrolide **28** can be obtained in only four linear steps. The intermediate **31**, which can be obtained, in analogy to the synthesis of rubrolide C analogue **27**, after Suzuki-Miyaura reaction between boronic acid **32** and **33**. The prenylated benzaldehyde derivative **36** can be obtained after Claisen rearrangement of allyl ether **37**.

Allyl ether **37** was obtained via Tsuji-Trost allylation, in the presence of a palladium catalyst, from aldehyde **38** and boc-protected carbonate **39**, which can be obtained by boc-protection of 2-methylbut-3-en-2-ol **40** (Scheme 7).

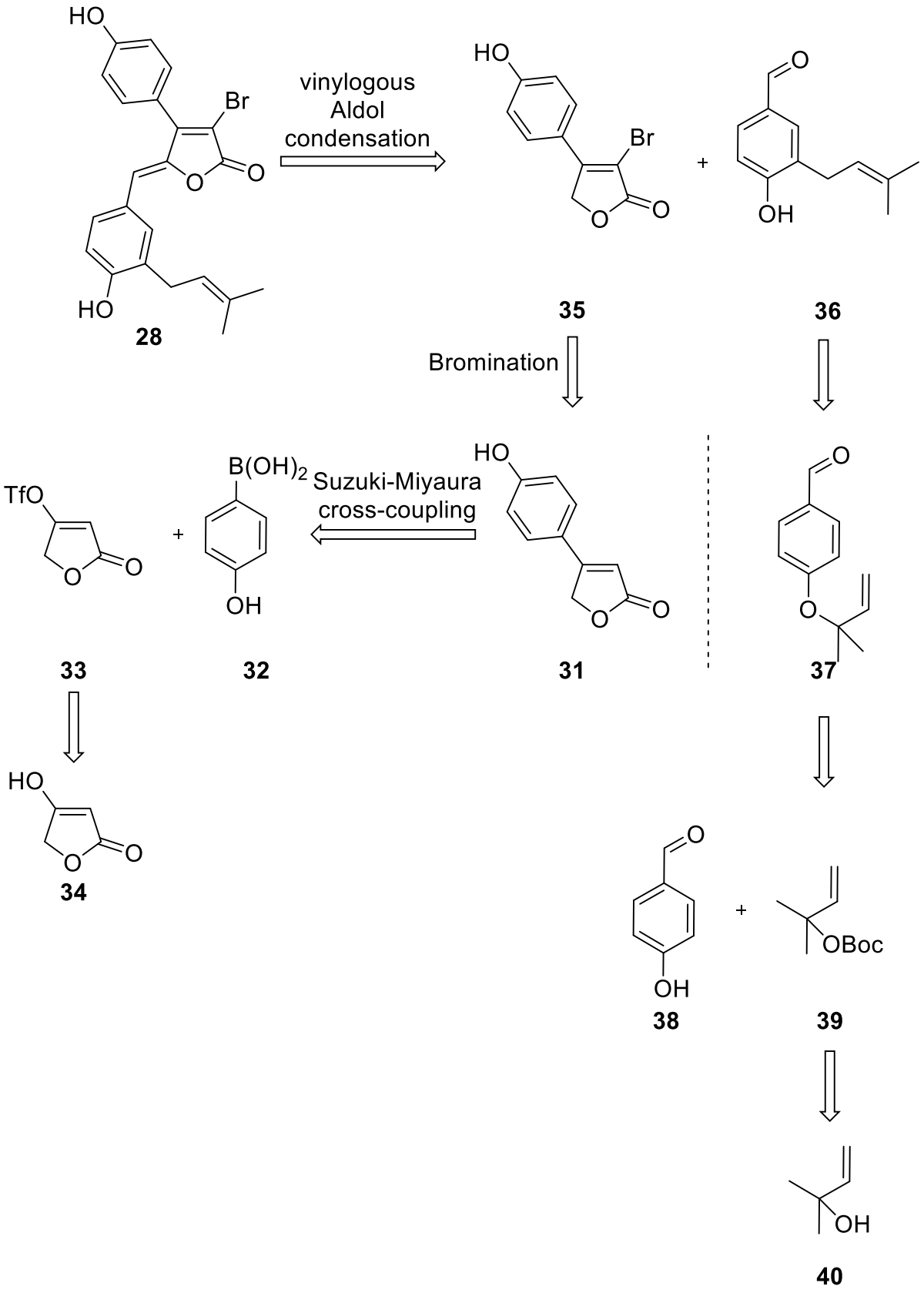

Scheme 7: Retrosynthetic approach for 3-bromo-rubrolide R **28**.

3. Results and Discussion

3.1. Synthesis of *tert*-butyl-1,1-dimethylallyl carbonate 39

The first step for the synthesis of rubrolide R derivative **28** was boc-protection of 2-methylbut-3-en-2-ol **40**. Without further purification, the desired *tert*-butyl-1,1-dimethylallyl carbonate **39** was obtained in 85% yield.

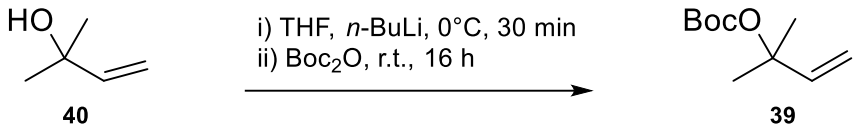

Scheme 8: Boc-protection of 2-methylbut-3-en-2-ol **40**.

This intermediate was required to implement the Tsuji-Trost reaction in the following step.

3.2. Synthesis of 4-[(2-methylbut-3-en-2-yl)oxy]benzaldehyde 37

The Tsuji-Trost product **37** was synthesized from carbonate **39** and aldehyde **38** in the presence of $Pd(PPh_3)_4$. After additional normal phase column chromatography, 4-[(2-methylbut-3-en-2-yl)oxy]benzaldehyde **37** was obtained in 58% yield.

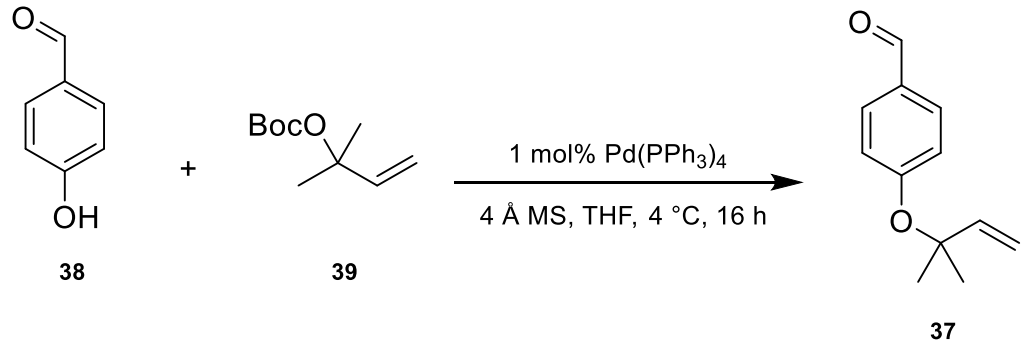

Scheme 9: Overview of the reaction to obtain aldehyde **37**.

A very important factor for the successful synthesis of the Tsuji-Trost product **37** is the quality of the palladium catalyst. For the reaction to be successful, the catalyst needs to be freshly prepared or stored under suitable conditions.

3.3. Synthesis of 4-hydroxy-3-(3-methylbut-2-en-1-yl)benzaldehyde 36

For the synthesis of compound **36**, a Claisen rearrangement was performed. Hereby, a solution of compound **37** in DMF was heated to 180 °C under microwave irradiation and subsequently purified by normal phase column chromatography to receive product **36** in 74% yield.

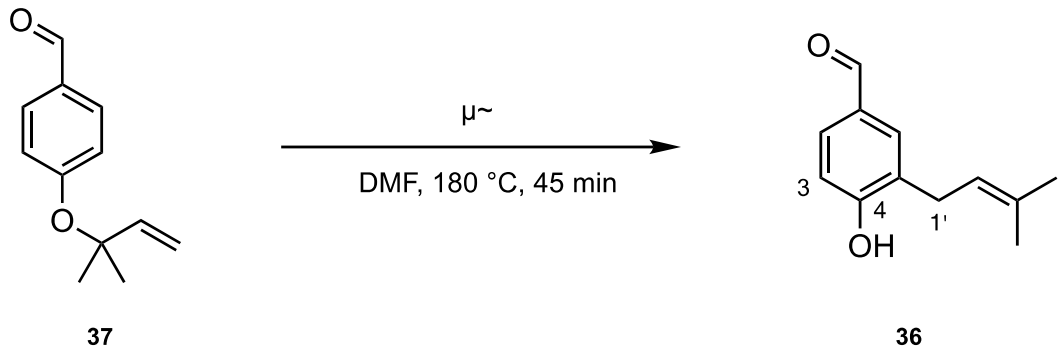

37 **36**

Scheme 10: Synthesis of aldehyde **36**.

3.4. Synthesis of 5-oxo-2,5-dihydrofuran-3-yl-trifluoromethanesulfonate 33

For both, rubrolide C derivative **27** and rubrolide R derivative **28**, the synthesis of triflate **33** was necessary as starting material for the planned Suzuki-Miyaura cross coupling reaction. This intermediate **33** was synthesized from tetronic acid **34** in the presence of triflic anhydride and triethylamine. It was carried out based on a modified procedure by Grigg *et al.*[36] Purification by Kugelrohr distillation yielded product **33** in 53% yield.

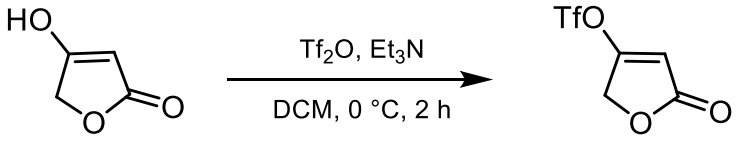

34 **33**

Scheme 11: Reaction conditions for requiring triflate **33**.

3.5. Synthesis of 4-(4-hydroxyphenyl)furan-2(5H)-one 31

The next reaction that needed to be performed was the Suzuki-Miyaura cross-coupling reaction, involving the prior synthesized triflate **33**, commercially available boronic acid **32**, a palladium catalyst, Na_2CO_3 as base and 1,4-dioxane as solvent. The starting materials **32** and **33** were

dissolved in 1,4-dioxane and degassed. After addition of base and catalyst $Pd(PPh_3)_4$, the reaction mixture was stirred for 16 hours. Reversed phase column chromatography yielded the intermediate furanone **31** in 31% yield.

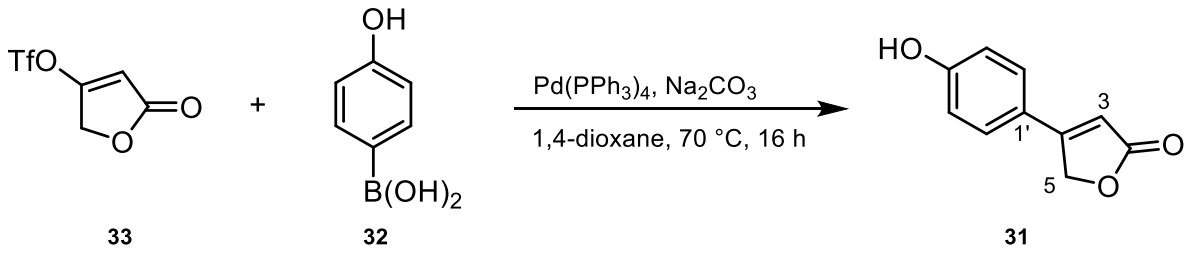

33 **32** **31**

Scheme 12: Synthesis of furanone **31**.

3.6. Synthesis of 3-iodo-4-(4-hydroxyphenyl)furan-2(5H)-one 30

For the synthesis of 3-iodo-4-(4-hydroxyphenyl)furan-2(5H)-one **30**, furanone **31** needed to react with *N*-iodosuccinimide, as iodine source, in the presence of triflic acid, which acts as Lewis acid. This product is a crucial intermediate in the synthesis of rubrolide C derivative **27**. Iodination exclusively took place in 3-position of the furanone ring, since this position is the most reactive position. Purification by reversed phase column chromatography generated a yield of 58%.

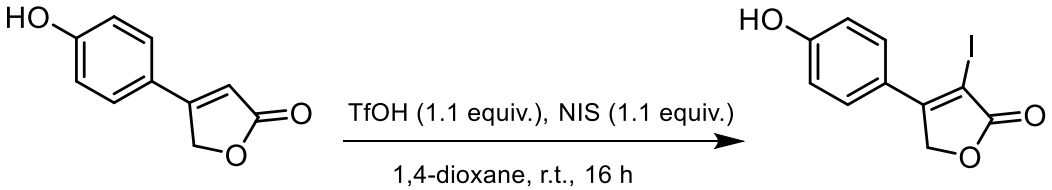

31 **30**

Scheme 13: Synthesis of furanone **30**.

3.7. Synthesis of 3-bromo-4-(4-hydroxyphenyl)furan-2(5H)-one 35

Suzuki product **31** is further required for the synthesis of 3-bromo-4-(4-hydroxyphenyl)furan-2(5H)-one **35** to be obtained. In this procedure, compound **31** reacts with *N*-bromosuccinimide, as bromine source, in the presence of triflic acid. This reaction is a key step in the synthesis of rubrolide R derivative **28**. After purification via reversed phase column chromatography, furanone **35** could be obtained in 57% yield.

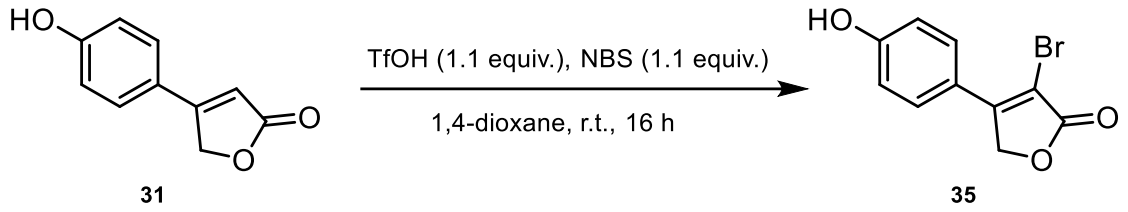

Scheme 14: Bromination of furanone **31**.

3.8. Synthesis of 3-iodo-rubrolide C 27

The desired compound 3-iodo-rubrolide C derivative **27** was obtained by a vinylogous aldol condensation of furanone **30** with aldehyde **29**. The required reagents for this reaction were triethylamine as base and TBDMSOTf in the first step. Activation of the carbonyl led to a charge transfer in the furanone ring. Therefore, the carbon atom in position 5 can attack the electrophilic carbon atom of the aldehyde moiety of **29**. After formation of the C-C-bond, a condensation reaction is initiated by addition of DBU as base. To ensure the deprotection of the TBDMS ether, which was formed during the first step, addition of water was required. Purification by normal phase column chromatography and additional reversed phase column chromatography yielded the desired rubrolide derivative **27** in 12% yield as pure *Z*-isomer.

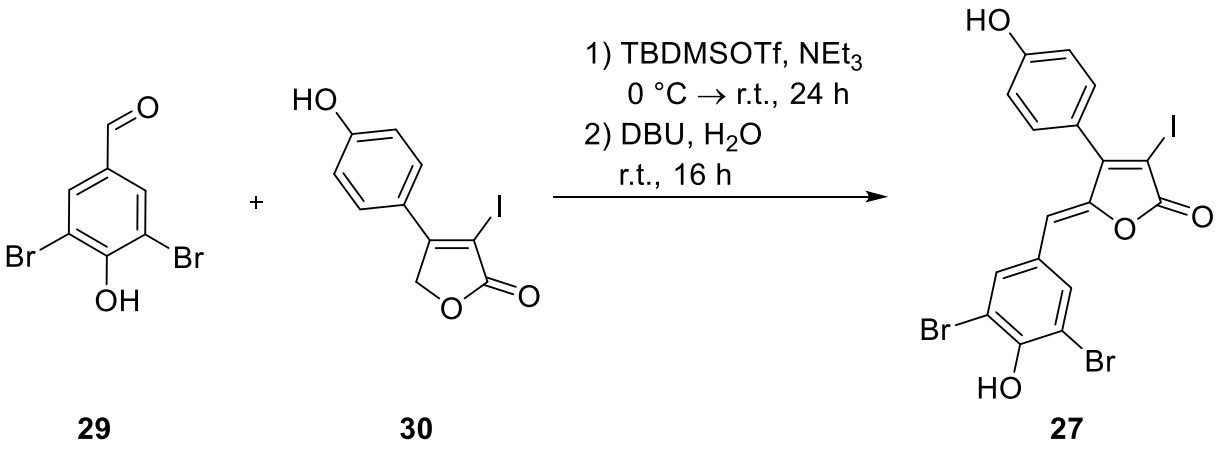

Scheme 15: Vinylogous aldol condensation to rubrolide C analogue **27**.

As demonstrated in figure 6 and figure 7, the chemical structure of **2**7 was confirmed via NMR spectroscopy, verifying the successful formation of rubrolide C analogue **27**. Figure 6 displays the ^{1}H-NMR of 3-iodo-rubrolide C **27**. At 6.23 ppm (s,1 H, 6-H), the characteristic signal of the benzylidene proton is found as singlet with an integral of 1 H. The doublets at 7.06 ppm (d, J = 8.7 Hz, 2 H, 3'-H, 5'-H) and 7.49 ppm (d, J = 8.8 Hz, 2 H, 2'-H, 6'-H) correspond to the

1,4-disubstituted aromatic substituent. Finally, the singlet at 8.08 ppm (s, 2 H, 2''-H, 6''-H) indicates the 2,6-dibrominated phenol, which was introduced by vinylogous aldol condensation.

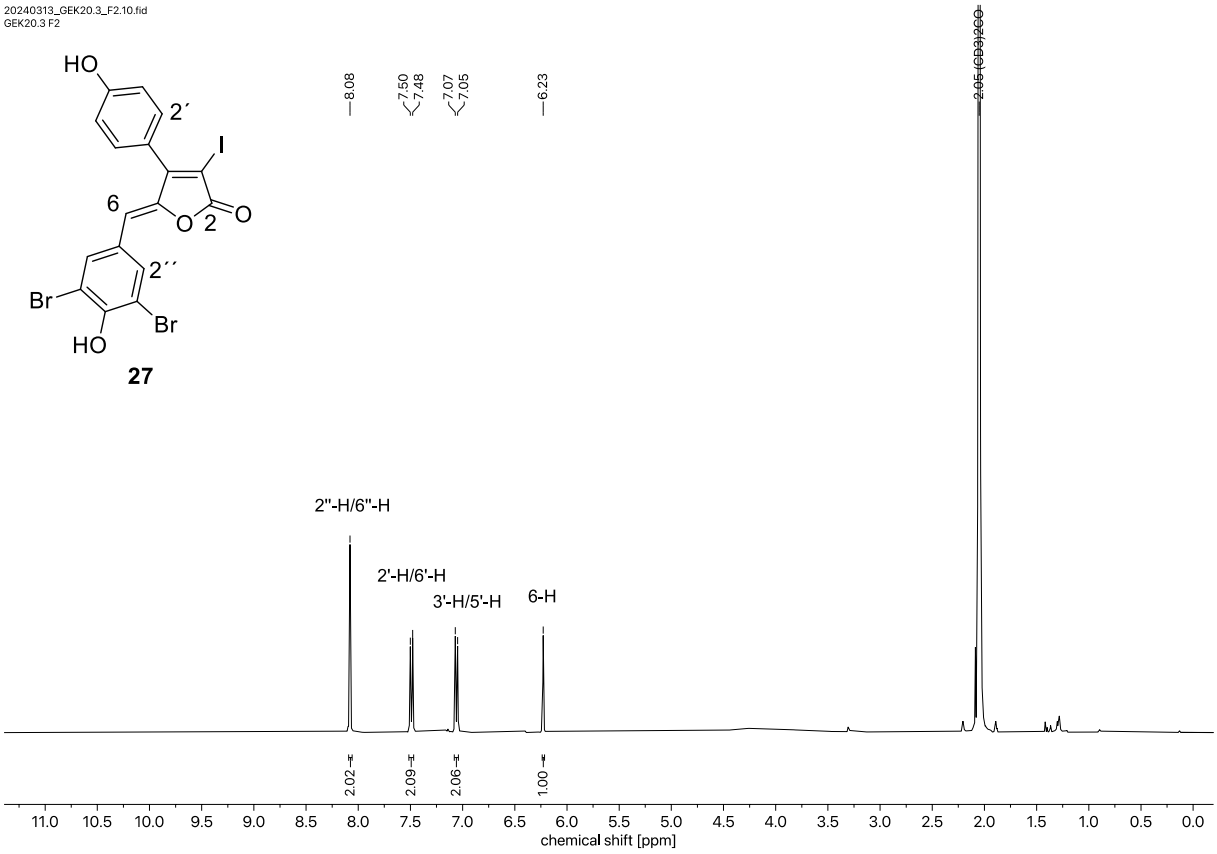

Figure 6: ^{1}H-NMR of rubrolide C analogue **27**, measured at 400 MHz in acetone-d_6.

The corresponding ^{13}C-NMR spectrum of 3-iodo-rubrolide C **27** is displayed in figure 7. The signal at 82.6 ppm represents C-3, which is substituted with iodine. C-6, the benzylidene carbon, is present as signal at 111.2 ppm. The 2,6-dibrominated phenol is represented by the signal of the two brominated carbons C-3'' and C-5'' (112.0 ppm), C-1'' at 128.4 ppm, C-2'' and C-6'' at 135.2 ppm and C-4'' at 152.9 ppm. The peaks at 116.6 ppm (C-3', C-5'), 122.3 ppm (C-1'), 131.7 ppm (C-2', C-6') and 160.4 ppm (C-4') correspond to the 1,4-disubstituted phenol. Furthermore, signals at 150.0 ppm (C-5) and 160.8 ppm (C-4) indicate the furanone ring and the carbonyl group resonates at 166.9 ppm (C-2).

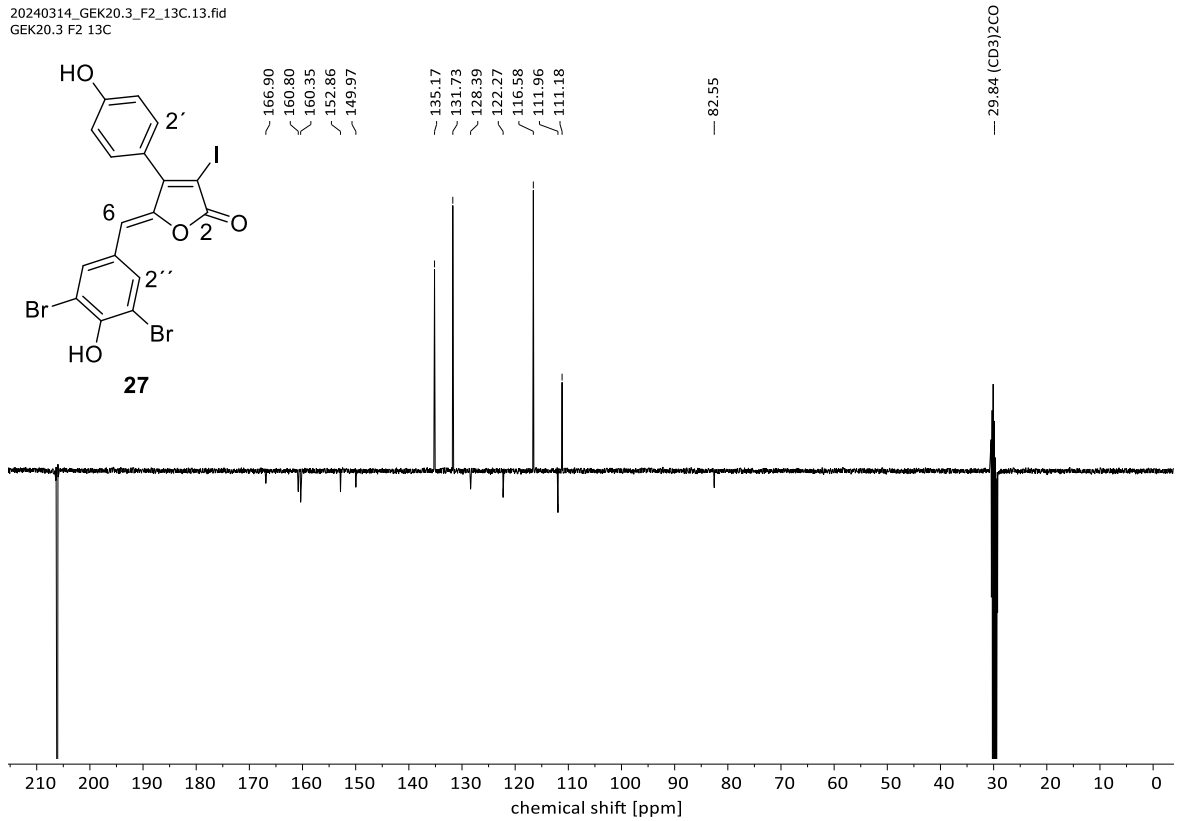

Figure 7: ^{13}C-NMR of 3-iodo-rubrolide C **27**, measured at 100 MHz in acetone-d_6.

The desired Z-configuration of the exocyclic double bond between C-5/C-6 is evident from additional NOESY experiment (Figure 8). The signal labelled in blue confirms the coupling between the benzylidene proton 6-H and proton 6'-H, whereas the signals labelled in orange mark the coupling between proton 6-H, aromatic proton 6'-H and aromatic proton 6''-H.

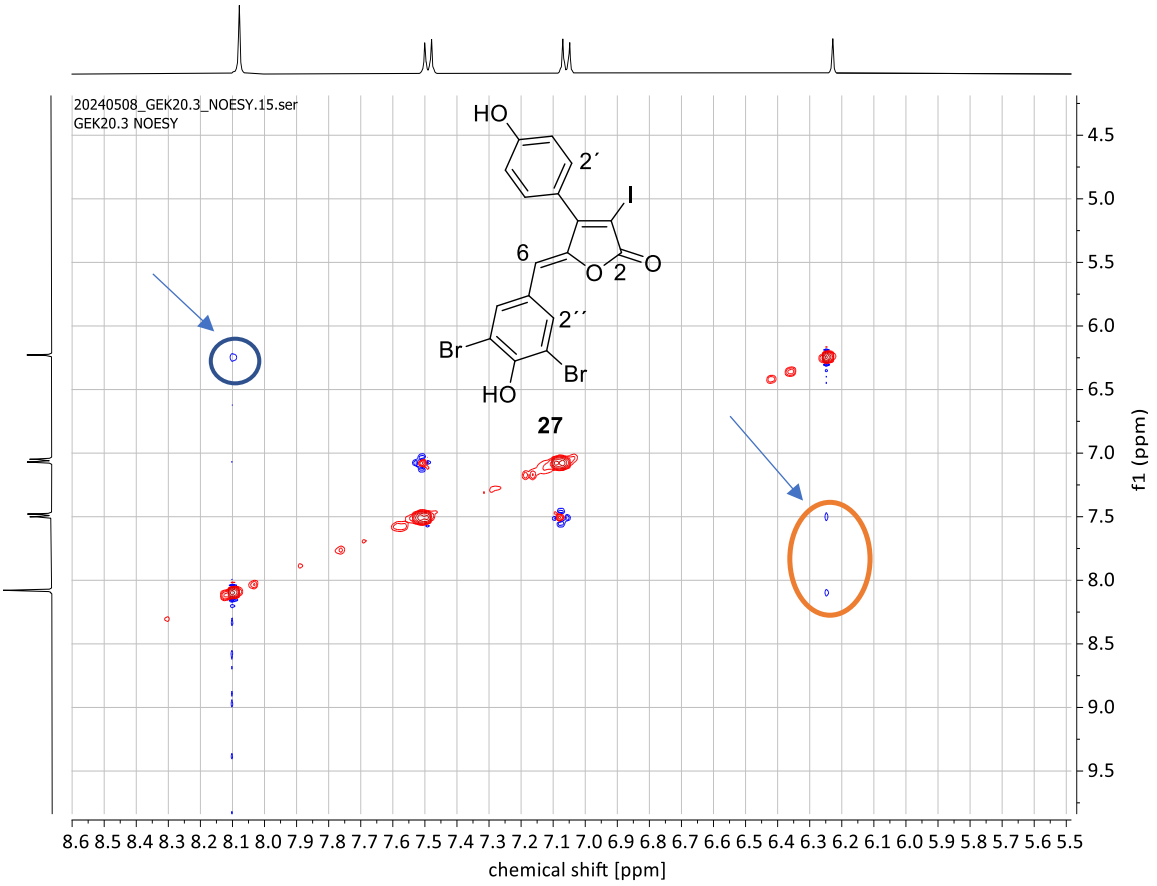

Figure 8: NOESY-NMR (400 MHz, acetone-d_6) experiment of rubrolide analogue C **27**.

3.9. Synthesis of 3-bromo-rubrolide R 28

The final step in the synthesis of 3-bromo-rubrolide R **28** incorporated the reaction of furanone **36** with aldehyde **35** in the presence of DIPEA, TBDMSOTf, DBU and water. DBU is again used to form the double bond in position 15 of the furanone. After purification by normal phase column chromatography and additional reversed phase column chromatography, the synthesis of the desired rubrolide derivative **28** was achieved in 15% yield.

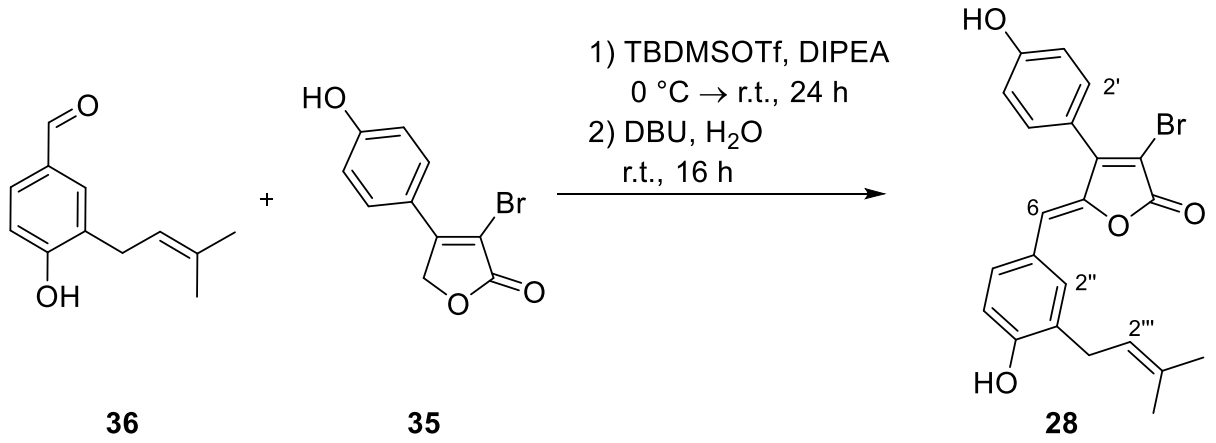

36 **35** **28**

Scheme 16: Vinylogous aldol condensation reaction to yield 3-bromo-rubrolide R **28**.

The structure of 3-bromo-rubrolide R **28** was confirmed by NMR spectroscopy. The ^{1}H-NMR spectrum shows signals for the prenyl side chain of **28**, in which the two methyl groups resonate as singlet at 1.72 ppm with an integral of 6 H. At 3.34 ppm, the doublet with a coupling constant of J = 7.4 Hz and an integral of 2 H can be assigned to 1’’’-H_2. The dddd at 5.34 ppm, with a coupling constant of J = 7.4, 6.1, 3.0, and 1.6 Hz and an integral of 1 H, couples with 1’’’-H_2 (7.4 Hz) and is assigned to 2’’’-H. The singlet at 6.22 ppm, with an integral of 1 H, is the characteristic signal for the benzylidene proton at 6-H. Further signals in the aromatic region are present. The doublet at 6.92 ppm, with a coupling constant of J = 8.3 Hz and an integral of 1 H, can be assigned to 5’’-H at the aromatic C-ring. This proton couples with the C-ring proton 6’’-H, which resonates as a doublet of doublets at 7.60 ppm with J = 8.3 and 2.2 Hz and an integral of 1 H. The second coupling of 6’’-H is induced by 2’’-H at 7.62 ppm, which resonates as a doublet with a coupling constant of J = 2.2 Hz and an integral of 1 H. Moreover, signals at 7.06 ppm (3’-H, 5’-H) and 7.49 ppm (2’-H, 6’-H) both resonate as doublets with a coupling constant of J = 8.7 Hz and an integral of 2 H and can be assigned to the protons of the 1,4-disubstituted A-ring (Figure 9).

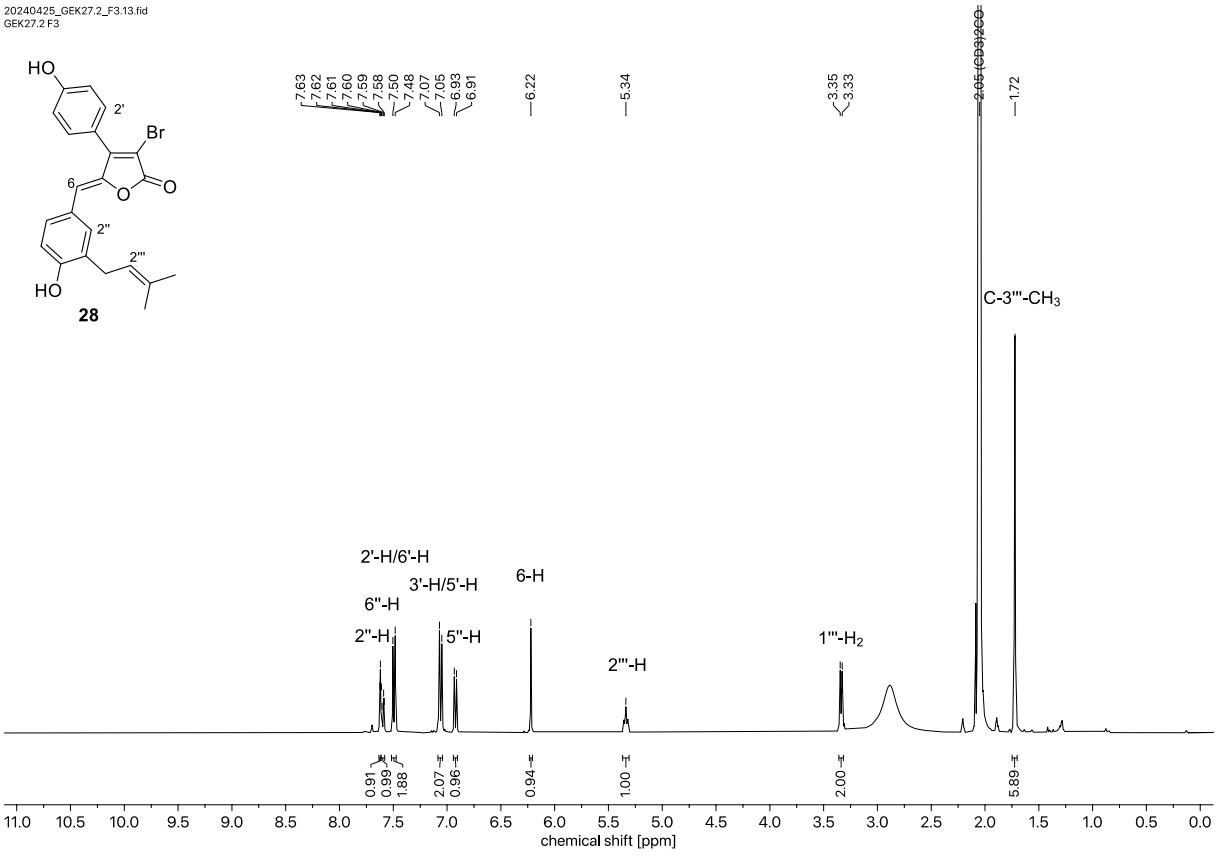

Figure 9: ^{1}H-NMR (400 MHz, acetone-d_6) of rubrolide derivative R **28**.

The ^{13}C-NMR spectrum of 3-bromo-rubrolide R **28** confirms the two methyl groups at C-3''' by signals at 17.87 ppm and 25.89 ppm. Further, the remaining carbon signal, caused by the CH_2-protons of the prenyl chain, is represented by the signal at 28.86 ppm (C-1''') and the signals for the alkene structure are present at 123.13 ppm (C-2''') and 133.15 ppm (C-3'''). The signal for the benzylidene carbon was found at 115.58 ppm (C-6), whereas the carbonyl group corresponds to the signal at 165.60 ppm (C-2). Signals at 105.77 ppm (C-3), 146.67 ppm (C-5) and 154.93 ppm (C-4) indicate the furanone ring. Furthermore, signals found at 116.34 ppm (C-5''), 125.77 ppm (C-1''), 129.52 ppm (C-3''), 131.11 ppm (C-6''), 133.74 ppm (C-2'') and 157.63 ppm (C-4'') can be assigned to the prenylated ring structure, whereas the carbon atom attached to the hydroxyl group (C-4'') holds the highest chemical shift. Lastly, the 1,4-disubstituted phenol ring is evident from signals at 116.64 ppm (C-3', C-5'), 121.04 ppm (C-1'), 131.80 ppm (C-2', C-6') and 160.38 ppm (C-4') (Figure 10).

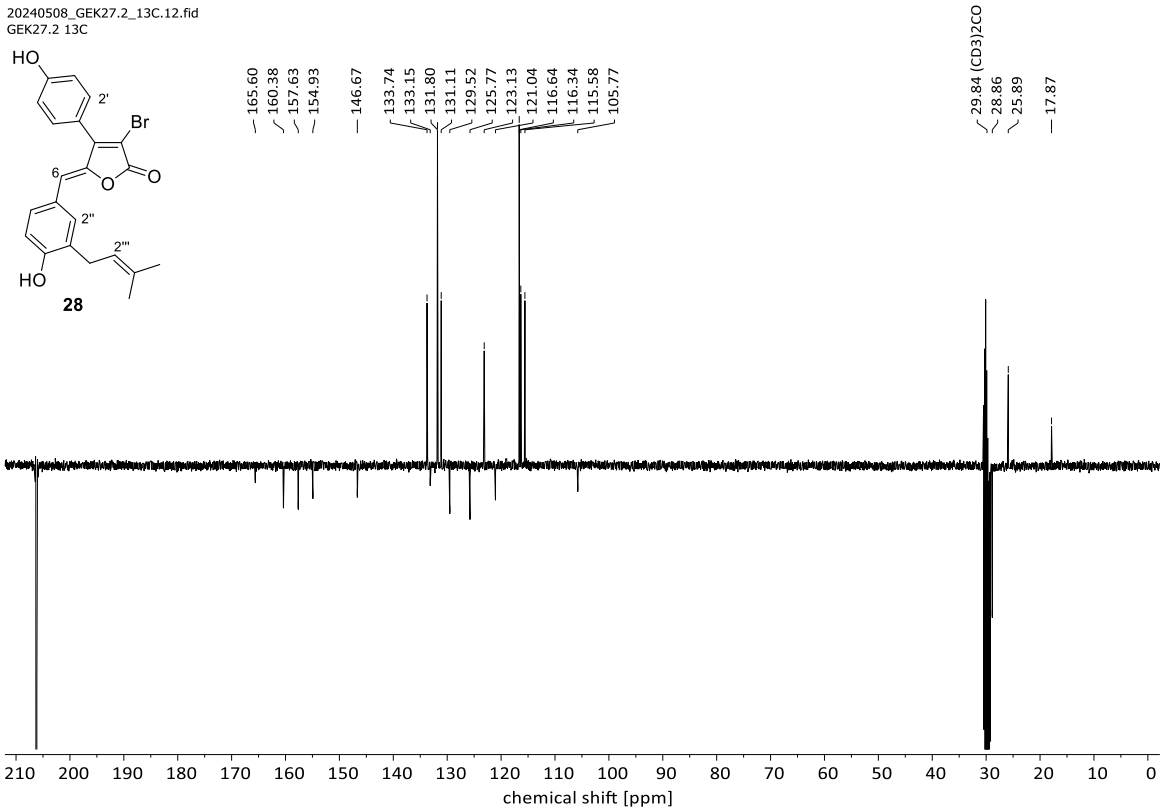

Figure 10: ^{13}C-NMR of rubrolide C analogue **28**, measured at 100 MHz in acetone-d_6.

The Z-configuration of the exocyclic double bond between C-5/C-6 of compound **28** could be confirmed via NOESY experiment (Figure 11). Signals marked in blue demonstrate the coupling between the benzylidene proton 6-H, aromatic proton 6'-H and aromatic proton 6''- H.

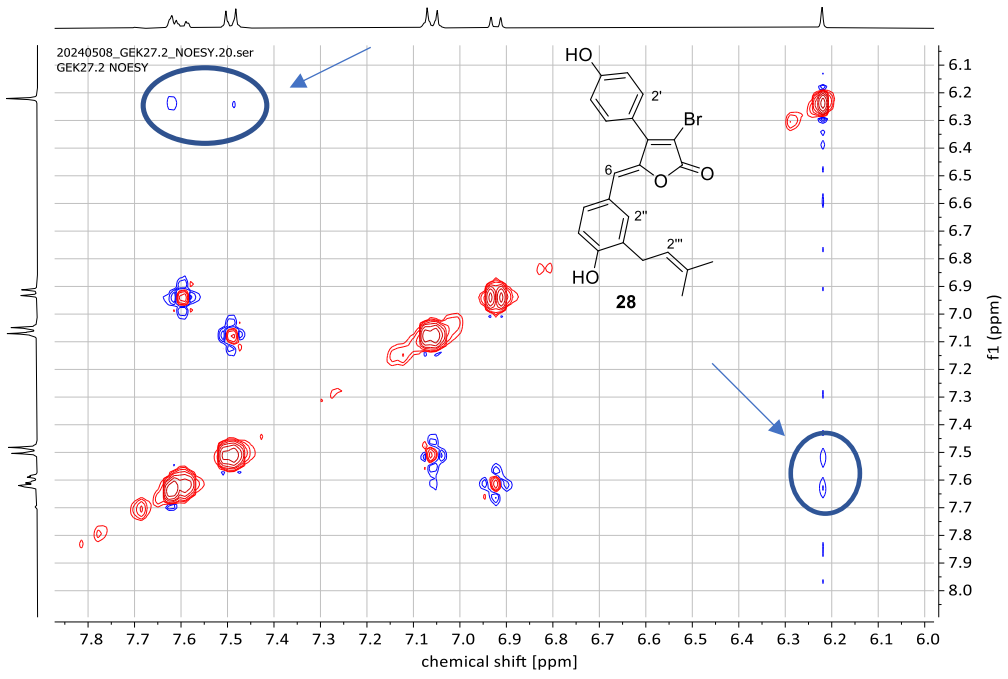

Figure 11: NOESY-NMR (400 MHz, acetone-d_6) spectrum of rubrolide derivative R **28**.

4. Conclusion

The aim of this thesis was the synthesis of two rubrolide analogues for subsequent bioactivity measurements. Both compounds were successfully obtained starting from tetronic acid **34** in four linear steps, employing a Suzuki-Miyaura reaction and a vinylogous aldol condensation as key steps.

The synthesis of the key intermediate, furanone **31**, starts from tetronic acid **34**, which reacted to triflate **33** in 53% yield. Following this, a Pd-catalyzed Suzuki-Miyaura cross-coupling reaction of triflate **33** and boronic acid **32** was performed to obtain furanone **31** in 31% yield. This furanone **31** serves as starting material for both rubrolide syntheses performed in this thesis.

For the synthesis of rubrolide C derivative **27,** furanone **31** was iodinated in position 3 to yield furanone **30** in 58% yield. Lastly, vinylogous aldol condensation was performed, in which furanone **30** needed to react with aldehyde **29** to form 3-iodo-rubrolide C **27**. Additionally, product **27** was purified by normal phase and reversed phase column chromatography to yield the pure *Z* isomer **27**.

For the preparation of rubrolide R analogue **28,** furanone **31** was brominated to yield furanone **35** in 57% yield. For building block **36**, which is necessary for the synthesis of the aromatic C-ring, 2-methylbut-3-en-2-ol **40** reacted to boc-protected carbonate **39** in 85% yield. Furthermore, Tsuji-Trost allylation with 4-hydroxybenzaldehyde **38** yielded allyl phenyl ether **37** in 58% yield and subsequent microwave-assisted Claisen rearrangement gave the prenylated aldehyde **36** in 74% yield. Finally, aldehyde **36** and brominated furanone **35** formed 3-bromo-rubrolide R **28** by vinylogous aldol condensation. The product was purified via normal phase and reversed phase column chromatography to yield the pure *Z* isomer **28**.

To conclude, this work represents the synthesis of the two rubrolide analogues, 3-iodo-rubrolide C **27** and 3-bromo-rubrolide R **28**, with the intention of further investigating their antiviral and antibacterial activities.

5. Experimental Part

5.1. General Information

Reactions

All reactions requiring anhydrous condition were performed under argon atmosphere using Schlenk technique. Reactions carried out at 0 °C incorporated an ice bath.

Reactions were monitored by thin layer chromatography on silica-coated aluminium plates (DC Kieselgel Alugram® Xtra SIL G/UV254, layer thickness 0.2 mm, by Macherey-Nagel). Detection was performed via UV-lamp (λ = 254, 366 nm). Low and non-fluorescent compounds were visualized by permanganate solution.

Reagents and solvents

All commercially purchased chemicals were used without further purification, unless otherwise noted. To perform reactions in the absence of water, solvents dried over molecular sieves were used. DCM, DMF, THF, toluene and 1,4-dioxane were kept under argon atmosphere. Tf_2O and trifluoromethanesulfonic acid were stored under argon atmosphere.

Sample processing

A laboratory evaporator from Heidolph Instruments, Laborota 4000-efficient, was operated to remove solvents *in vacuo*. When necessary, samples were dried further, using a rotary vane vacuum pump from Vacuubrand®.

Instruments

IR spectra were measured between 4000 and 400 cm^{-1} with an Alpha, Platinum-ATR from Bruker.

UV/Vis spectra were obtained with a GeneQuant™ 1300 UV/Vis spectrometer by Healthcare Life Sciences. Samples were measured between 200 and 600 nm.

Melting points were acquired with a Galen III heating tabletop microscope with integrated thermometer by the brand Leica.

^{1}H NMR and ^{13}C NMR spectra were recorded on an Avance III HD 400 MHz spectrometer by Bruker. The residual proton signals of deuterated DMSO-d_6 (chemical shift of δ = 2.50 ppm (^{1}H) and δ = 39.52 ppm (^{13}C)), $CDCl_3$ (chemical shift of δ = 7.26 ppm (^{1}H) and δ = 77.16 ppm (^{13}C)) or acetone-d_6 (chemical shift of δ = 2.05 ppm (^{1}H) and δ = 29.84, 206.26 ppm (^{13}C)) were used as internal standards. To describe the multiplicity of the signals, s (singlet), d (doublet), t (triplet), dd (doublet of doublet), dddd (doublet of doublet of doublet of doublet), m (multiplet) were used as abbreviations. Signals were listed as follows: chemical shift, multiplicity, coupling constant(s), number of protons, assignment.

HRMS were measured on an electrospray-quadrupole time-of-flight mass spectrometer (ESI QTOF) by Bruker with a *m/z* ratio of 100-1000.

Microwave reactions were performed in an Initiator+, Robot Eight by Biotage®.

Advanced automated Flash Purification was performed on a Selekt by Biotage®. Detection was performed via UV-absorption at 254 nm and 280 nm and via absorption of visible light between 198 nm and 810 nm.

5.2. Synthetic procedures

5.2.1. Synthesis of *tert*-butyl-1,1-dimethylallyl carbonate 39

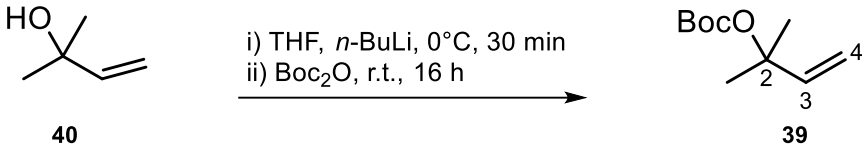

40 **39**

A solution of 2-methylbut-3-en-2-ol **40** (1.50 mL, 14.5 mmol, 1.00 equiv.) in THF (25.0 mL) was cooled to 0 °C and *n*-BuLi (9.00 mL, 14.5 mmol, 1.00 equiv., 1.6 M in hexane) was added dropwise. The reaction was stirred at 0 °C for 30 min. Afterwards, di-*tert*-butyl dicarbonate (3.47 g, 15.9 mmol, 1.10 equiv.) was added, the reaction mixture was warmed to room temperature and stirred for 16 h. Then, the mixture was diluted with MTBE (50.0 mL) and washed with sat. aq. $NaHCO_3$ solution (75.0 mL), H_2O (25.0 mL) and brine (75.0 mL). The organic layer was dried over $MgSO_4$, filtered and the solvent was removed in vacuum. The allyl carbonate **39** (2.30 g, 12.4 mmol, 85%) was obtained as yellow oil.[18]

TLC: $\mathbf{R_f}$ = 0.35 (PE/EtOAc 30:1 v/v).

IR (ATR): 2979, 2933, 1807, 1738, 1463, 1369, 1282, 1255, 1119, 1074, 995, 924, 842, 791, 712 cm^{-1}.

^{1}H-NMR (400 MHz, $CDCl_3$): δ (ppm) = 1.47 (s, 9 H, $C(CH_3)_3$), 1.53 (s, 6 H, 2 × CH_3), 5.14 (m, 2 H, 4-H_2), 6.11 (dd, J = 17.5, 10.9 Hz, 1 H, 3-H).

^{13}C-NMR (100 MHz, $CDCl_3$): δ (ppm) = 26.9 (2 C, 2 × C-2-CH_3), 28.3 (3 C, $C(\underline{C}H_3)_3$), 81.9 ($\underline{C}(CH_3)_3$), 81.9 (C-2), 113.5 (C-4), 142.8 (C-3), 152.4 (C=O).

$C_{10}H_{18}O_3$ (186.25 g/mol).

5.2.2. Synthesis of 4-[(2-methylbut-3-en-2-yl)oxy]benzaldehyde 37

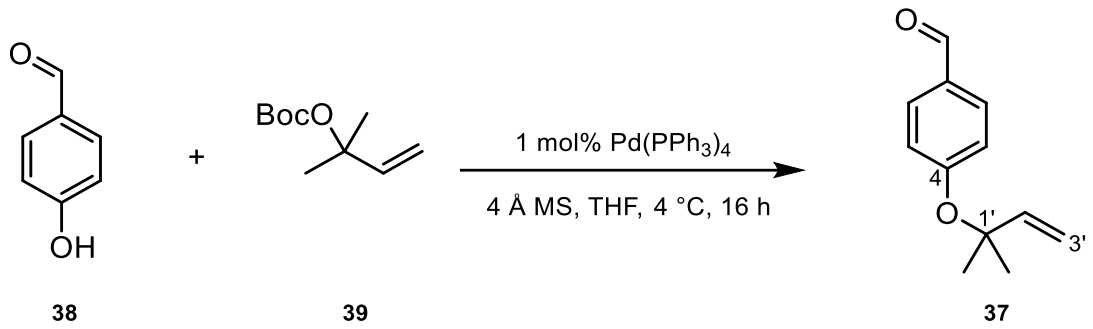

38 **39** **37**

A solution of 4-hydroxybenzaldehyde **38** (200 mg, 1.64 mmol, 1.00 equiv.) and boc-protected 2-methylbut-3-en-2-ol **39** (1.07 g, 5.73 mmol, 3.50 equiv.) in anhydrous THF (4.00 mL) was cooled to 0 °C. Afterwards, $Pd(PPh_3)_4$ (18.9 mg, 16.0 µmol, 1.0 mol%) was added and the mixture was stirred at 4 °C for 16 h. The reaction mixture was filtered through a syringe filter and the solvent was removed in vacuum. The residue was purified by column chromatography (silica gel, PE/EtOAc 33:1 → 20:1) to obtain aldehyde **37** (180 mg, 0.94 mmol, 58%) as colourless oil.[18]

TLC: $\mathbf{R_f}$ = 0.49 (PE/EtOAc 9:1 v/v).
IR (ATR): 2930, 1691, 1596, 1502, 1247, 1126, 904, 833, 694 cm^{-1}.
UV/Vis (MeOH): λ_{max} (nm) = 211, 277.
^{1}H-NMR (400 MHz, $CDCl_3$): δ (ppm) = 1.54 (s, 6 H, 2 × CH_3), 5.23 (m, 2 H, 3'-H_2), 6.14 (dd, J = 17.7, 10.9 Hz, 1 H, 2'-H), 7.08 (d, J = 8.7 Hz, 2 H, 3-H, 5-H), 7.75 (d, J = 8.7 Hz, 2 H, 2-H, 6-H), 9.87 (s, 1 H, CHO).
^{13}C-NMR (100 MHz, $CDCl_3$): δ (ppm) = 27.4 (2 C, 2 × CH_3), 80.8 (C-1'), 114.3 (C-3'), 119.7 (2 C, C-3, C-5), 130.2 (C-1), 131.4 (2 C, C-2, C-6), 143.8 (C-2'), 162.3 (C-4), 191.1 (CHO).
MS (ESI$^+$): *m/z* calcd.: 191.1067 $C_{12}H_{15}O_2^+$; *m/z* found 191.1071.
$C_{12}H_{14}O_2$ (190.24 g/mol).

5.2.3. Synthesis of 4-hydroxy-3-(3-methylbut-2-en-1-yl)benzaldehyde 36

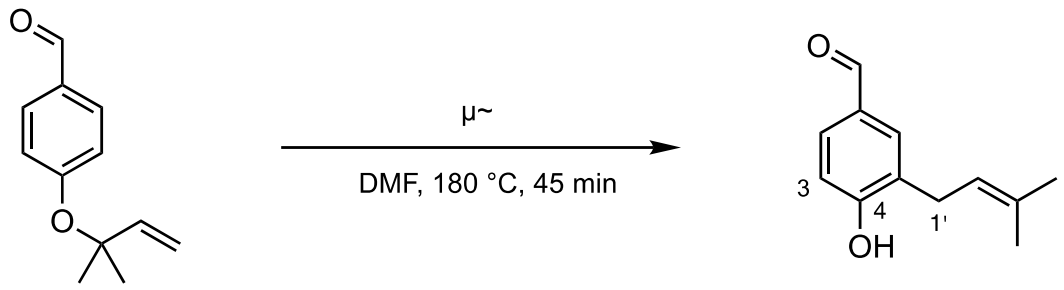

37 **36**

A solution of 4-[(2-methylbut-3-en-2-yl)oxy]benzaldehyde **37** (262 mg, 1.38 mmol, 1.00 equiv.) in DMF (3.00 mL) was stirred at 180 °C for 45 min under microwave irradiation. The reaction mixture was diluted with EtOAc (5.0 mL) and the solvent was removed in vacuum. The crude product was purified by column chromatography (silica gel, PE/EtOAc 33:1 → 5:1) to yield aldehyde **35** (195 mg, 1.02 mmol, 74%) as light yellow solid.[18]

TLC: R_f = 0.20 (PE/EtOAc 4:1 v/v).

MP: 51 °C.

IR (ATR): 3140, 1653, 1583, 1432, 1379, 1276, 1239, 1200, 939, 838, 765, 630, 570, 441 cm^{-1}.

UV/Vis (MeOH): λ_{max} (nm) = 226, 287.

^{1}H-NMR (400 MHz, $CDCl_3$): δ (ppm) = 1.80 (dd, J = 2.9, 1.4 Hz, 6 H, 2 × CH_3), 3.42 (d, J = 7.3 Hz, 2 H, CH_2), 5.32 (dddd, J = 7.3, 5.9, 2.9, 1.5 Hz, 1 H, 2'-H), 6.91 (d, J = 8.8 Hz, 1 H, 3-H), 7.67 (m, 2 H, 2-H, 6-H), 9.85 (s, 1 H, CHO).

^{13}C-NMR (100 MHz, $CDCl_3$): δ (ppm) = 26.0, 18.1 (2 C, 2 × CH_3), 29.7 (C-1'), 116.3 (C-3), 120.7 (C-2'), 127.7 (C-5), 130.2 (C-2), 130.7 (C-3'), 132.0 (C-1), 136.3 (C-6), 160.2 (C-4), 191.3 (CHO).

MS (ESI^+): *m/z* calcd.: 191.1067 $C_{12}H_{15}O_2^+$; *m/z* found 191.1074.

$C_{12}H_{14}O_2$ (190.24 g/mol).

5.2.4. Synthesis of 5-oxo-2,5-dihydrofuran-3-yl-trifluoromethanesulfonate 33

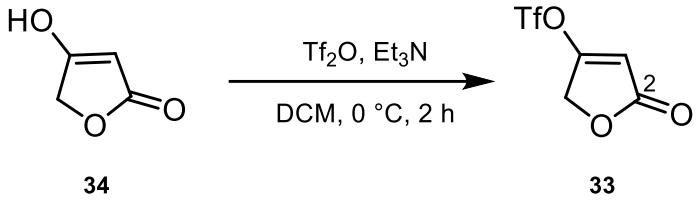

A solution of 4-hydroxyfuran-2(5H)-one **34** (500 mg, 5.00 mmol, 1.00 equiv.) in anhydrous DCM (30.0 mL) was cooled to 0 °C and Et_3N (0.84 mL, 0.61 g, 6.00 mmol, 1.20 equiv.) and Tf_2O (1.01 mL, 1.69 g, 6.00 mmol, 1.20 equiv.) were added dropwise. The mixture was stirred for 2 h at 0 °C. Afterwards, the mixture was diluted with DCM (20.0 mL) and washed with H_2O (4 × 100 mL). The organic layer was dried over $MgSO_4$, filtered and the solvent was removed in vacuum. The residue was purified by Kugelrohr distillation to yield triflate **33** (617 mg, 2.66 mmol, 53%) as yellow liquid.[18]

UV/Vis (MeOH): λ_{max} (nm) = 209, 248.
IR (ATR): 1787, 1645, 1436, 1301, 1215, 1126, 1047, 930, 808, 761, 601, 617 cm^{-1}.
^{1}H-NMR (400 MHz, $CDCl_3$): δ (ppm) = 4.89 (d, J = 1.8 Hz, 2 H, 5-H_2), 6.07 (t, J = 1.8 Hz, 1 H, 3-H).
^{13}C-NMR (100 MHz, $CDCl_3$): δ (ppm) = 67.6 (C-5), 104.7 (C-3), 118.6 (q, J_{CF} = 322 Hz, CF_3), 167.0 (C-2), 168.9 (C-4),
HRMS (ESI$^-$): *m/z* calcd.: 230.9581 $C_5H_2F_3O_5S^-$; m/z found 230.9581.
$C_5H_3F_3O_5S$ (232.13 g/mol).

5.2.5. Synthesis of 4-(4-hydroxyphenyl)furan-2(5H)-one 31

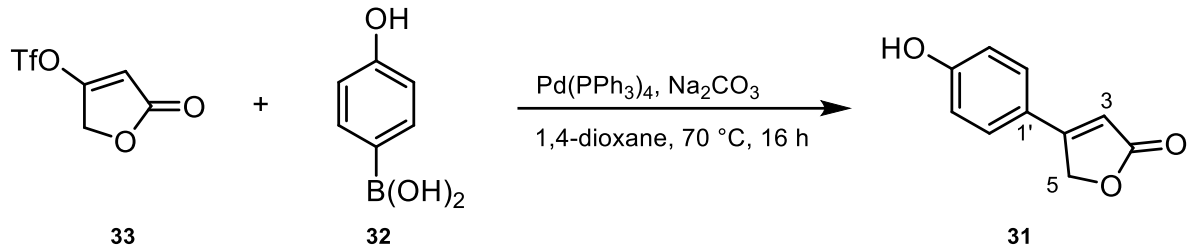

A solution of 5-oxo-2,5-dihydrofuran-3-yltrifluoromethane sulfonate **33** (176 mg, 0.76 mmol, 1.00 equiv.), arylboronic acid **32** (125 mg, 0.91 mmol, 1.20 equiv.) and Na_2CO_3 (240 mg,

2.27 mmol, 3.00 equiv.) was dissolved in 1,4-dioxane (5.62 mL) and degassed with argon for 10 min. Afterwards, $Pd(PPh_3)_4$ (3.76 mg, 2.14 mol%) was added to the solution and stirred for 16 h at 70 °C. The reaction was cooled to room temperature, filtered through celite® and the solvent was removed in vacuum. The crude product was purified by reversed phase column chromatography (25 g RP-C_{18}, H_2O/ MeCN 7:1 → 1:1) to yield the product **31** (40.7 mg, 0.23 mmol, 31%).[18]

TLC: $\mathbf{R_f}$ = 0.40 (PE/EtOAc 1:1 v/v).
MP: 232 °C.
IR (ATR): 2921, 1698, 1580, 1510, 1326, 1272, 1168, 1038, 901, 820, 703, 588, 546, 480 cm^{-1}.
UV/Vis (MeOH): λ_{max} (nm) = 223, 304.
^{1}H-NMR (400 MHz, DMSO-d_6): δ (ppm) = 5.30 (d, J = 1.7 Hz, 2 H, 5-H_2), 6.47 (t, J = 1.7 Hz, 1 H, 3-H), 6.86 (d, J = 8.7 Hz, 2 H, 3'-H, 5'-H), 7.56 (d, J = 8.7 Hz, 2 H, 2'-H, 6'-H), 10.21 (s, 1 H, OH),
^{13}C-NMR (100 MHz, DMSO-d_6): δ (ppm) = 70.9 (C-5), 108.8 (C-3), 115.8 (2 C, C-3', C-5'), 120.7 (C-1'), 129.0 (2 C, C-2', C-6'), 160.6 (C-4'), 165.0 (C-4), 174.2 (C-2).
MS (ESI$^+$): *m/z* calcd.: 175.0401 $C_{10}H_7O_3^-$; *m/z* found 175.0407.
$C_{10}H_8O_3$ (176.17 g/mol).

5.2.6. Synthesis of 3-iodo-4-(4-hydroxyphenyl)furan-2(5H)-one 30

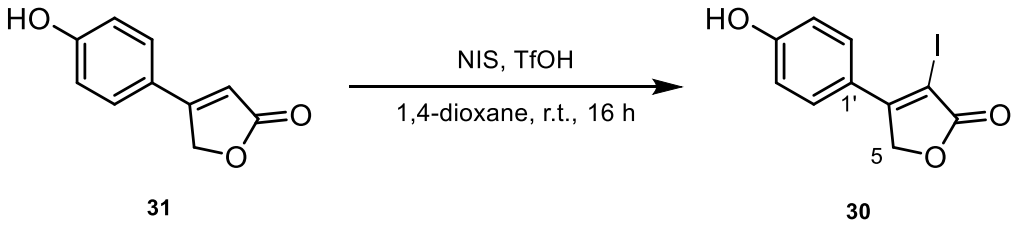

31 **30**

To a suspension of furanone **31** (50.0 mg, 0.29 mmol, 1.00 equiv.) in abs. 1,4-dioxane (2.00 mL), trifluoromethanesulfonic acid (27.5 µL, 0.31 mmol, 1.10 equiv.) and *N*-iodosuccinimide were added (70.3 mg, 0.31 mmol, 1.10 equiv.) and the mixture was stirred at room temperature for 16 h. Afterwards, saturated sodium hydrogen sulfite solution (6.00 mL) was added and the aqueous layer was extracted with EtOAc (3 × 6.00 mL). The combined organic layers were dried over $MgSO_4$, filtered, and the solvent was removed in vacuum.

Purification by reversed phase column chromatography (25 g RP-C_{18}, H_2O/ MeCN 10:1 → 1:1) yielded 3-iodo-4-(4-hydroxyphenyl)furan-2(5H)-one **30** (50.3 mg, 0.17 mmol, 58%).[37]

TLC: $\mathbf{R_f}$ = 0.35 (PE/EtOAc 3:2 v/v).
MP: 215 °C.
IR (ATR): 3225, 1707, 1601, 1568, 1503, 1317, 1264, 1172, 1029, 967, 823, 727, 569, 492 cm^{-1}
UV/Vis (MeCN): λ_{max} (nm) = 222, 309.
^{1}H-NMR (400 MHz, DMSO-d_6): δ (ppm) = 5.37 (s, 2 H, 5-H_2), 6.94 (d, J = 8.8 Hz, 2 H, 3'-H, 5'-H), 7.85 (d, J = 8.8 Hz, 2 H, 2'-H, 6'-H), 10.32 (s, 1 H, OH).
^{13}C-NMR (100 MHz, DMSO-d_6): δ (ppm) = 73.8 (C-5), 76.8 (C-3), 115.7 (C-3', C-5'), 120.9 (C-1'), 129.3 (C-2', C-6'), 160.7 (C-4'), 163.3 (C-4), 172.2 (C-2).
MS (ESI$^-$): *m/z* calcd.: 300.9367 $C_{10}H_6IO_3^-$; *m/z* found 300.9371.
$C_{10}H_7IO_3$ (302.07 g/mol).

5.2.7. Synthesis of 3-bromo-4-(4-hydroxyphenyl)furan-2(5H)-one 35

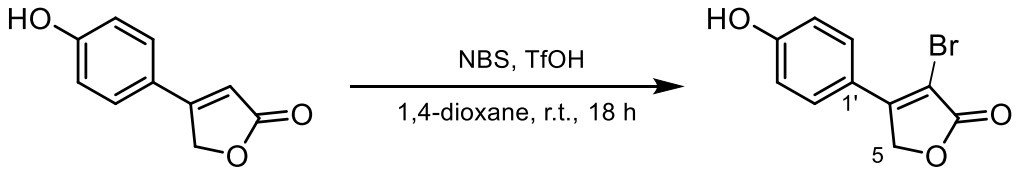

31 **35**

To a solution of furanone **31** (43.6 mg, 248 µmol, 1.00 equiv.) in abs. 1,4-dioxane (1.74 mL) trifluoromethanesulfonic acid (3.27 µL, 37.1 µmol, 15.0 mol-%) and *N*-bromosuccinimide were added (46.0 mg, 260 µmol, 1.05 equiv.), and the mixture was stirred at room temperature for 18 h. Then, saturated sodium hydrogen sulfite solution (10.0 mL) was added and the aqueous layer was extracted with EtOAc (3 × 25.0 mL). The combined organic layers were dried over $MgSO_4$, filtered, and the solvent was removed in vacuum. Purification by column chromatography (25 g RP-C_{18}, H_2O/MeCN 10:1 → 1:1) yielded 3-bromo-4-(4-hydroxy-phenyl)furan-2(5H)-one **35** (35.9 mg, 0.14 mmol, 57%) as white solid.[37]

TLC: $\mathbf{R_f}$ = 0.35 (PE/EtOAc 3:2 v/v).
MP: 234 °C.

IR (ATR): 3257, 1724, 1576, 1508, 1324, 1270, 1177, 1037, 988, 829, 742, 671, 572, 493 cm^{-1}.

UV/Vis (MeCN): λ_{max} (nm) = 204, 308.

^{1}H-NMR (400 MHz, DMSO-d_6): δ (ppm) = 5.39 (s, 2 H, 5-H_2), 6.94 (d, J = 8.8 Hz, 2 H, 3'-H, 6'-H), 7.83 (d, J = 8.8 Hz, 2 H, 2'-H, 6'-H), 10.38 (s, 1 H, OH).

^{13}C-NMR (100 MHz, DMSO-d_6): δ (ppm) = 72.0 (C-5), 101.0 (C-3), 115.9 (C-3', C-5'), 119.8 (C-1'), 129.6 (C-2', C-6'), 157.1 (C-4), 160.8 (C-4'), 170.0 (C-2).

MS (ESI$^-$): *m/z* calcd.: 252.9506 $C_{10}H_6BrO_3^-$; *m/z* found 252.9512.

$C_{10}H_7BrO_3$ (255.07 g/mol).

5.2.8. Synthesis of 3-iodo-rubrolide C 27

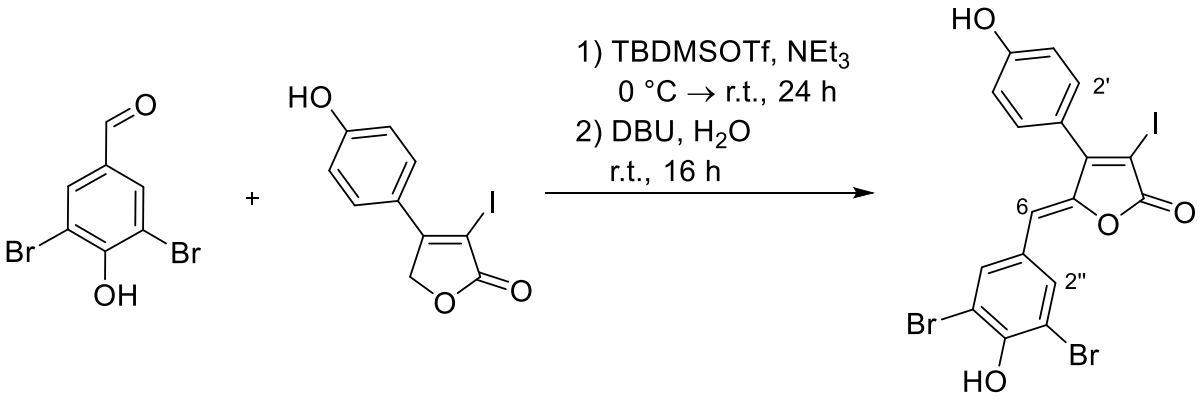

29 **30** **27**

A solution of furanone **30** (70.0 mg, 0.23 mmol, 1.00 equiv.) in abs. DCM (2.00 mL) was cooled to 0 °C and triethylamine (117 mg, 1.16 mmol, 5.00 equiv.) and TBDMSOTf (276 mg, 1.04 mmol, 4.50 equiv.) were added dropwise. The solution was stirred at 0 ° for 30 min, before aldehyde **29** (84.3 mg, 0.30 mmol, 1.30 equiv.) was added. The solution was allowed to warm to room temperature and stirred for 24 h. Then, DBU (212 mg, 1.39 mmol, 6.00 equiv.) and water (0.75 mL) were added, and the solution was stirred for 16 h. The reaction mixture was washed with aqueous HCl solution (1 M, 5.00 mL), the phases were separated, and the aqueous phase was extracted with EtOAc (3 × 25.0 mL). The combined organic phases were washed with brine (25.0 mL), dried over $MgSO_4$, filtered, and the solvent was removed in vacuum. Purification by column chromatography (25 g SiO_2, PE/EtOAc 9:1 → 2:1) yielded the *E*/*Z* mixed isomers in a 1:5 ratio. Additional purification by reversed phase column chromatography (12 g RP-C_{18}, H_2O/MeCN 2:1 → 1:2) yielded the pure *Z* isomer of 3-iodo-rubrolide C **27** (15.4 mg, 30.0 µmol, 12%) as orange solid.[37]

TLC: R_f = 0.46 (PE/EtOAc 2:1 v/v).

MP: 201 °C.

IR (ATR): 3292, 1732, 1604, 1471, 1218, 1165, 954, 888, 835, 744, 640, 536 cm^{-1}.

UV/Vis (MeOH): λ_{max} (nm) = 206, 350, 502.

^{1}H-NMR (400 MHz, acetone-d_6): δ (ppm) = 6.23 (s, 1 H, 6-H), 7.06 (d, J = 8.7 Hz, 2 H, 3'-H, 5'-H), 7.49 (d, J = 8.8 Hz, 2 H, 2'-H, 6'-H), 8.08 (s, 2 H, 2''-H, 6''-H).

^{13}C-NMR (100 MHz, acetone-d_6): δ (ppm) = 82.6 (C-3), 111.2 (C-6), 112.0 (2 C, C-3'', C-5''), 116.6 (C-3', C-5'), 122.3 (C-1'), 128.4 (C-1''), 131.7 (2 C, C-2', C-6'), 135.2 (2 C, C-2'', C-6''), 150.0 (C-5), 152.9 (C-4''), 160.4 (C-4'), 160.8 (C-4), 166.9 (C-2).

MS (ESI$^-$): *m/z* calcd.: 560.7840 $C_{17}H_8Br_2IO_4^-$; *m/z* found 560.7843.

$C_{17}H_9Br_2IO_4$ (563.97 g/mol).

5.2.9. Synthesis of 3-bromo-rubrolide R 28

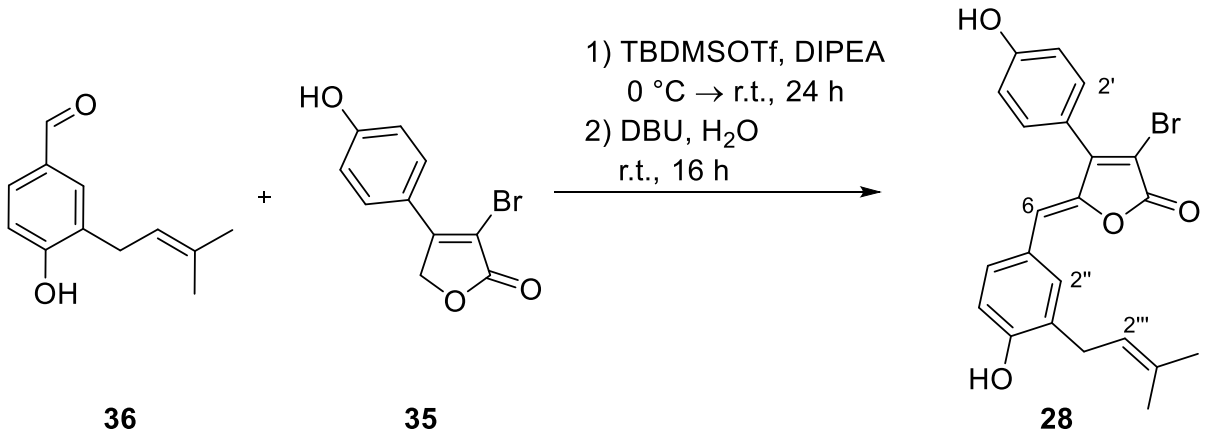

36 **35** **28**

A solution of furanone **35** (22.3 mg, 87.0 µmol, 1.00 equiv.) in abs. DCM (1.50 mL) was cooled to 0 °C and DIPEA (56.5 mg, 437 µmol, 5.00 equiv.) and TBDMSOTf (104 mg, 393 µmol, 4.50 equiv.) were added dropwise. The solution was stirred at 0 ° for 30 min. Afterwards, aldehyde **36** (21.6 mg, 114 µmol, 1.30 equiv.) was added, the solution was allowed to warm to room temperature, and was stirred for 24 h. Then, DBU (79.9 mg, 525 µmol, 6.00 equiv.) and water (0.50 mL) were added and the solution was stirred for 16 h. The reaction mixture was washed with aqueous HCl solution (1 M, 5.00 mL), the phases were separated, and the aqueous phase was extracted with EtOAc (3 × 25.0 mL). The combined organic phases were washed with sodium bicarbonate solution (25.0 mL) and brine (25.0 mL), dried over $MgSO_4$, filtered, and the solvent was removed in vacuum. Purification by column chromatography (25 g SiO_2, PE/EtOAc 19:1 → 1:3) yielded the *E*/*Z* mixture of the isomers in a ratio of 1:13. Purification

by reversed phase column chromatography (12 g RP-C_{18}, H_2O/MeCN 3:2 → 1:2) yielded the pure *Z* isomer of 3-bromo-rubrolide R **28** (5.50 mg, 12.9 µmol, 15%) as yellow solid.[37]

TLC: $\mathbf{R_f}$ = 0.27 (PE/EtOAc 2:1 v/v).

MP: 174 °C.

IR (ATR): 3316, 1730, 1687, 1592, 1500, 1424, 1363, 1272, 1096, 1011, 819, 746, 677, 542 cm^{-1}.

UV/Vis (MeOH): λ_{max} (nm) = 253, 375.

^{1}H-NMR (400 MHz, acetone-d_6): δ (ppm) = 1.72 (s, 6 H, 2 × C-3'''-$\underline{C}H_3$), 3.34 (d, *J* = 7.4 Hz, 2 H, 1'''-H_2), 5.34 (dddd, *J* = 7.5, 6.1, 3.0, 1.6 Hz, 1 H, 2'''-H), 6.22 (s, 1 H, 6-H), 6.92 (d, *J* = 8.3 Hz, 1 H, 5''-H), 7.06 (d, *J* = 8.7 Hz, 2 H, 3'-H, 5'-H), 7.49 (d, *J* = 8.6 Hz, 2 H, 2'-H, 6'-H), 7.60 (dd, *J* = 8.3, 2.4 Hz, 1 H, 6''-H), 7.62 (d, *J* = 2.2 Hz, 1 H, 2''-H).

^{13}C-APT-NMR (100 MHz, acetone-d_6): δ (ppm) = 17.87 (C-3'''-CH_3), 25.89 (C-3'''-CH_3), 28.86 (C-1'''), 105.77 (C-3), 115.58 (C-6), 116.34 (C-5''), 116.64 (C-3', C-5'), 121.04 (C-1'), 123.13 (C-2'''), 125.77 (C-1''), 129.52 (C-3''), 131.11 (C-6''), 131.80 (C-2', C-6'), 133.15 (C-3'''), 133.74 (C-2''), 146.67 (C-5), 154.93 (C-4), 157.63 (C-4''), 160.38 (C-4'), 165.60 (C-2).

MS (ESI$^+$): *m/z* calcd.: 427.0539 $C_{22}H_{20}BrO_4^+$; *m/z* found 427.0538.

$C_{22}H_{19}BrO_4$ (427.29 g/mol).

6. Appendix

6.1. NMR Spectra

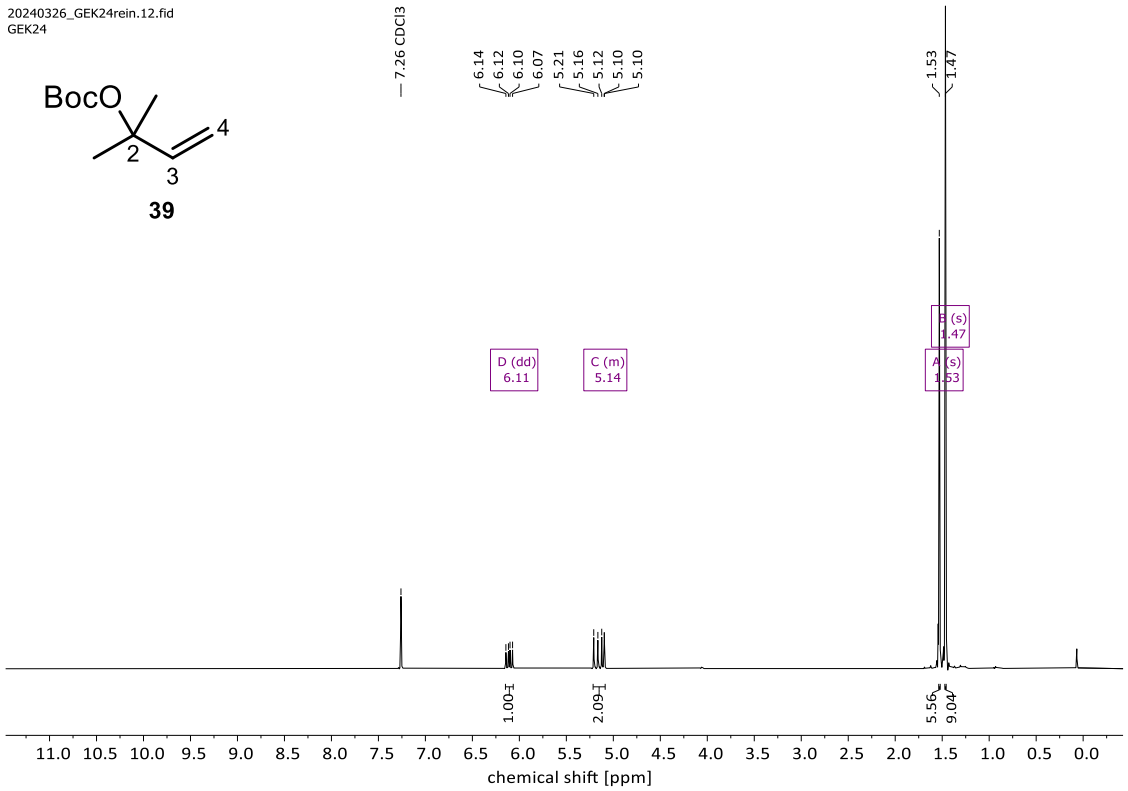

Figure 12: ^{1}H-NMR spectrum of compound **39** (400 MHz, $CDCl_3$).

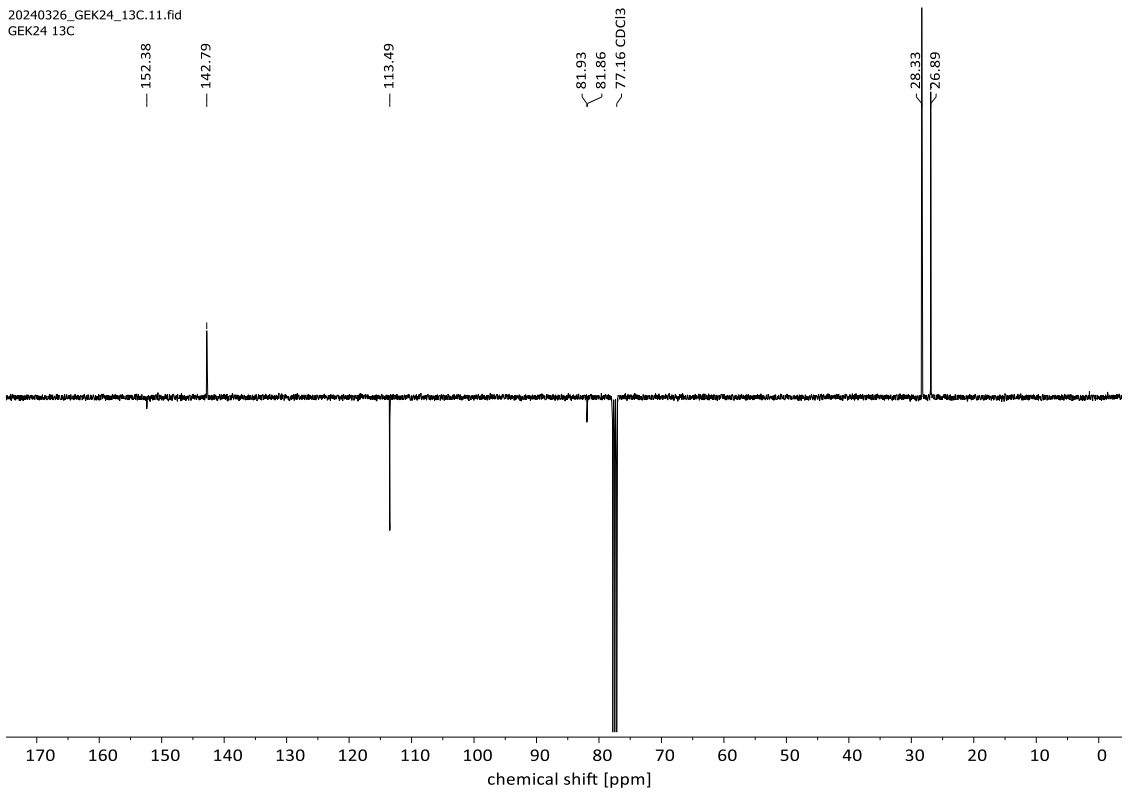

Figure 13: ^{13}C-NMR spectrum of compound **39** (APT, 100 MHz, $CDCl_3$).

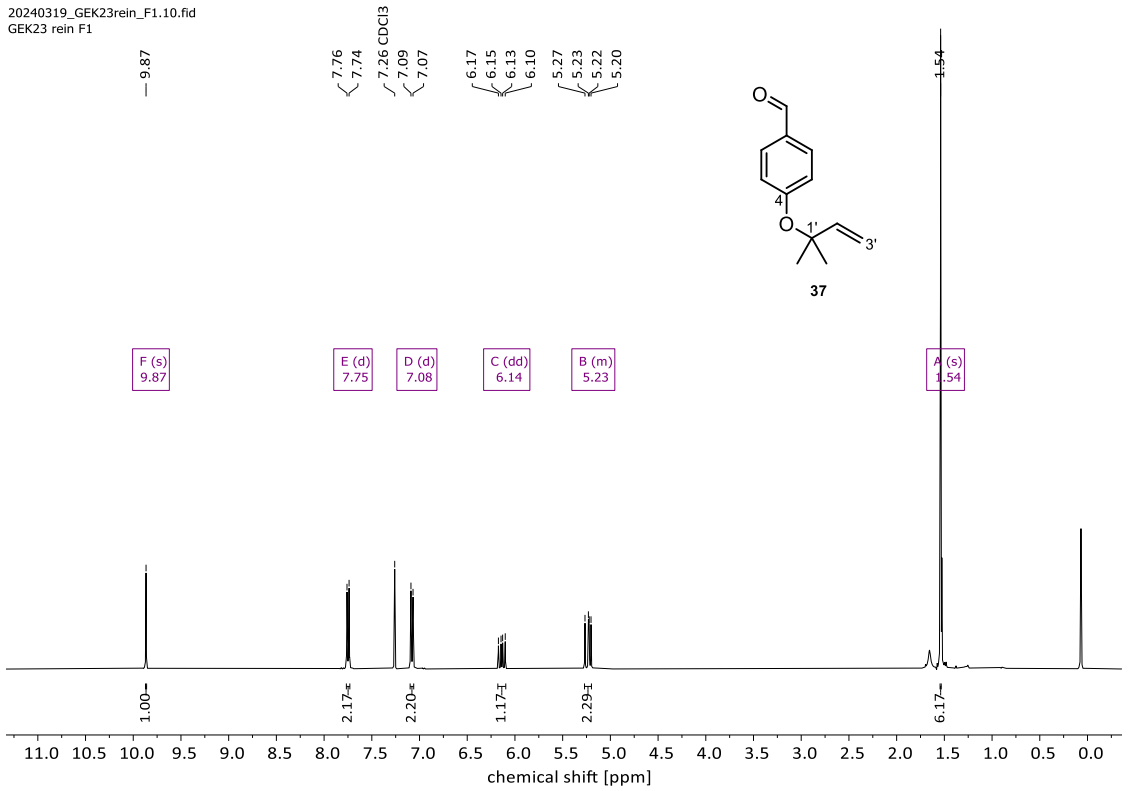

Figure 14: ^{1}H-NMR spectrum of aldehyde **37** (400 MHz, $CDCl_3$).

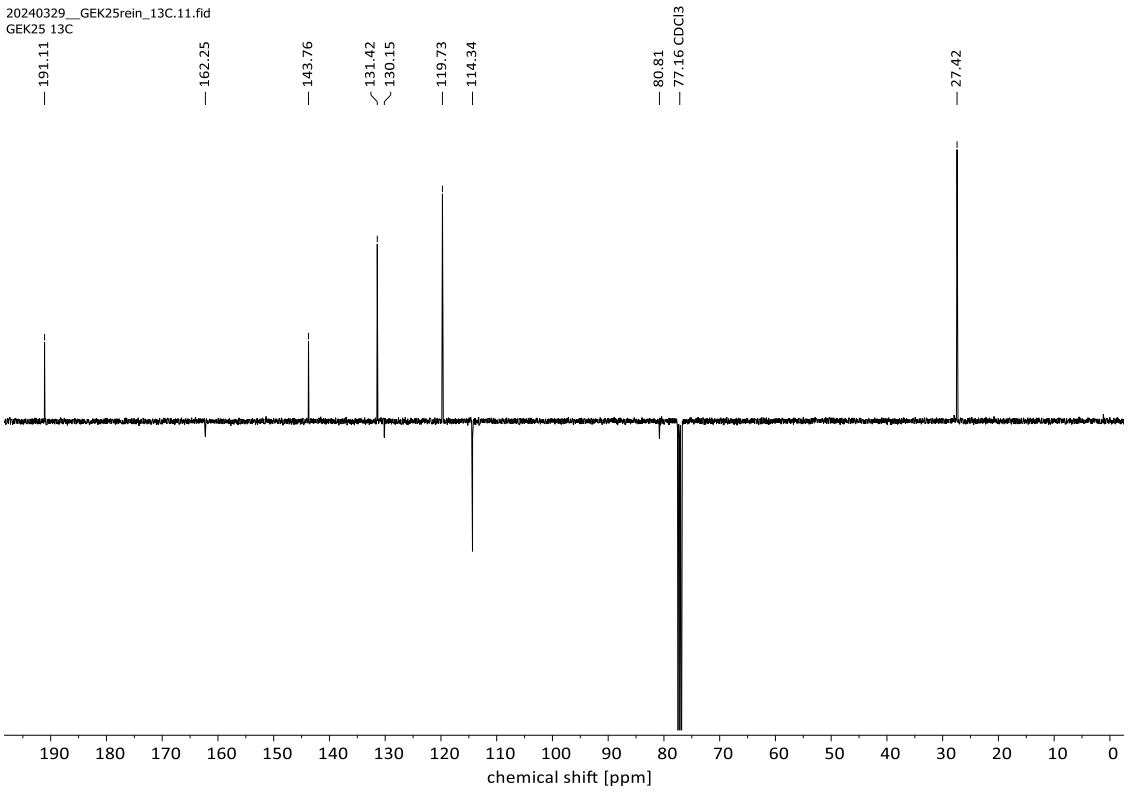

Figure 15: ^{13}C-NMR spectrum of aldehyde **37** (APT, 100 MHz, $CDCl_3$).

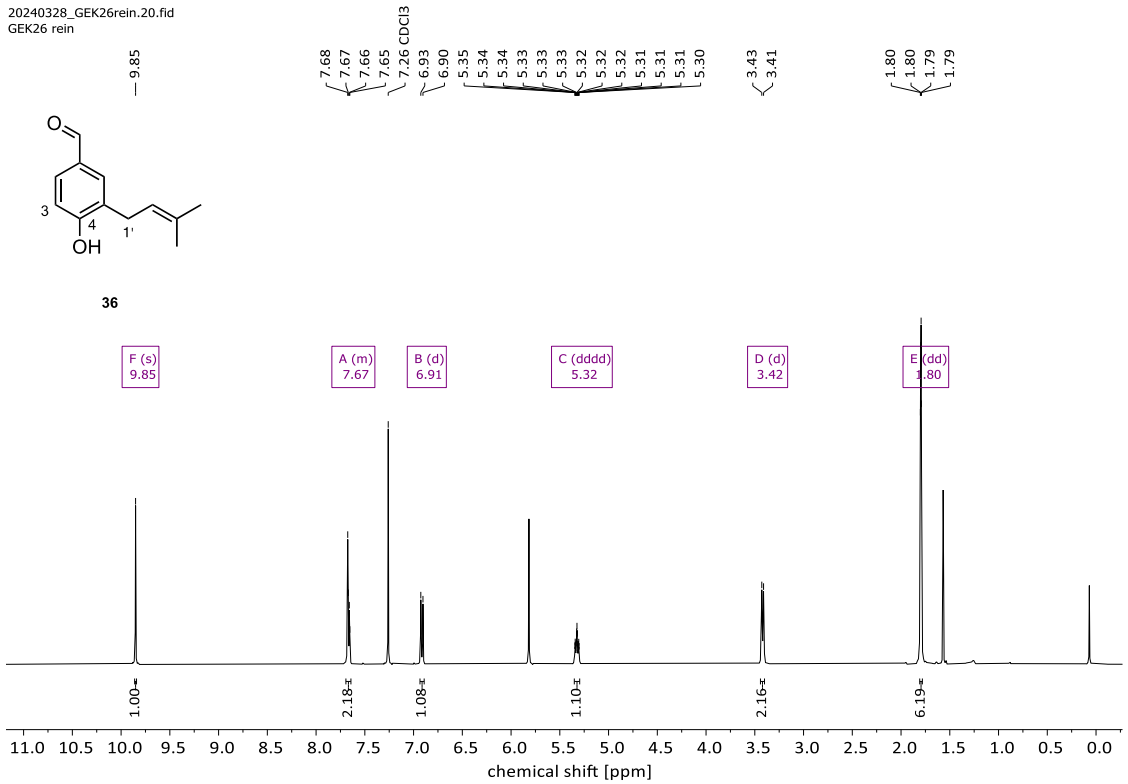

Figure 16: ^{1}H-NMR spectrum of aldehyde **36** (400 MHz, $CDCl_3$).

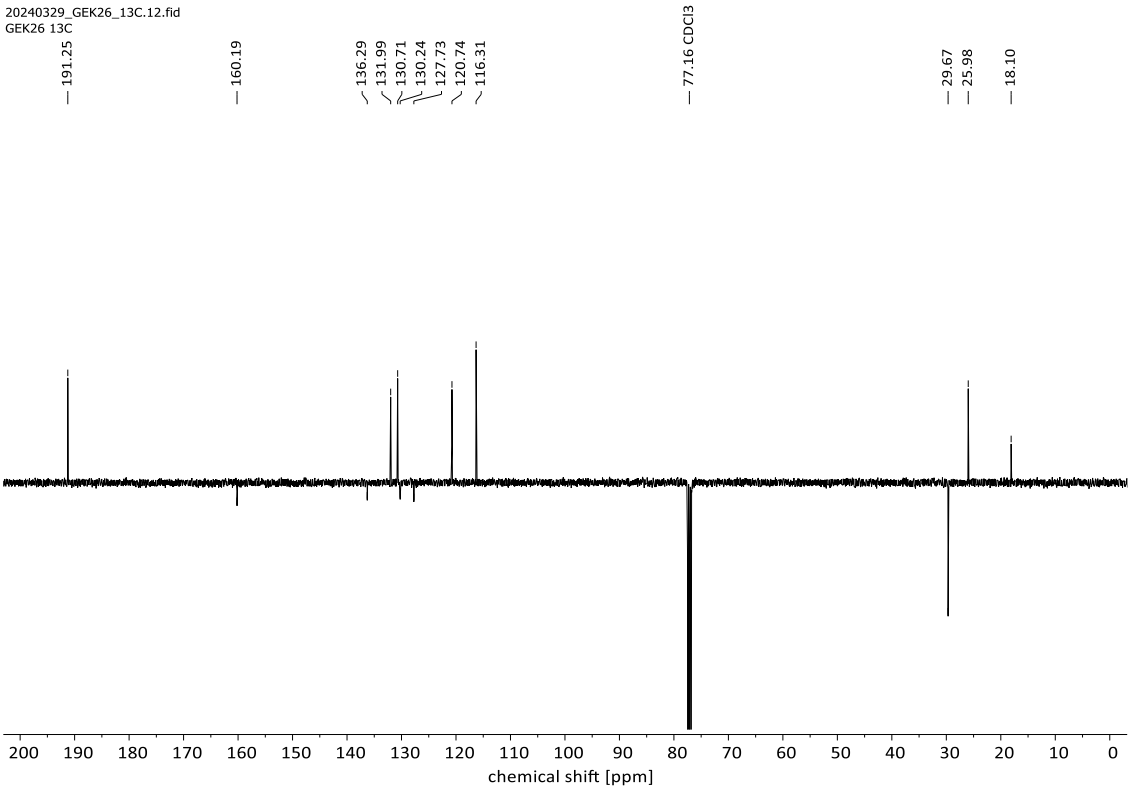

Figure 17: ^{13}C-NMR spectrum of aldehyde **36** (APT, 100 MHz, $CDCl_3$).

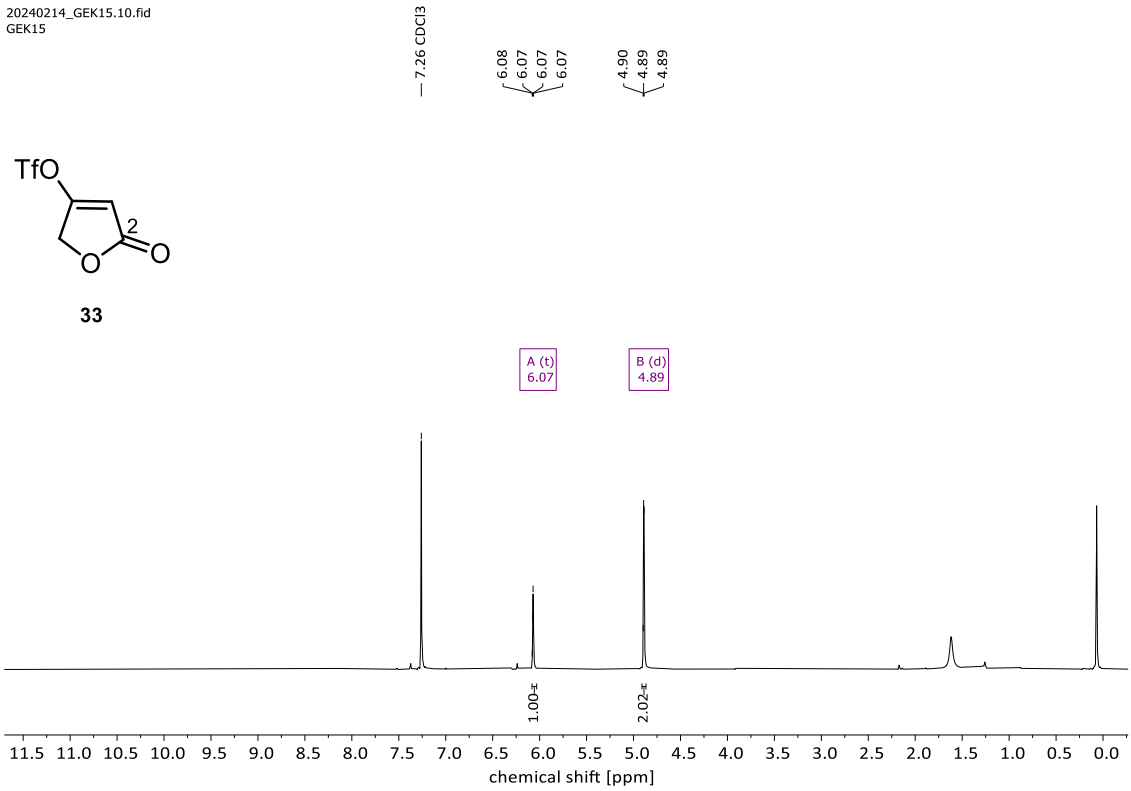

Figure 18: ^{1}H-NMR spectrum of triflate **33** (400 MHz, $CDCl_3$).

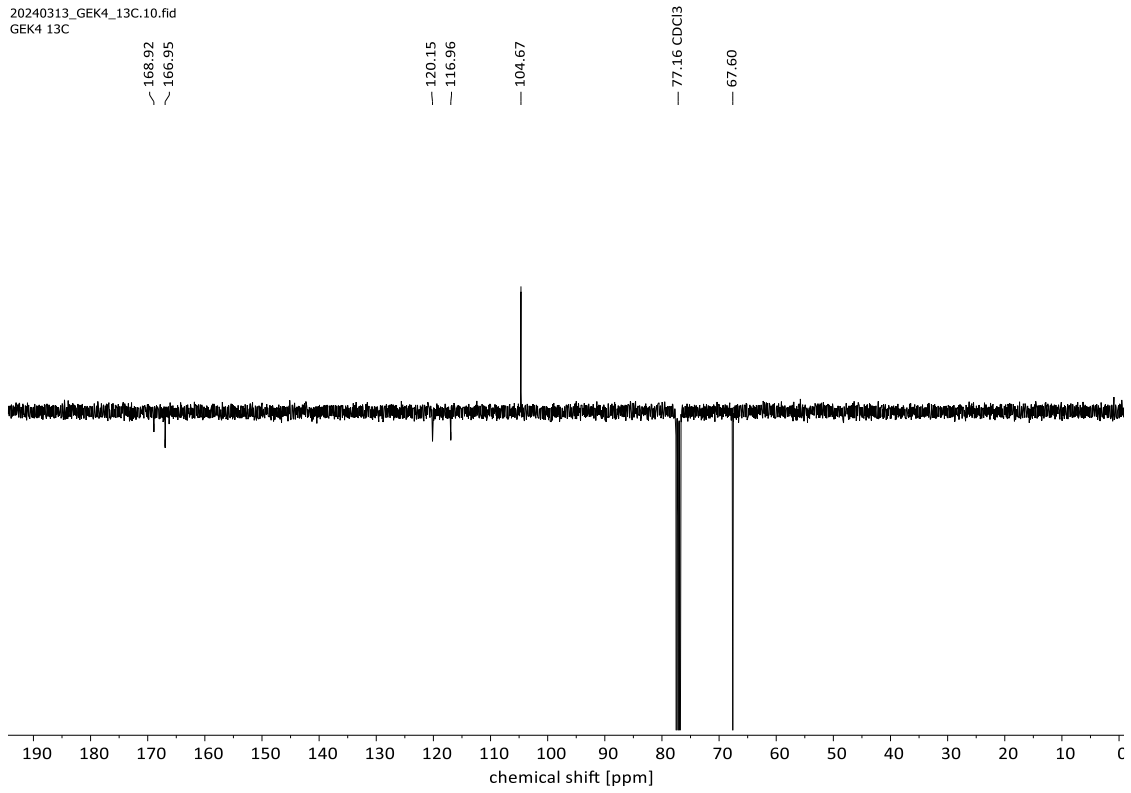

Figure 19: ^{13}C-NMR spectrum of triflate **33** (APT, 100 MHz, $CDCl_3$).

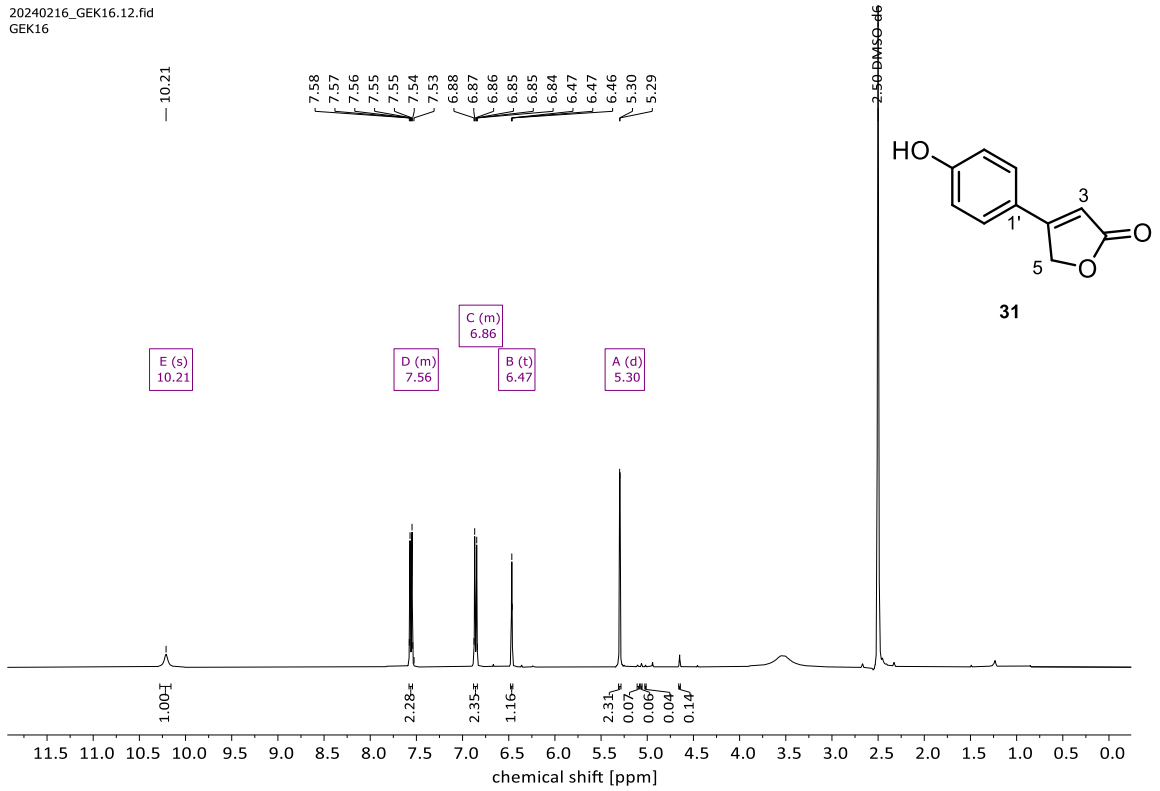

Figure 20: ^{1}H-NMR spectrum of furanone **31** (400 MHz, DMSO-d_6).

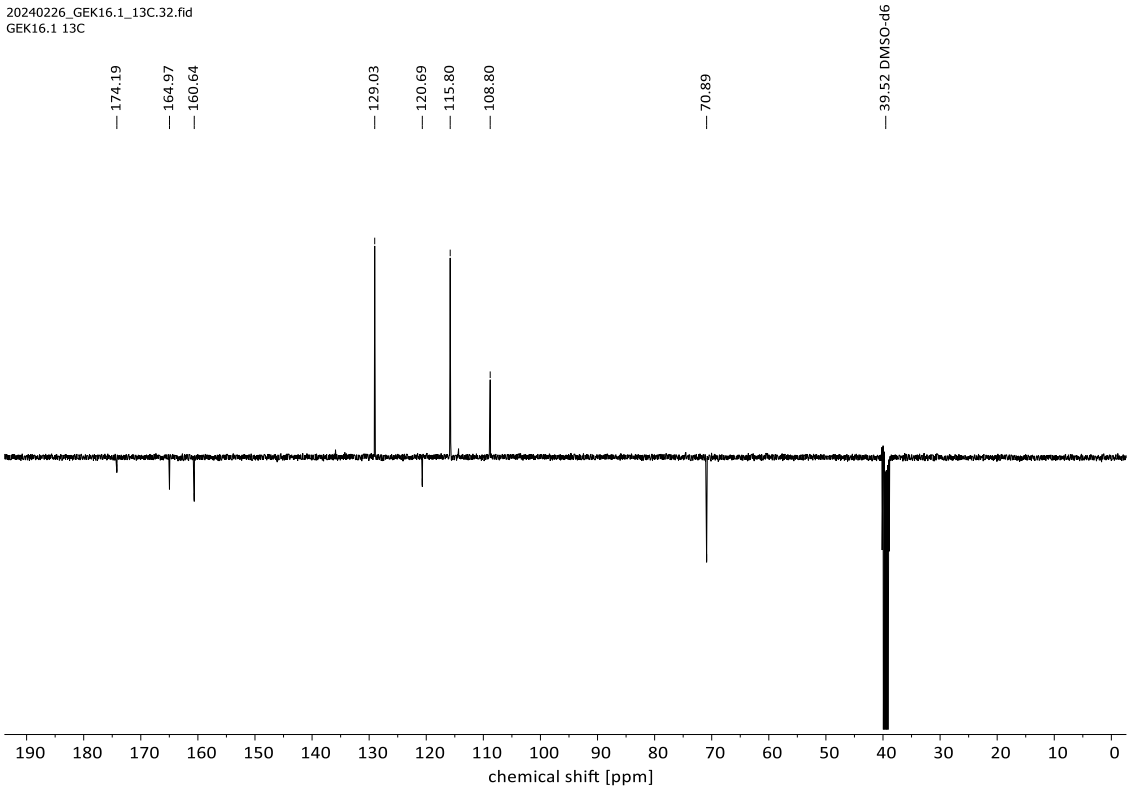

Figure 21: ^{13}C-NMR spectrum of furanone **31** (APT, 100 MHz, DMSO-d_6).

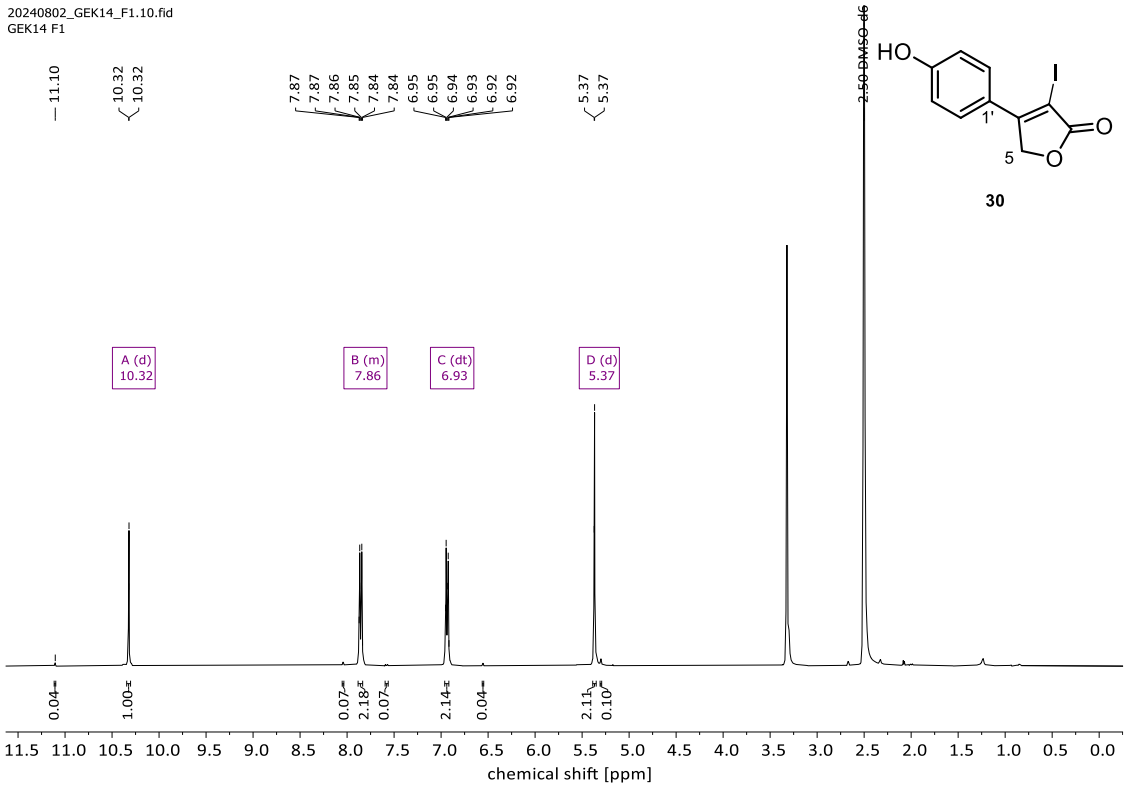

Figure 22: ^{1}H-NMR spectrum of furanone **30** (400 MHz in DMSO-d_6).

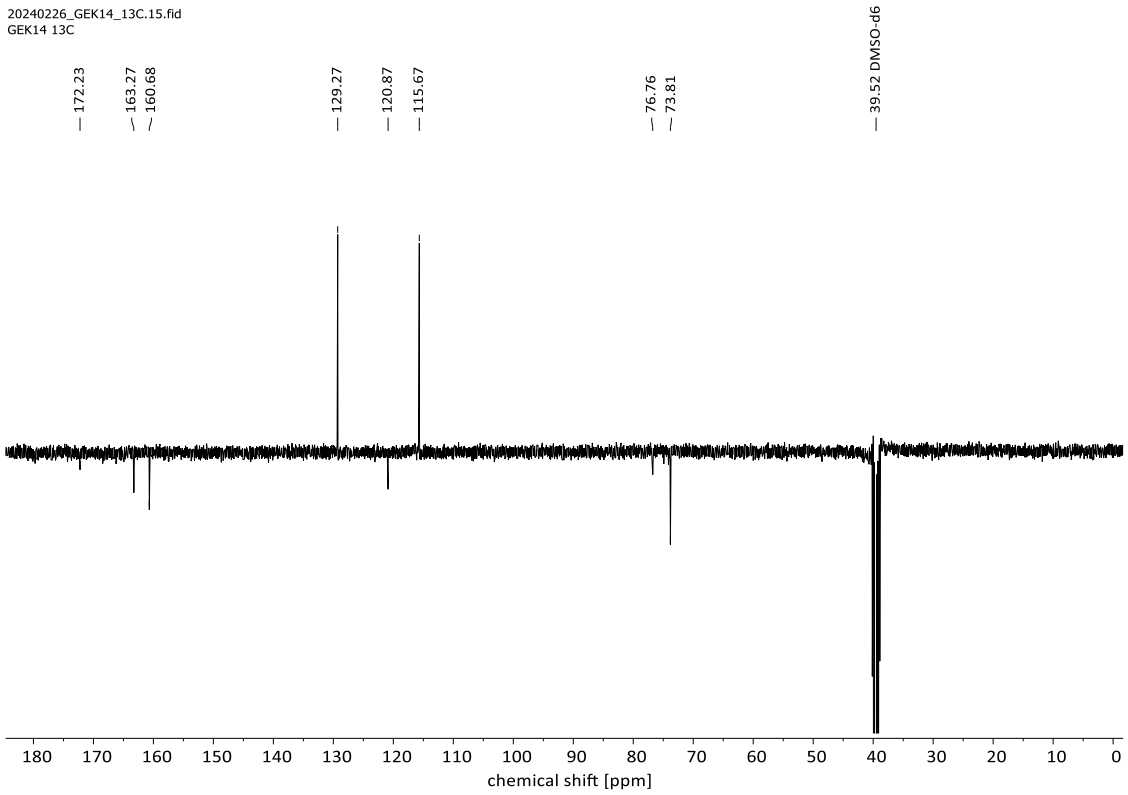

Figure 23: ^{13}C-NMR spectrum of furanone **30** (APT, 100 MHz in DMSO-d_6).

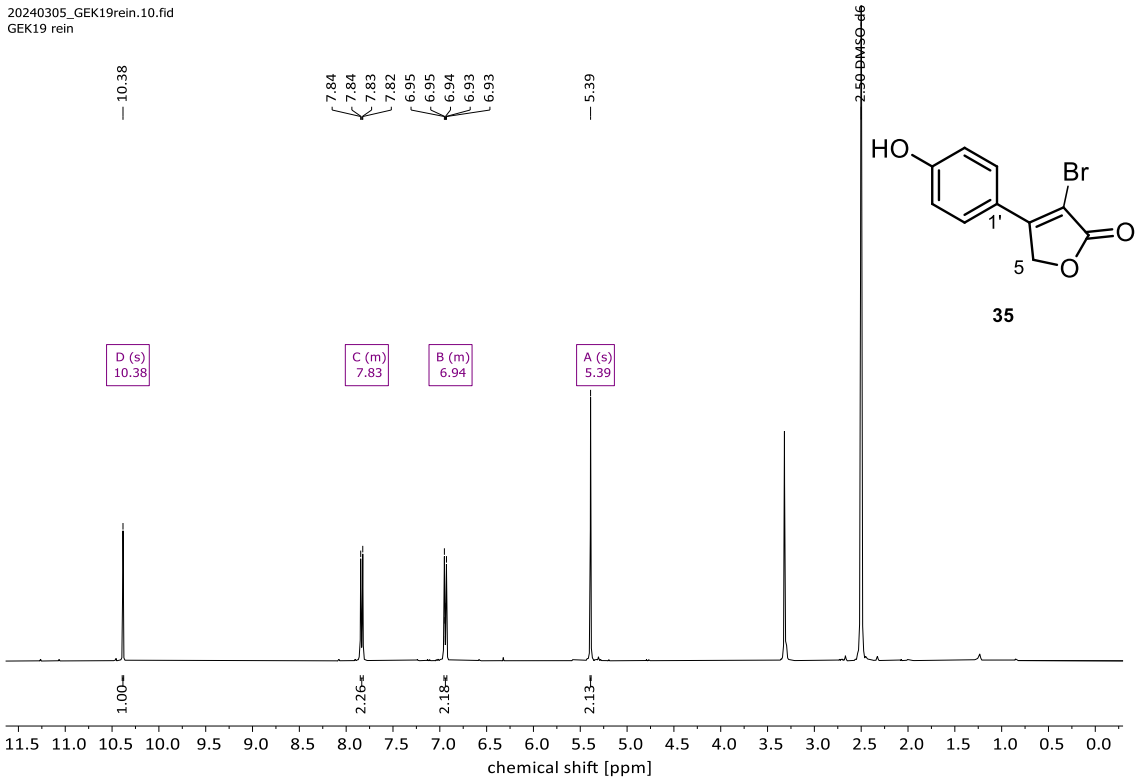

Figure 24: ^{1}H-NMR spectrum of furanone **35** (400 MHz, DMSO-d_6).

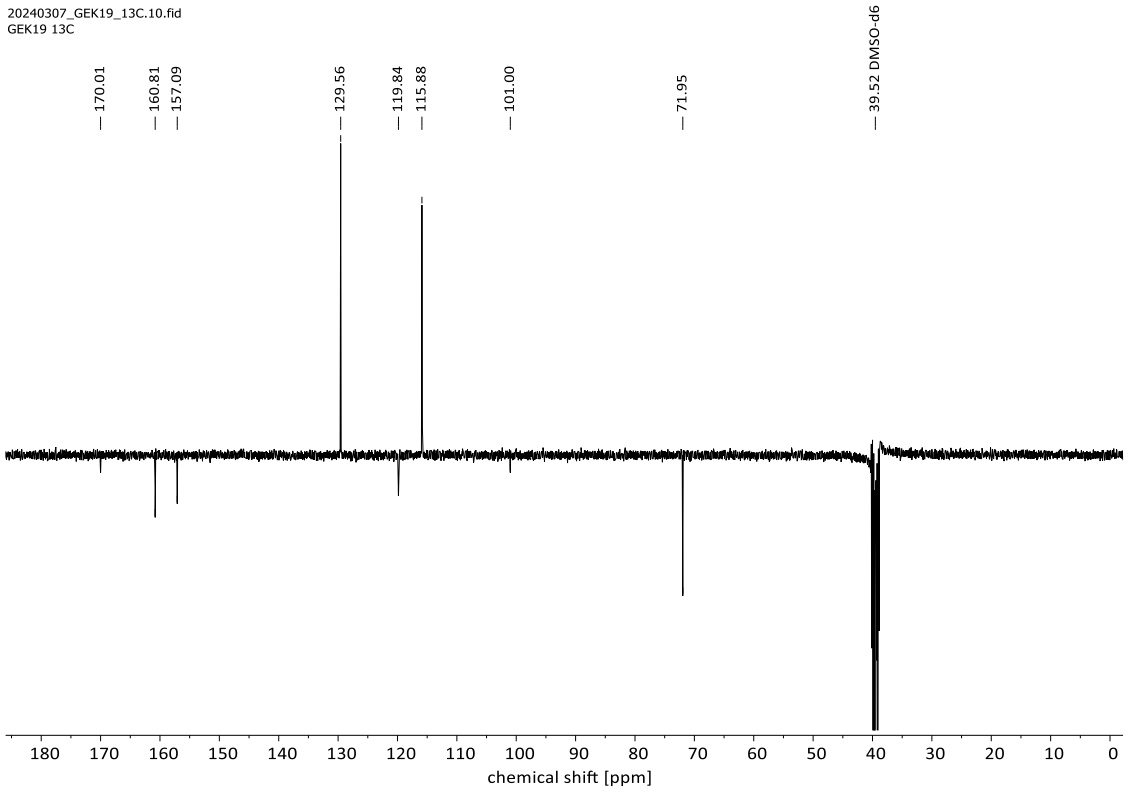

Figure 25: ^{13}C-NMR spectrum of furanone **35** (APT, 100 MHz, DMSO-d_6).

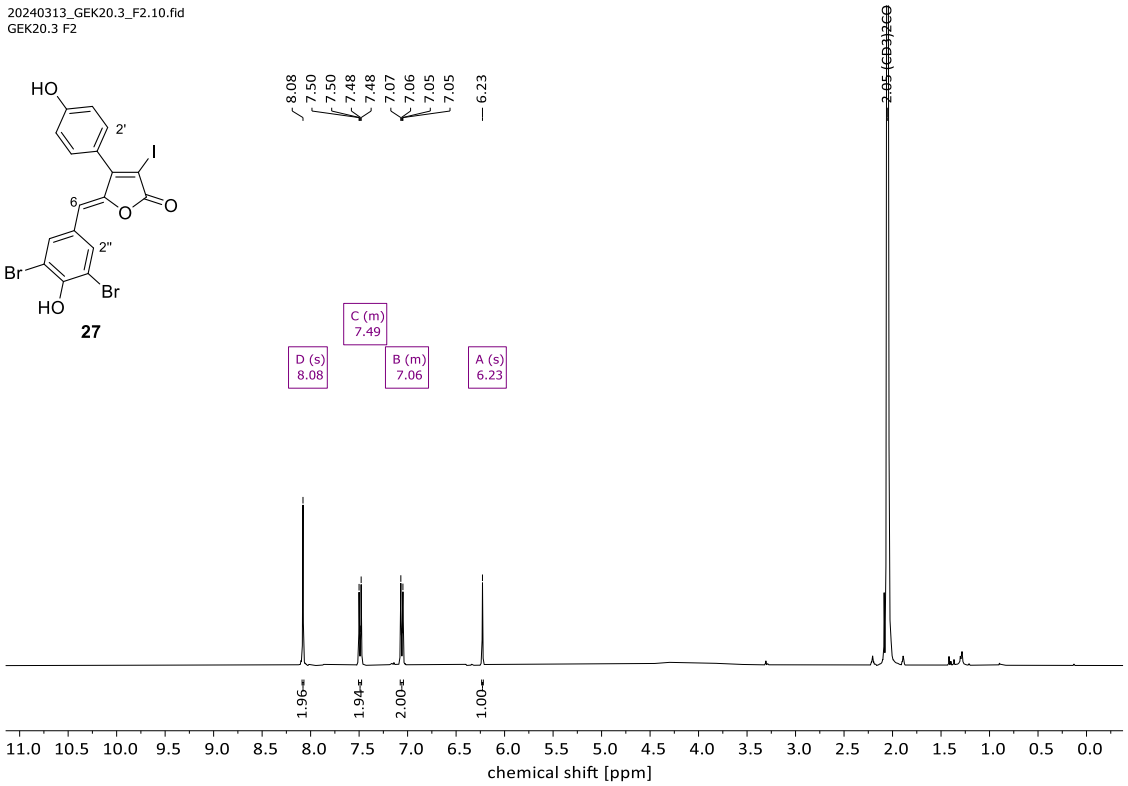

Figure 26: ^{1}H-NMR spectrum of rubrolide C derivative **27** (400 MHz, acetone-d_6).

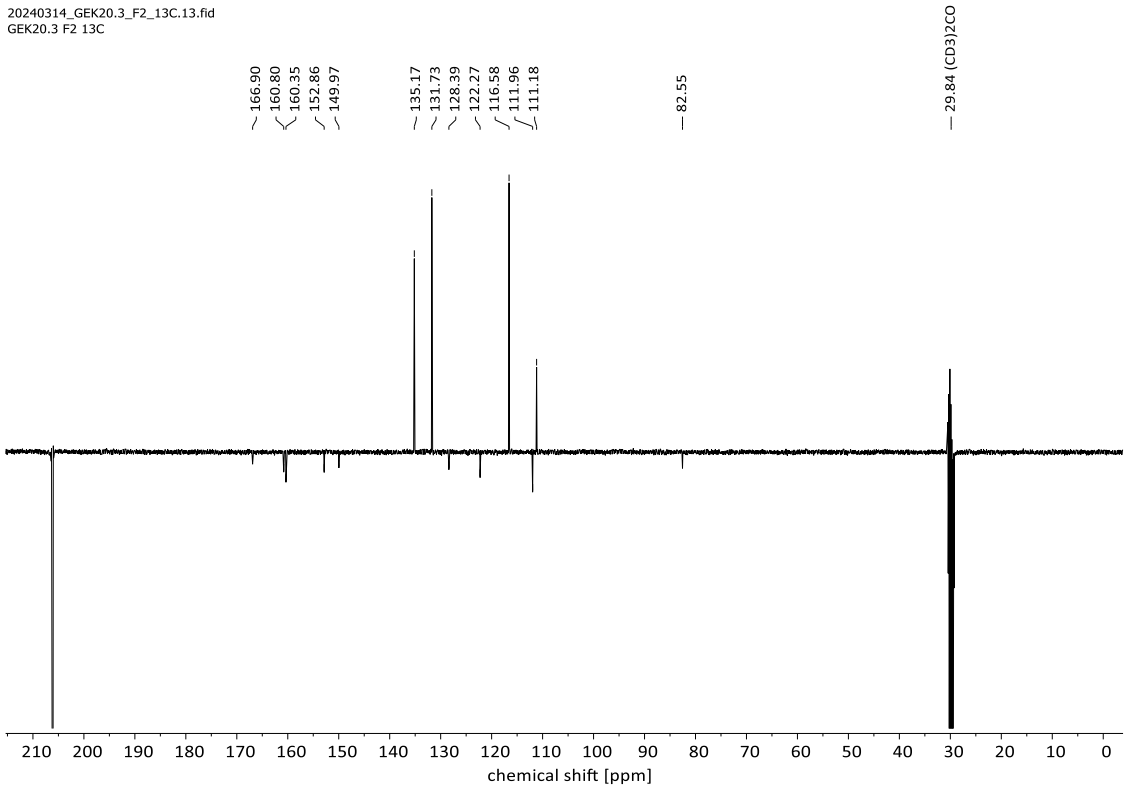

Figure 27: ^{13}C-NMR spectrum of rubrolide C derivative **27** (APT, 100 MHz, acetone-d_6).

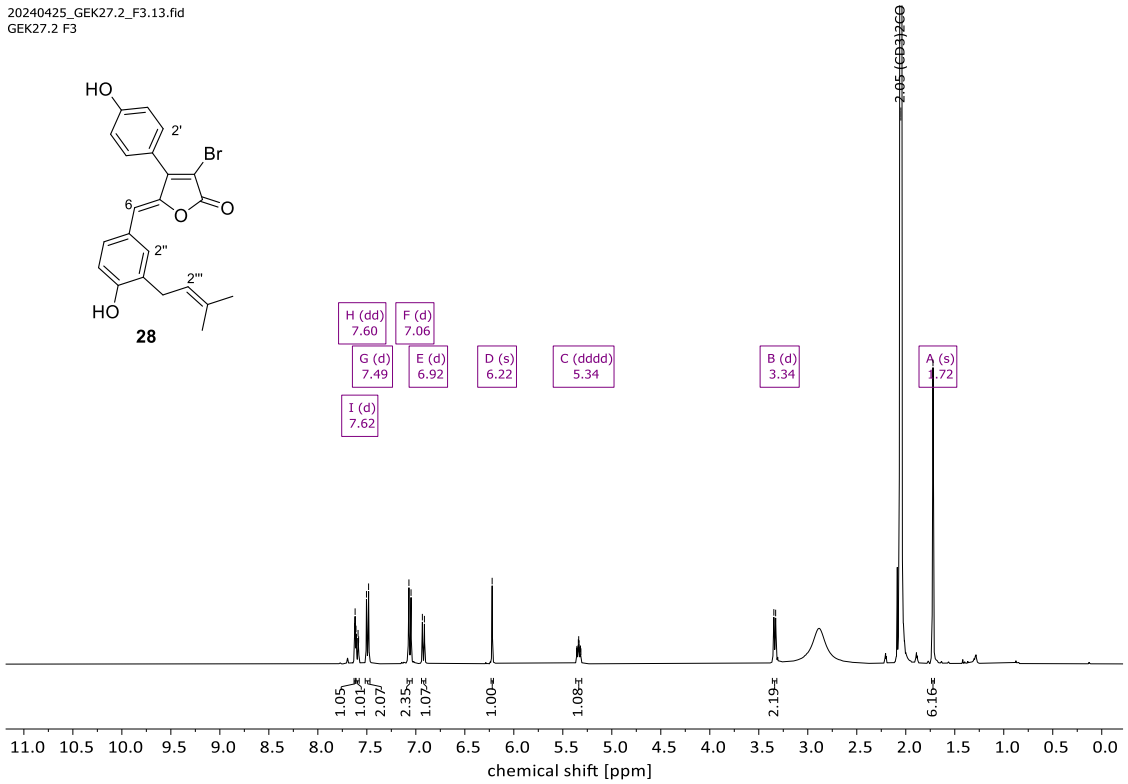

Figure 28: ^{1}H-NMR spectrum of rubrolide derivative R **28** (400 MHz, acetone-d_6).

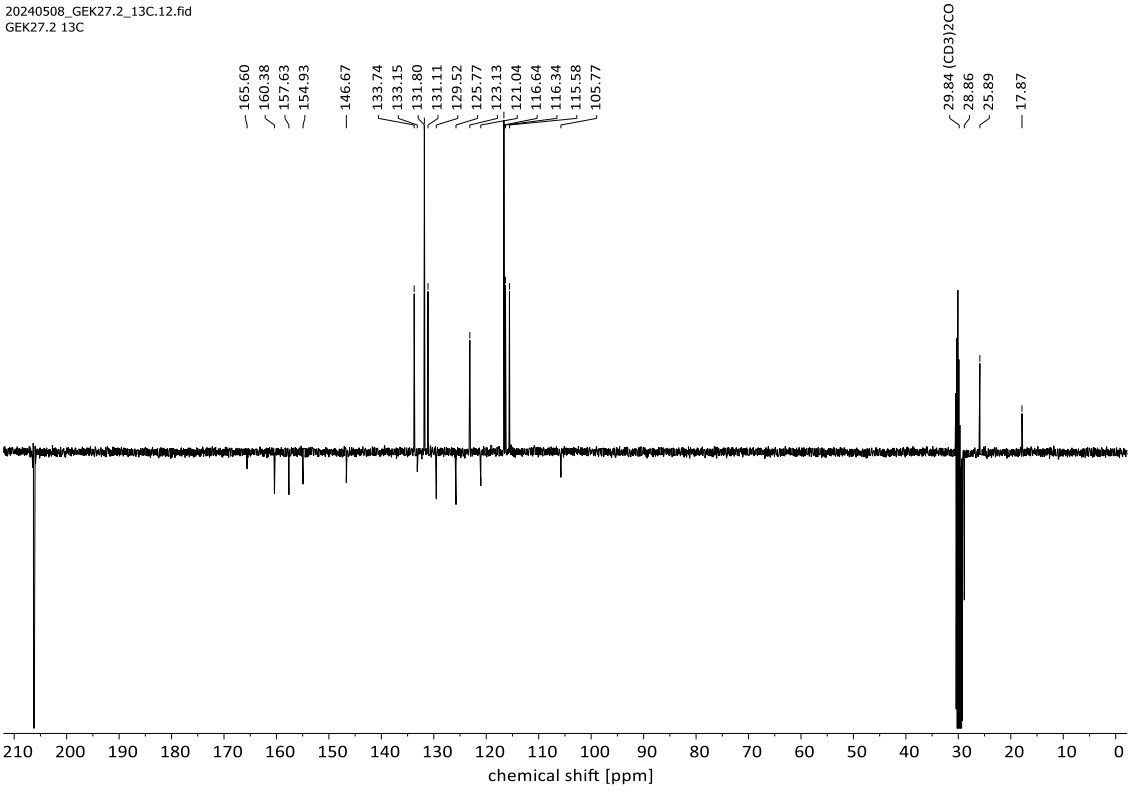

Figure 29: ^{13}C-NMR spectrum of rubrolide derivative R **28** (APT, 100 MHz, acetone-d_6).

6.2. HRMS Spectra

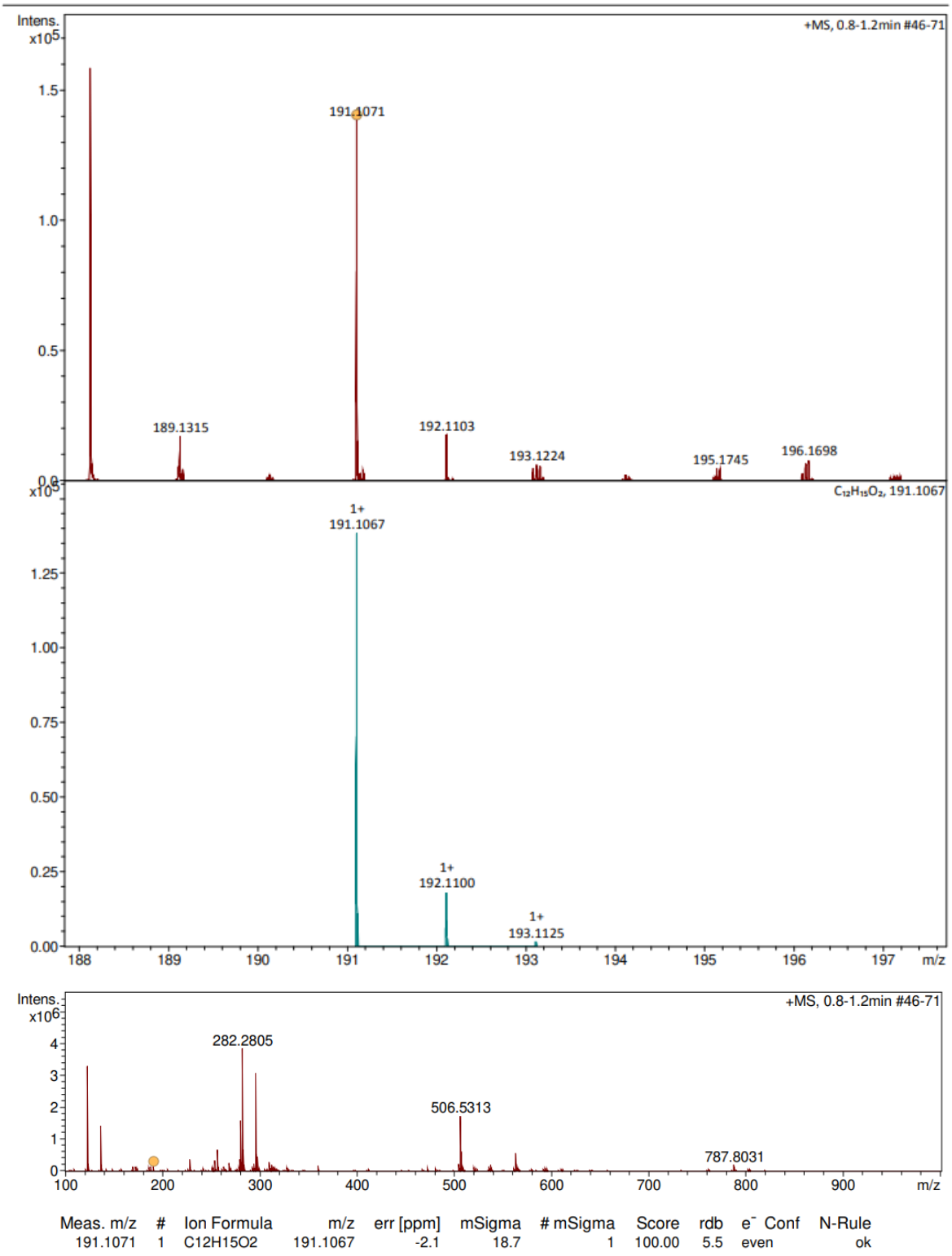

Figure 30: HRMS spectrum of 4-[(2-methylbut-3-en-2-yl)oxy]benzaldehyde **37**.

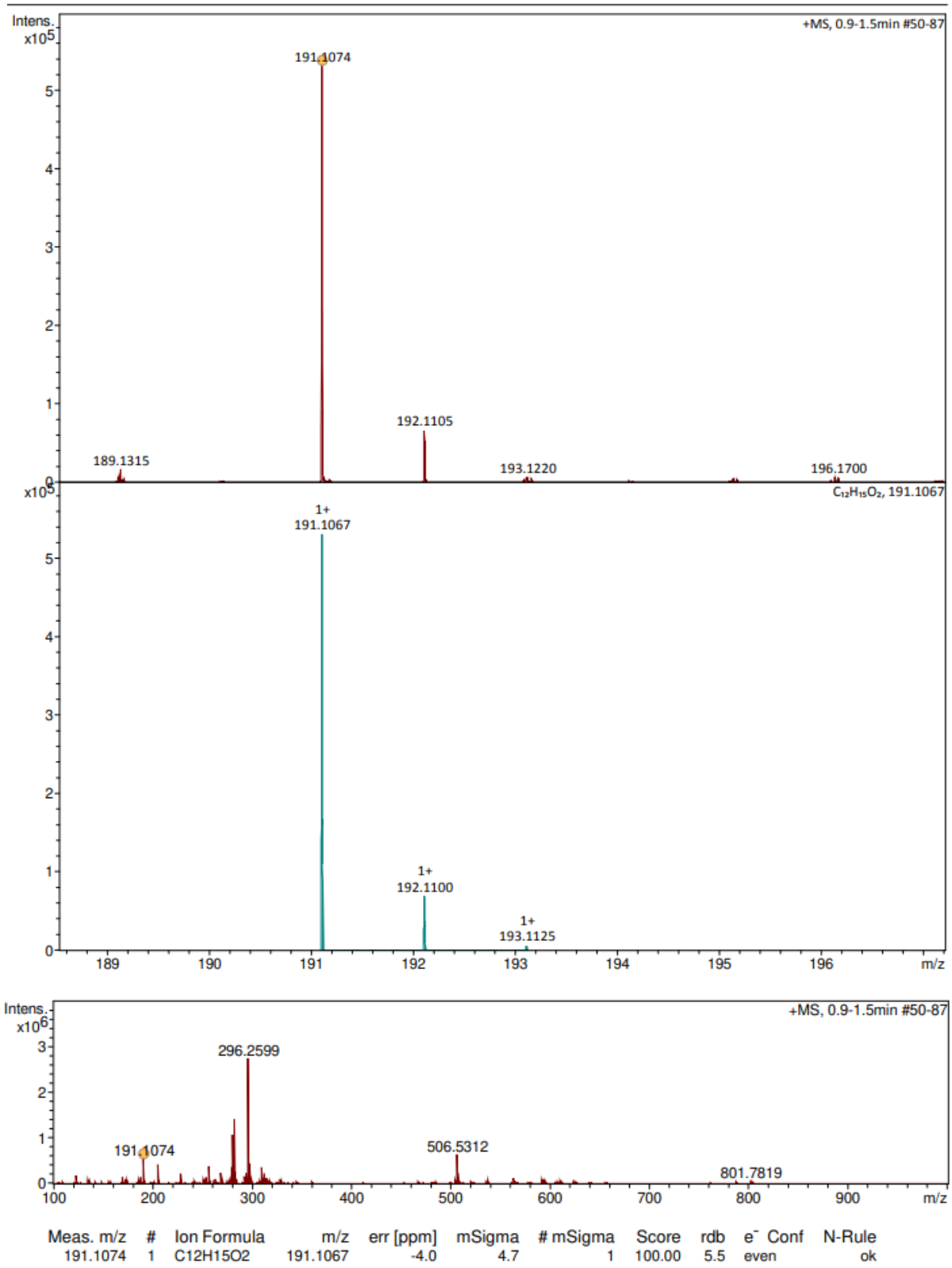

Figure 31: HRMS spectrum of 4-hydroxy-3-(3-methylbut-2-en-1-yl)benzaldehyde **36**.

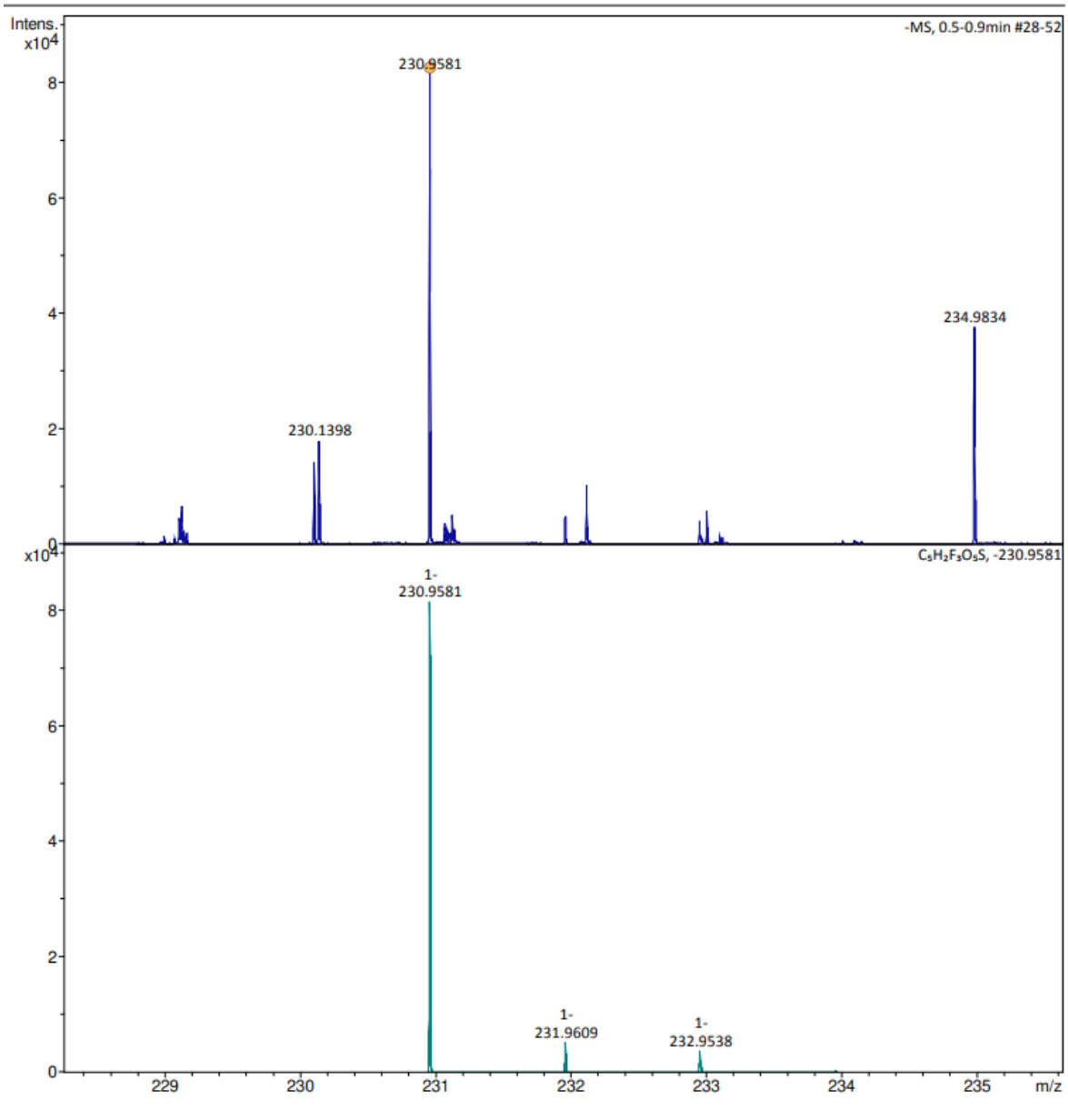

Meas. m/z	#	Ion Formula	m/z	err [ppm]	mSigma	# mSigma	Score	rdb	e⁻ Conf	N-Rule
230.9581	1	C5H2F3O5S	230.9581	-0.2	n.a.	1	82.18	3.5	even	ok
	2	C3H4F5O2S2	230.9578	-1.1	n.a.	2	100.00	-0.5	even	ok
	3	C6H6F3S3	230.9589	3.6	n.a.	3	94.41	2.5	even	ok
	4	C2H3F4O6S	230.9592	4.8	n.a.	4	48.54	-0.5	even	ok
	5	C6H3F4OS2	230.9567	-6.1	n.a.	5	53.92	3.5	even	ok

Figure 32: HRMS spectrum of 5-oxo-2,5-dihydrofuran-3-yl-trifluoromethanesulfonate **33**.

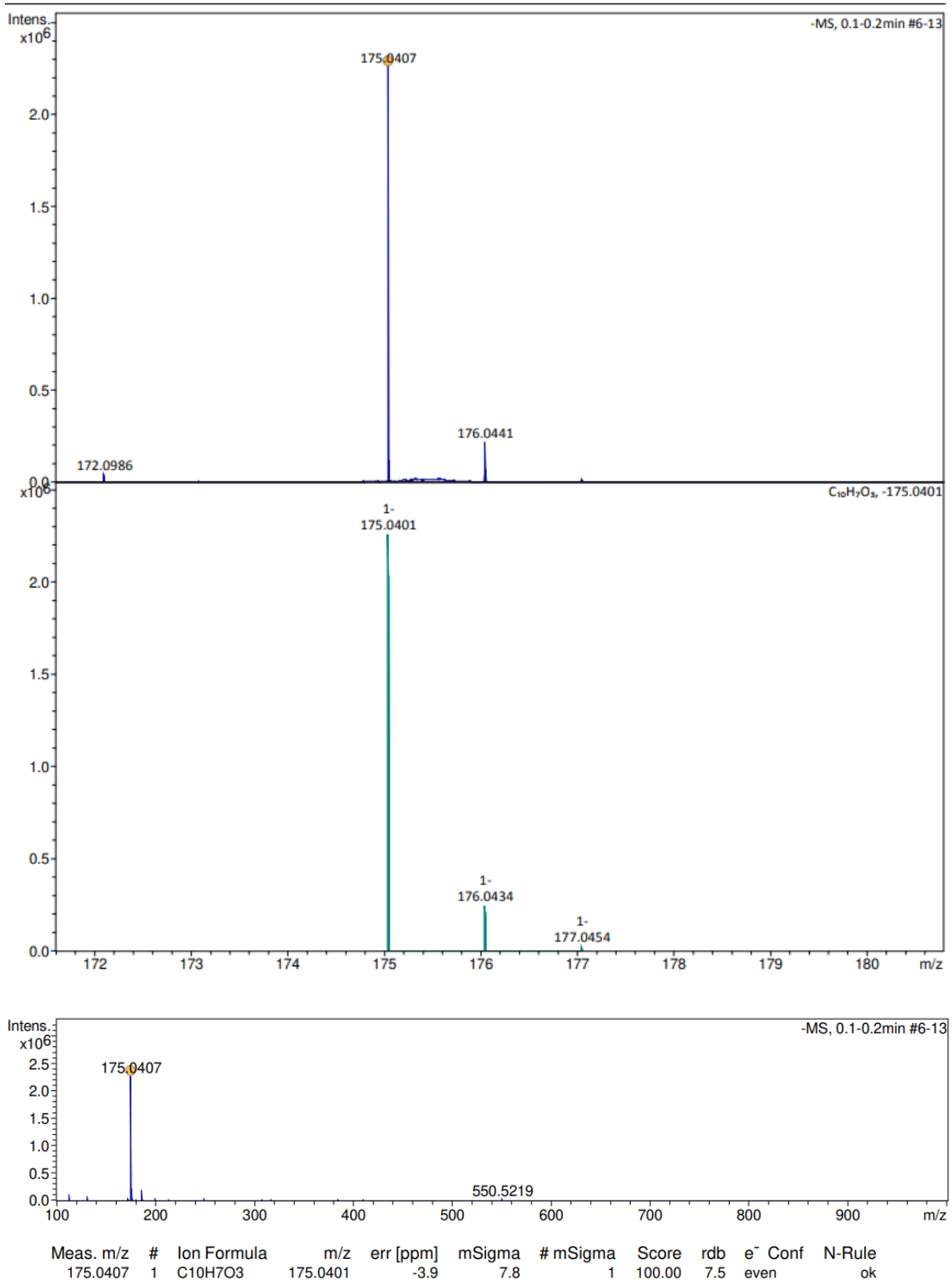

Figure 33: HRMS spectrum of 4-(4-hydroxyphenyl)furan-2(5H)-one **31**.

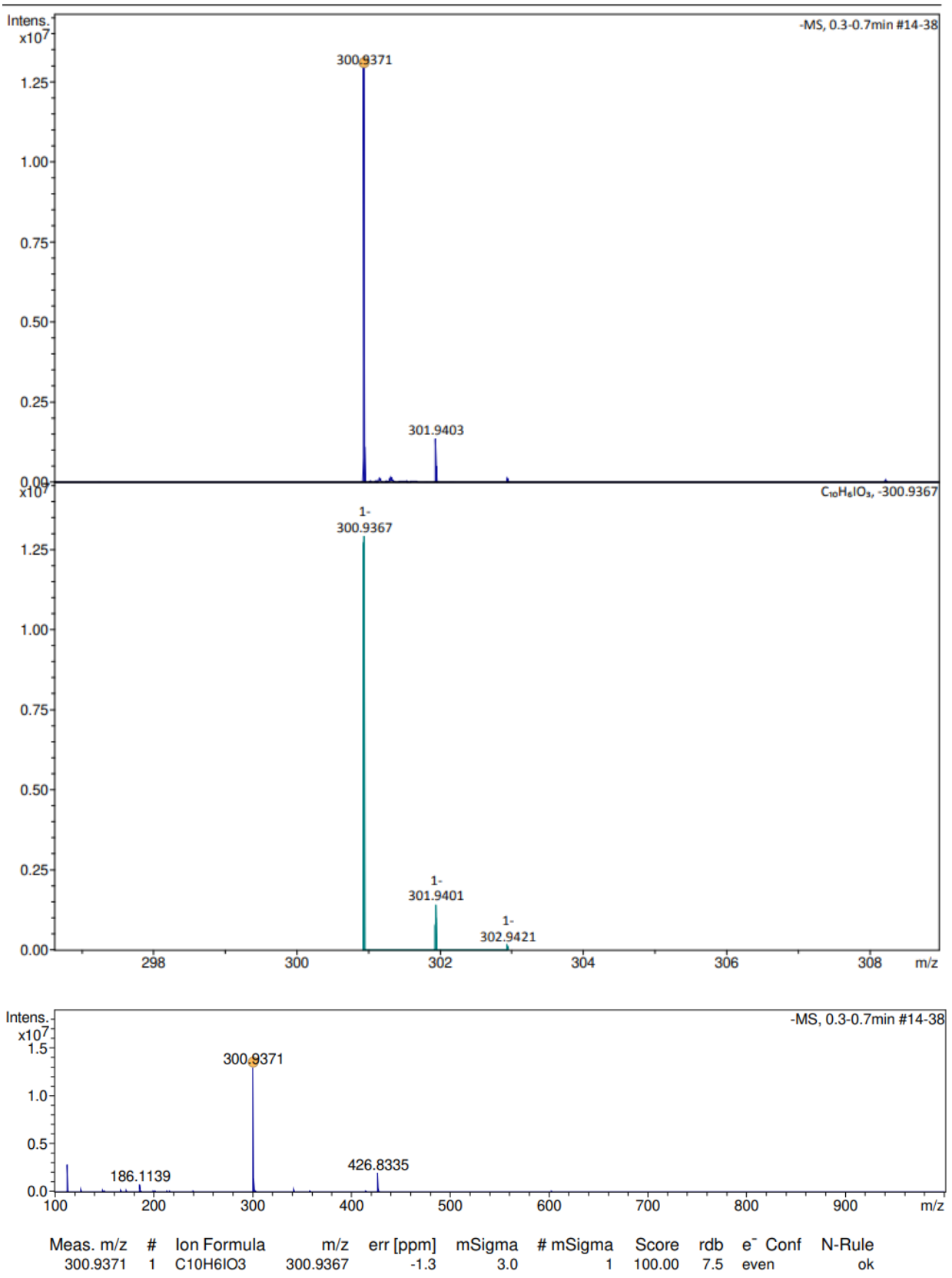

Figure 34: HRMS spectrum of 3-iodo-4-(4-hydroxyphenyl)furan-2(5H)-one **30.**

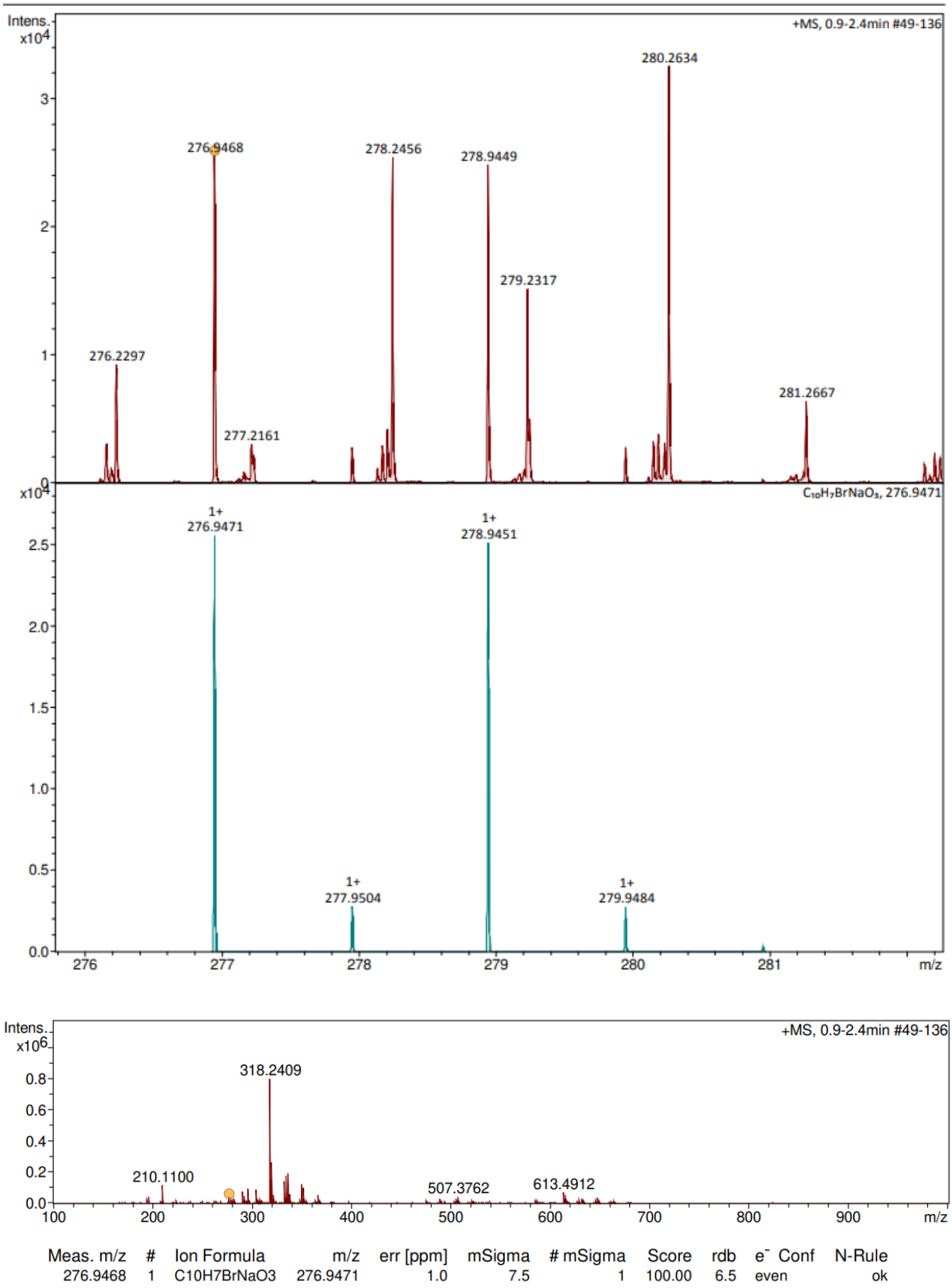

Meas. m/z	#	Ion Formula	m/z	err [ppm]	mSigma	# mSigma	Score	rdb	e⁻ Conf	N-Rule
276.9468	1	C10H7BrNaO3	276.9471	1.0	7.5	1	100.00	6.5	even	ok

Figure 35: HRMS spectrum of 3-bromo-4-(4-hydroxyphenyl)furan-2(5H)-one **35**.

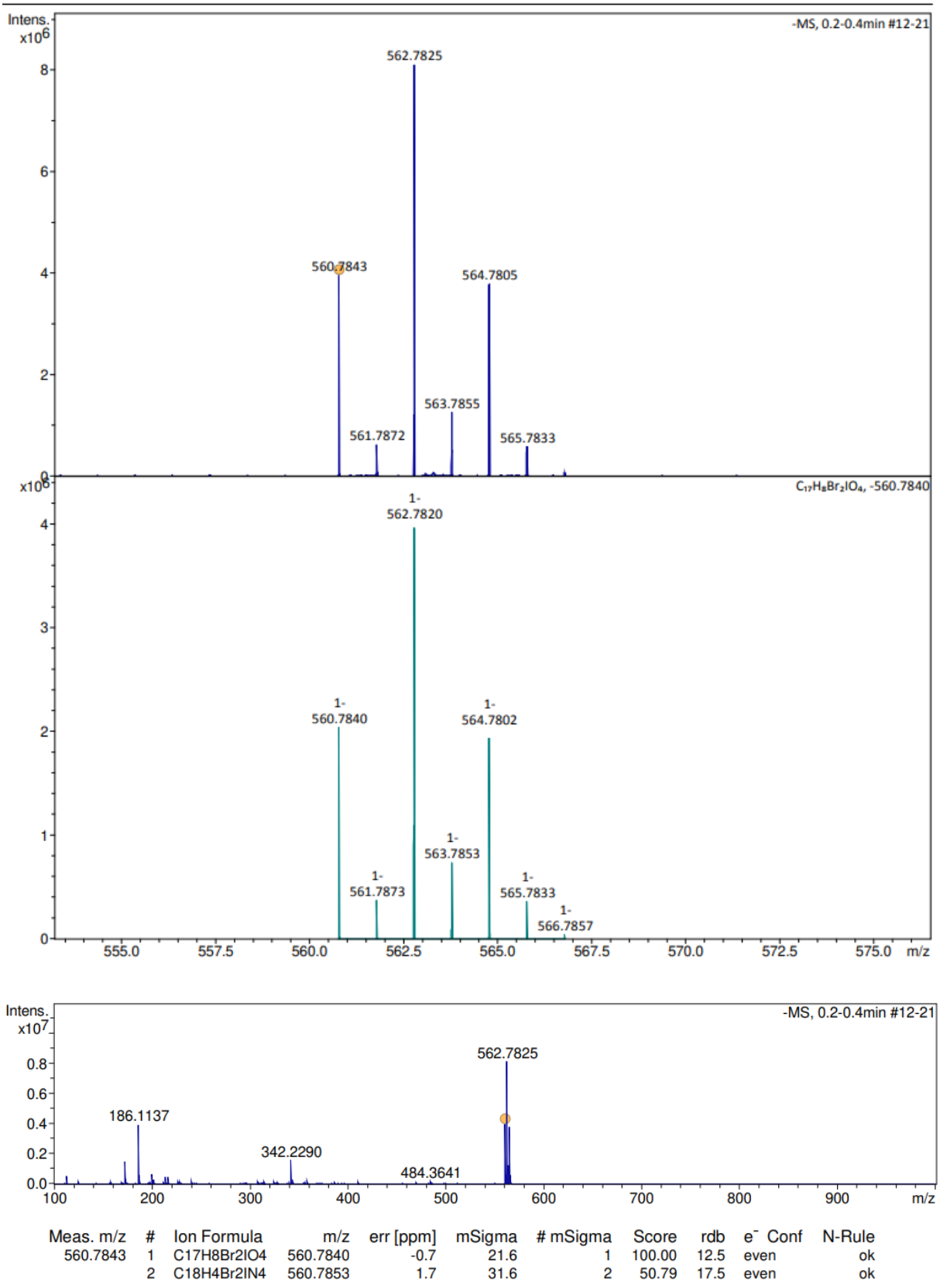

Meas. m/z	#	Ion Formula	m/z	err [ppm]	mSigma	# mSigma	Score	rdb	e⁻ Conf	N-Rule
560.7843	1	C17H8Br2IO4	560.7840	-0.7	21.6	1	100.00	12.5	even	ok
	2	C18H4Br2IN4	560.7853	1.7	31.6	2	50.79	17.5	even	ok

Figure 36: HRMS spectrum of 3-iodo-rubrolide C **27**.

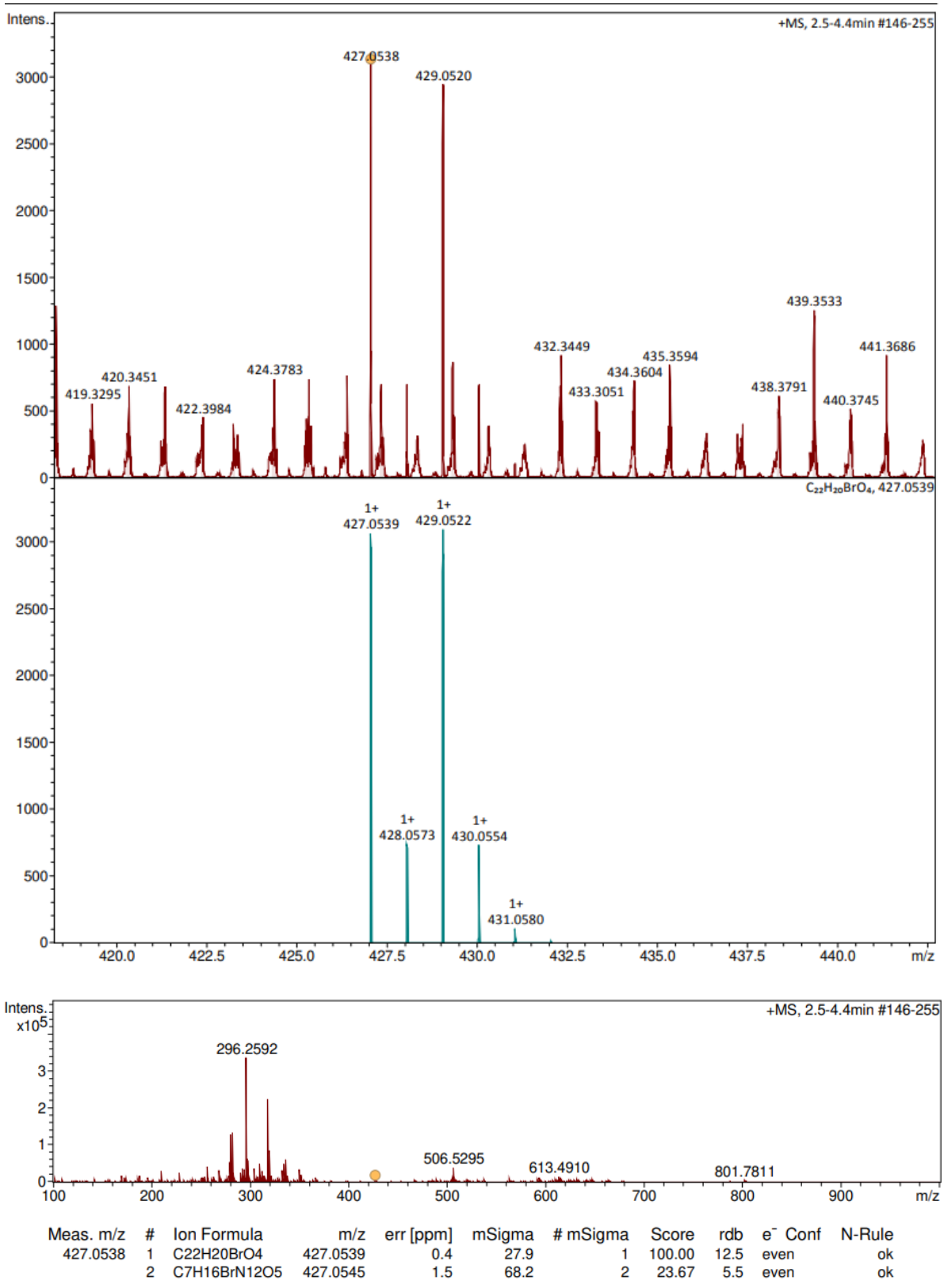

Meas. m/z	#	Ion Formula	m/z	err [ppm]	mSigma	# mSigma	Score	rdb	e⁻ Conf	N-Rule
427.0538	1	C22H20BrO4	427.0539	0.4	27.9	1	100.00	12.5	even	ok
	2	C7H16BrN12O5	427.0545	1.5	68.2	2	23.67	5.5	even	ok

Figure 37: HRMS spectrum of 3-bromo-rubrolide R **28**.

6.3. IR Spectra

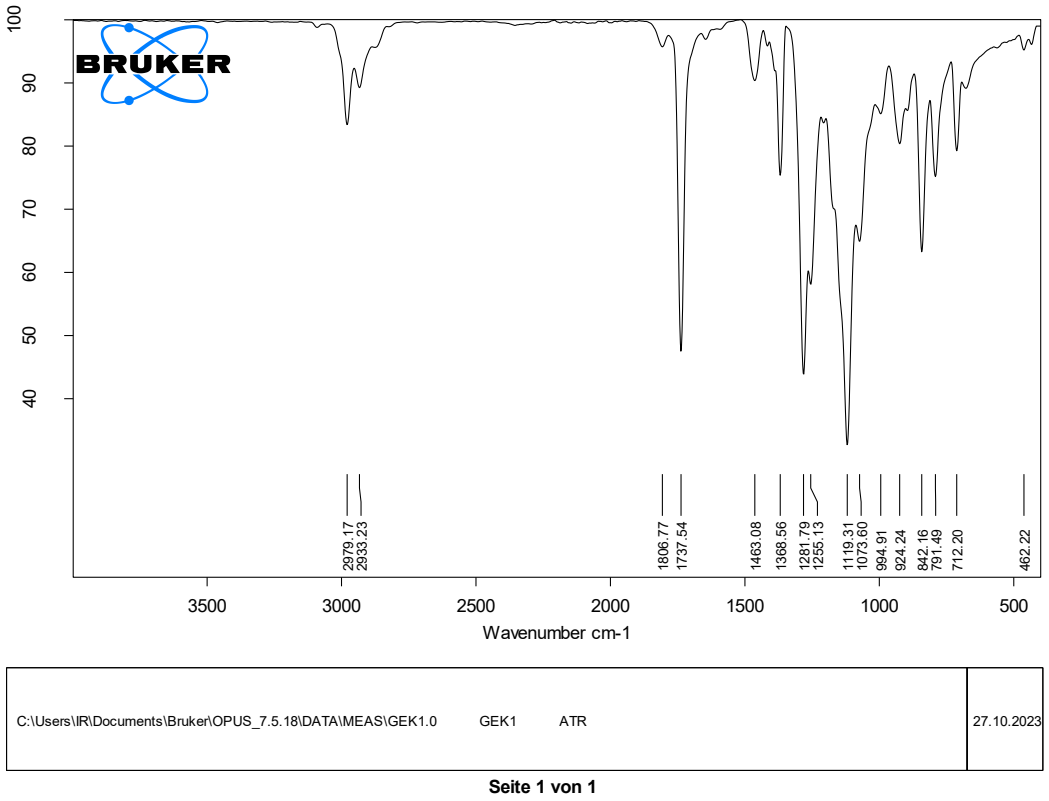

Figure 38: IR spectrum of tert-butyl-1,1-dimethylallyl carbonate **39**.

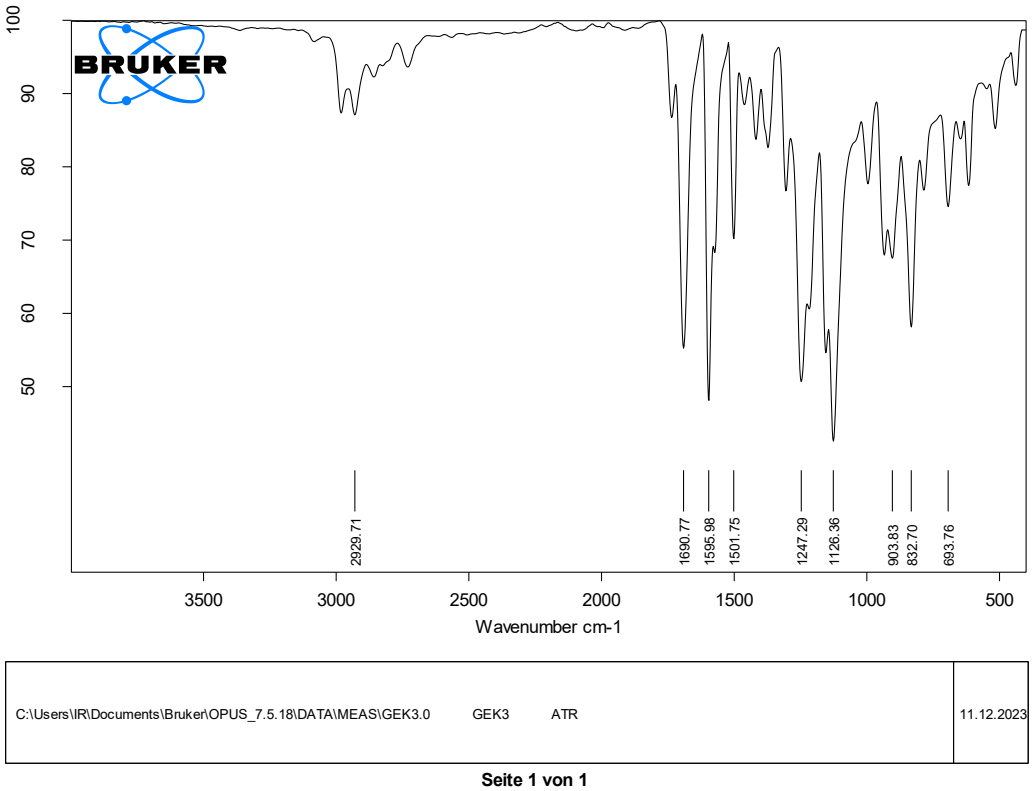

Figure 39: IR spectrum of 4-[(2-methylbut-3-en-2-yl)oxy]benzaldehyde **37**.

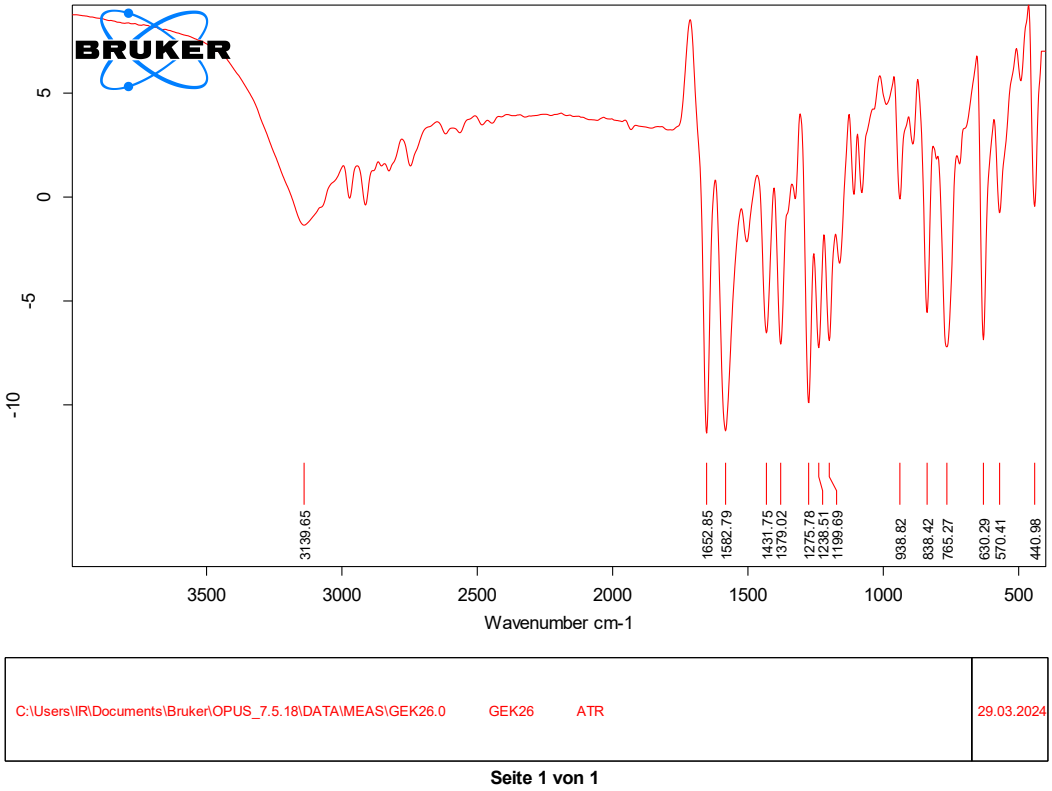

Figure 40: IR spectrum of 4-hydroxy-3-(3-methylbut-2-en-1-yl)benzaldehyde **36**.

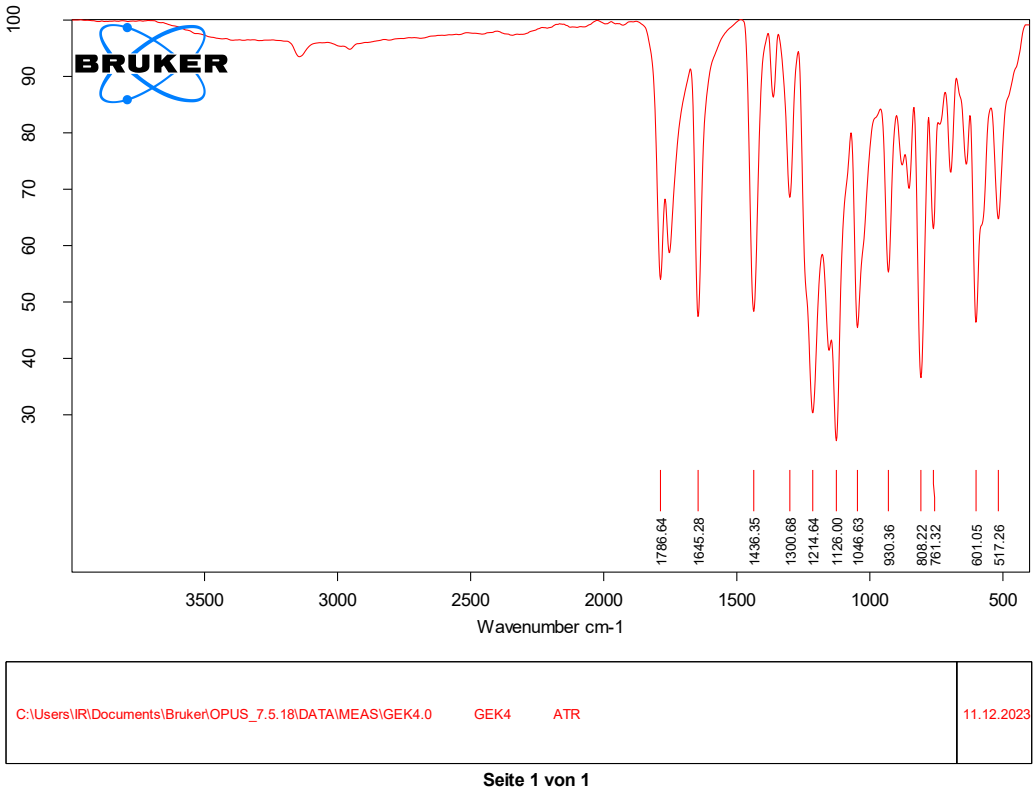

Figure 41: IR spectrum of 5-oxo-2,5-dihydrofuran-3-yl-trifluoromethanesulfonate **33**.

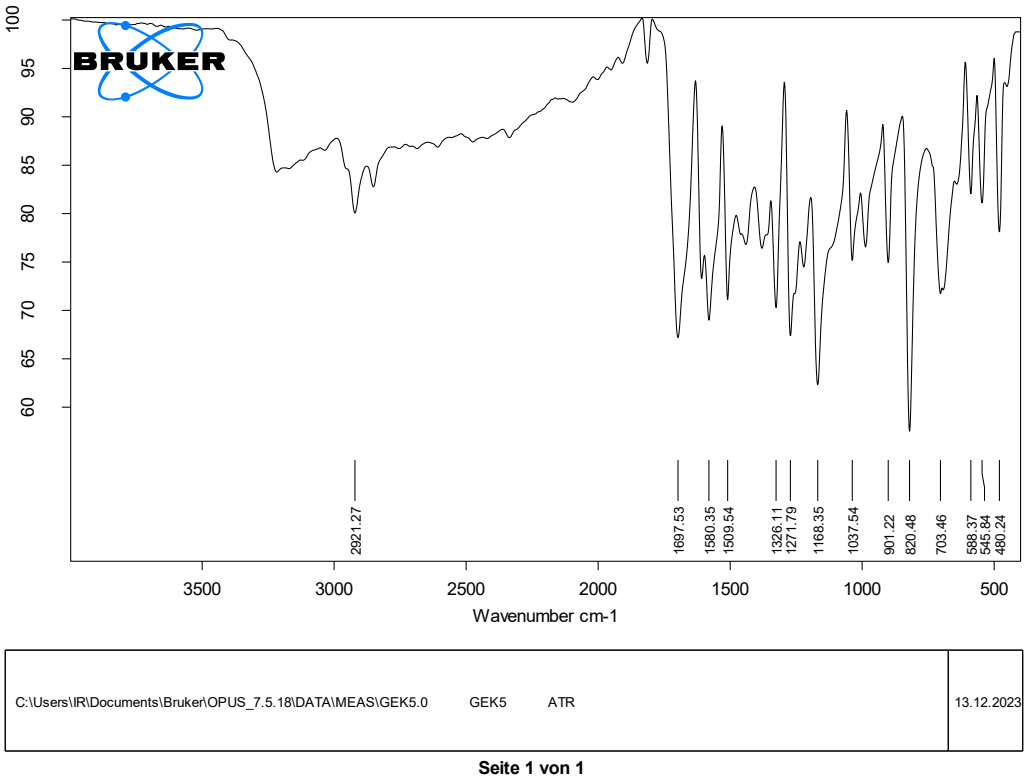

Figure 42: IR spectrum of 4-(4-hydroxyphenyl)furan-2(5H)-one **31**.

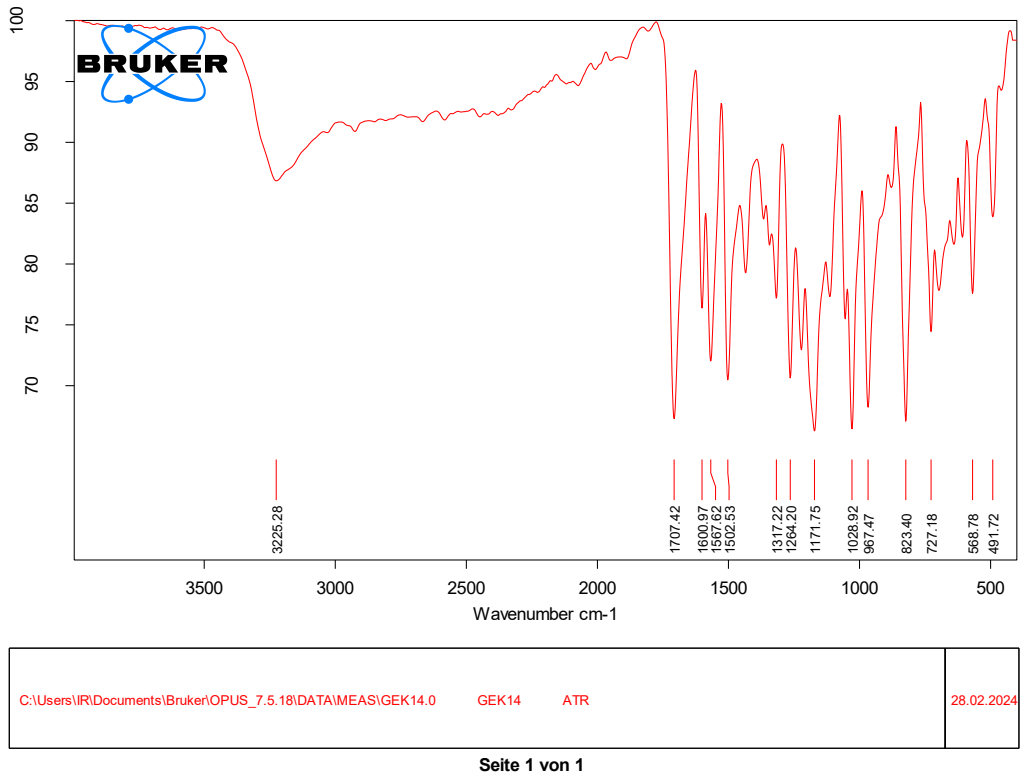

Figure 43: IR spectrum of 3-iodo-4-(4-hydroxyphenyl)furan-2(5H)-one **30.**

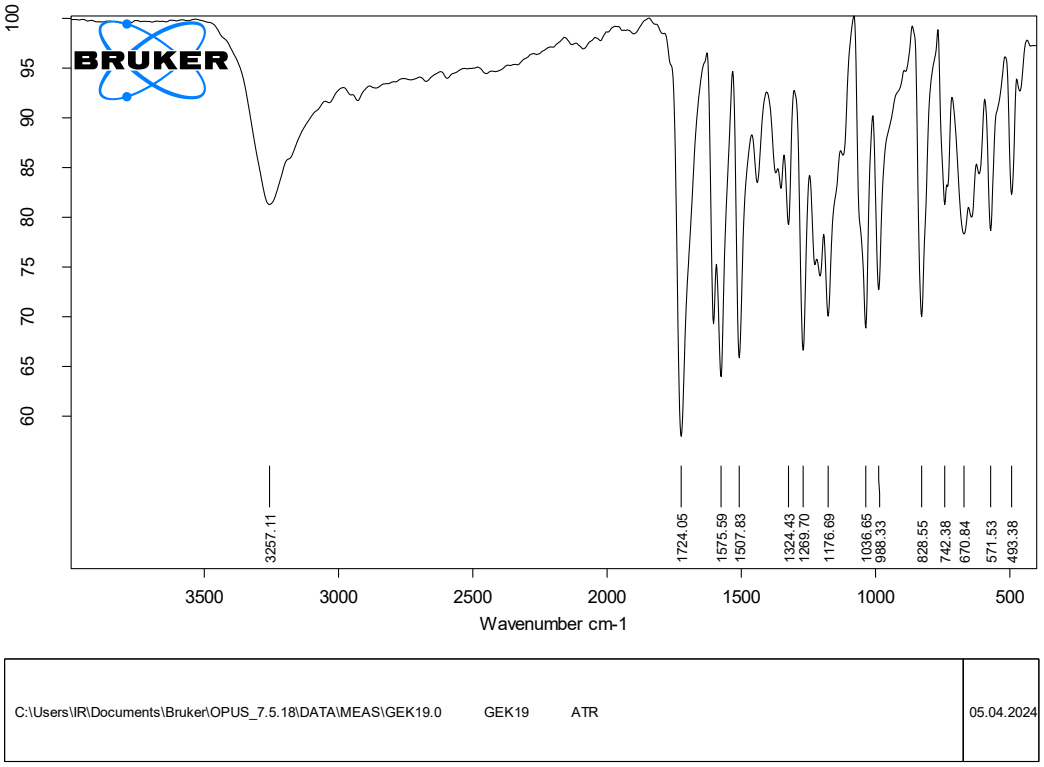

Figure 44: IR spectrum of 3-bromo-4-(4-hydroxyphenyl)furan-2(5H)-one **35**.

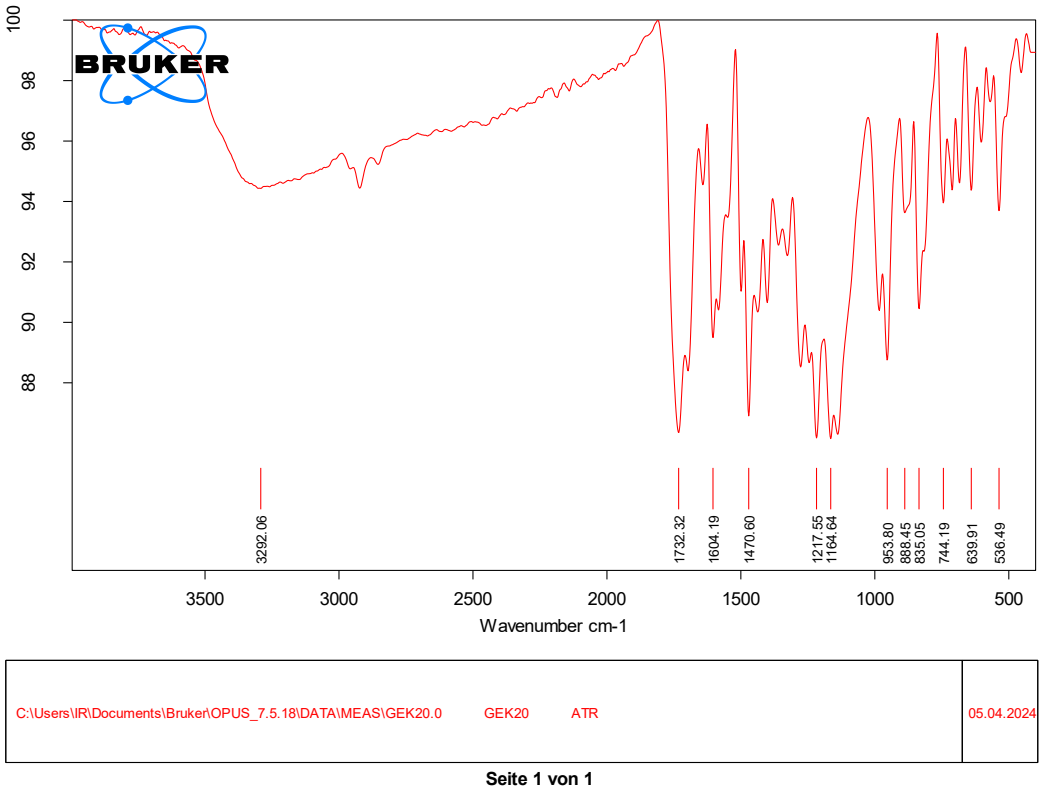

Figure 45: IR spectrum of 3-iodo-rubrolide C **27**.

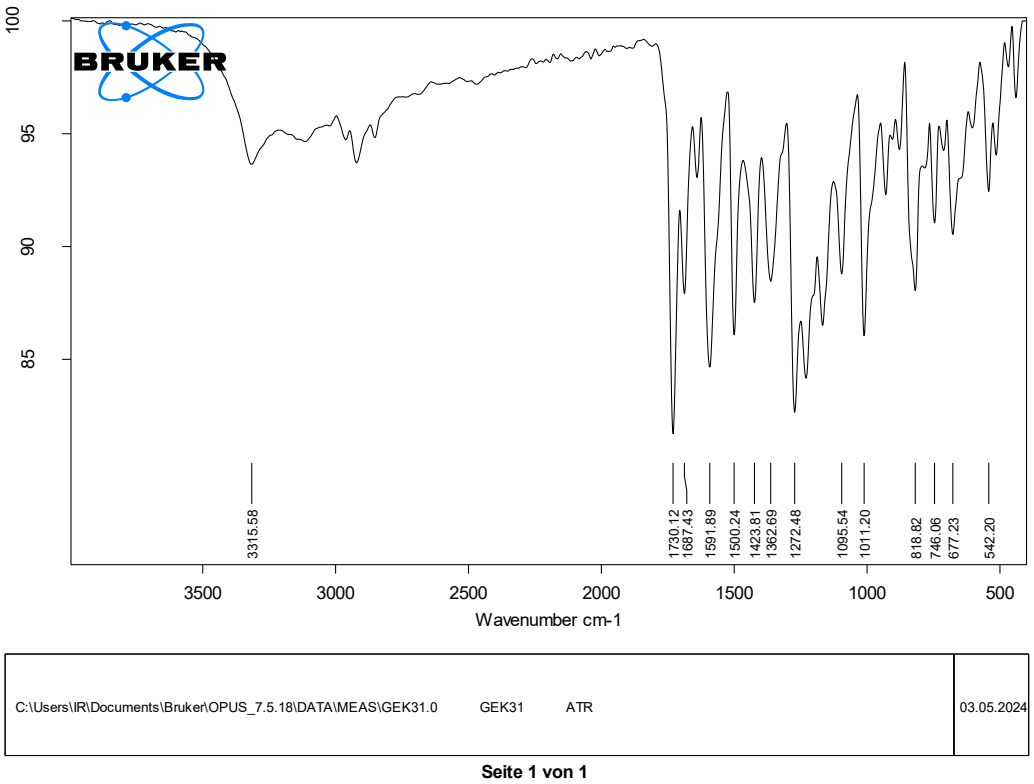

Figure 46: IR spectrum of 3-bromo-rubrolide R **28**.

7. References

[1] McArthur, D. B. Emerging Infectious Diseases. *Nursing Clinics of North America*, **2019**, *54* (2), 297–311. https://doi.org/https://doi.org/10.1016/j.cnur.2019.02.006.

[2] Jones, K. E.; Patel, N. G.; Levy, M. A.; Storeygard, A.; Balk, D.; Gittleman, J. L.; Daszak, P. Global Trends in Emerging Infectious Diseases. *Nature*, **2008**, *451* (7181), 990–993. https://doi.org/10.1038/nature06536.

[3] The Lancet Microbe. Climate Change: Fires, Floods, and Infectious Diseases. *The Lancet Microbe*. Elsevier Ltd September 1, 2021, p e415. https://doi.org/10.1016/S2666-5247(21)00220-2.

[4] Caminade, C.; McIntyre, K. M.; Jones, A. E. Impact of Recent and Future Climate Change on Vector-Borne Diseases. *Annals of the New York Academy of Sciences*. Blackwell Publishing Inc. January 1, 2019, pp 157–173. https://doi.org/10.1111/nyas.13950.

[5] Moreira, T. A.; Lafleur-Lambert, R.; Barbosa, L. C. A.; Boukouvalas, J. Concise, Stereocontrolled and Modular Syntheses of the Anti-Influenza Rubrolides R and S. *Tetrahedron Lett*, **2019**, *60* (50). https://doi.org/10.1016/j.tetlet.2019.151307.

[6] Miao, S.; Andersen, R. J. Rubrolides A-H, Metabolites of the Colonial Tunicate Ritterella Rubra. *J Org Chem*, **1991**, *56* (22), 6275–6280. https://doi.org/10.1021/jo00022a012.

[7] Abbott, D. P.; Trason, W. B. *RITTERELLA RUBRA AND DISTAPLIA SMITHI: TWO NEW COLONIAL ASCIDIANS FROM THE WEST COAST OF NORTH AMERICA*.

[8] Chen, L.; Hu, J. S.; Xu, J. L.; Shao, C. L.; Wang, G. Y. Biological and Chemical Diversity of Ascidian-Associated Microorganisms. *Marine Drugs*. MDPI AG October 1, 2018. https://doi.org/10.3390/md16100362.

[9] Lass-Flörl, C.; Dietl, A. M.; Kontoyiannis, D. P.; Brock, M. Aspergillus Terreus Species Complex. *Clinical Microbiology Reviews*. American Society for Microbiology December 1, 2021. https://doi.org/10.1128/CMR.00311-20.

[10] Zhu, T.; Chen, Z.; Liu, P.; Wang, Y.; Xin, Z.; Zhu, W. New Rubrolides from the Marine-Derived Fungus Aspergillus Terreus OUCMDZ-1925. *Journal of Antibiotics*, **2014**, *67* (4), 315–318. https://doi.org/10.1038/ja.2013.135.

[11] de Vries, J.; Assmann, M.; Janneschütz, J.; Krauß, J.; Gudzuhn, M.; Stanelle-Bertram, S.; Gabriel, G.; Streit, W. R.; Schützenmeister, N. Synthesis of Natural Rubrolides B, I, K, L, M, O and Analogues. *European J Org Chem*, **2021**, *2021* (29), 4195–4200. https://doi.org/10.1002/ejoc.202100526.

[12] Karak, M.; Acosta, J. A. M.; Barbosa, L. C. A.; Boukouvalas, J. Late-Stage Bromination Enables the Synthesis of Rubrolides B, I, K, and O. *European J Org Chem*, **2016**, *2016* (22), 3780–3787. https://doi.org/10.1002/ejoc.201600473.

[13] Gong, M.; Cai, J.; Lu, X.; Zhou, X.; Li, J.; Wu, Q.; Wu, J. Total Synthesis and Herbicidal Activity of Natural Rubrolides C, E and F. *Nat Prod Res*, **2024**.

[14] Miranda, A. C. M.; Barbosa, L. C. A.; Masood, M. A.; Varejão, J. O. S.; Sordi, M.; Benfatti, C. A. M.; Pimenta, A. L. Inhibitory Effect on Biofilm Formation of Pathogenic Bacteria Induced by Rubrolide Lactam Analogues. *ACS Omega*, **2018**, *3* (12), 18475–18480. https://doi.org/10.1021/acsomega.8b02334.

[15] Smitha, D.; Kumar, M. M. K.; Ramana, H.; Rao, D. V. Rubrolide R: A New Furanone Metabolite from the Ascidian *Synoicum* of the Indian Ocean. *Nat Prod Res*, **2014**, *28* (1), 12–17. https://doi.org/10.1080/14786419.2013.827194.

[16] Zhu, T.; Chen, Z.; Liu, P.; Wang, Y.; Xin, Z.; Zhu, W. New Rubrolides from the Marine-Derived Fungus Aspergillus Terreus OUCMDZ-1925. *Journal of Antibiotics*, **2014**, *67* (4), 315–318. https://doi.org/10.1038/ja.2013.135.

[17] Schacht, M.; Boehlich, G. J.; de Vries, J.; Bertram, S.; Gabriel, G.; Zimmermann, P.; Heisig, P.; Schützenmeister, N. Protecting-Group-Free Total Syntheses of Rubrolide R and S. *European J Org Chem*, **2017**, *2017* (13), 1745–1748. https://doi.org/10.1002/ejoc.201700158.
[18] Schacht, M. Synthesis of Natural Abundant Butenolides and Analogues, Hamburg, 2019.
[19] Damodar, K.; Kim, J.-K.; Jun, J.-G. Efficient, Collective Synthesis and Nitric Oxide Inhibitory Activity of Rubrolides E, F, R, S and Their Derivatives. *Tetrahedron Lett*, **2017**, *58* (1), 50–53. https://doi.org/10.1016/j.tetlet.2016.11.096.
[20] The Nobel Prize in Chemistry 2010. NobelPrize.org.
[21] Miyaura, N.; Yamada, K.; Suzuki, A. A NEW STEREOSPECIFIC CROSS-COUPLING BY THE PALLADIUM-CATALYZED REACTION OF 1-ALKENYLBORANES WITH 1-ALKENYL OR l-ALKYNYL HALIDES. *Tetrahedron Letters*. OPergamon Press Ltd 1979, pp 3437–3440.
[22] Boukouvalas, J.; Lachance, N.; Ouellet, M.; Trudeau, M. Facile Access to 4-Aryl-2(5H)-Furanones by Suzuki Cross Coupling: Efficient Synthesis of Rubrolides C and E. *Tetrahedron Lett*, **1998**, *39* (42), 7665–7668. https://doi.org/10.1016/S0040-4039(98)01715-8.
[23] Han, J.; Liu, Y.; Guo, R. Facile Synthesis of Highly Stable Gold Nanoparticles and Their Unexpected Excellent Catalytic Activity for Suzuki−Miyaura Cross-Coupling Reaction in Water. *J Am Chem Soc*, **2009**, *131* (6), 2060–2061. https://doi.org/10.1021/ja808935n.
[24] Saito, S.; Oh-tani, S.; Miyaura, N. Synthesis of Biaryls via a Nickel(0)-Catalyzed Cross-Coupling Reaction of Chloroarenes with Arylboronic Acids. *J Org Chem*, **1997**, *62* (23), 8024–8030. https://doi.org/10.1021/jo9707848.
[25] Thomas, A. A.; Denmark, S. E. Pre-Transmetalation Intermediates in the Suzuki-Miyaura Reaction Revealed: The Missing Link. *Science (1979)*, **2016**, *352* (6283), 329–332. https://doi.org/10.1126/science.aad6981.
[26] Miyaura, Norio.; Suzuki, Akira. Palladium-Catalyzed Cross-Coupling Reactions of Organoboron Compounds. *Chem Rev*, **1995**, *95* (7), 2457–2483. https://doi.org/10.1021/cr00039a007.
[27] Gillie, A.; Stille, J. K. Mechanisms of 1,1-Reductive Elimination from Palladium. *J Am Chem Soc*, **1980**, *102* (15), 4933–4941. https://doi.org/10.1021/ja00535a018.
[28] Carrow, B. P.; Hartwig, J. F. Distinguishing Between Pathways for Transmetalation in Suzuki−Miyaura Reactions. *J Am Chem Soc*, **2011**, *133* (7), 2116–2119. https://doi.org/10.1021/ja1108326.
[29] Lamblin, M.; Nassar-Hardy, L.; Hierso, J.; Fouquet, E.; Felpin, F. Recyclable Heterogeneous Palladium Catalysts in Pure Water: Sustainable Developments in Suzuki, Heck, Sonogashira and Tsuji–Trost Reactions. *Adv Synth Catal*, **2010**, *352* (1), 33–79. https://doi.org/10.1002/adsc.200900765.
[30] Trost, B. M.; Van Vranken, D. L. Asymmetric Transition Metal-Catalyzed Allylic Alkylations. *Chem Rev*, **1996**, *96* (1), 395–422. https://doi.org/10.1021/cr9409804.
[31] Brückner, R. *Reaktionsmechanismen*, 3rd ed.; Springer Berlin Heidelberg: Berlin, Heidelberg, 2004. https://doi.org/10.1007/978-3-662-45684-2.
[32] Denmark, S. E.; Heemstra, J. R.; Beutner, G. L. Catalytic, Enantioselective, Vinylogous Aldol Reactions. *Angewandte Chemie International Edition*, **2005**, *44* (30), 4682–4698. https://doi.org/10.1002/anie.200462338.
[33] Casiraghi, G.; Zanardi, F.; Appendino, G.; Rassu, G. The Vinylogous Aldol Reaction: A Valuable, Yet Understated Carbon−Carbon Bond-Forming Maneuver. *Chem Rev*, **2000**, *100* (6), 1929–1972. https://doi.org/10.1021/cr990247i.

[34] Bellina, F.; Anselmi, C.; Viel, S.; Mannina, L.; Rossi, R. Selective Synthesis of (Z)-4-Aryl-5-[1-(Aryl)Methylidene]-3-Bromo-2(5H)-Furanones. *Tetrahedron*, **2001**, *57* (50), 9997–10007. https://doi.org/10.1016/S0040-4020(01)01017-1.
[35] Gudzuhn, M.; Alio, I.; Moll, R.; de Vries, jessica; Boehlich, J.; Assmann, M.; Janneschütz, J.; Schützenmeister, N.; Himmelbach, A.; Poehlein, A.; et al. Molecular Insight into Gene Response of Diorcinol- and Rubrolide-Treated Biofilms of the Emerging Pathogen Stenotrophomonas Maltophilia. *Microbiol Spectr*, **2022**, *10* (3).
[36] Grigg, R.; Savic, V.; Thornton-Pett, M. 4-Substituted Protoanemonin in Intramolecular Cycloaddition Reactions of Non-Stabilised Azomethine Ylides. *Tetrahedron*, **1997**, *53* (30), 10633–10642. https://doi.org/10.1016/S0040-4020(97)00674-1.
[37] Assmann, M. Totalsynthese Der Rubrolide I, K, L, M, O Und Analoga Als Leitstruktur Zur Steigerung Der Antiviralen Aktivität, Hamburg, 2020.

8. Acknowledgements

First and foremost, I would like to thank Prof. Dr. Nina Schützenmeister for giving me the opportunity to write my thesis in her group. I am grateful for being able to contribute to the research on new anti-infective drug candidates and for gaining valuable experience in the laboratory. I also thank her for her constant support during my work in the lab and during my writing, which was a huge help for me.

Special thanks also go to PhD student Jasmin Janneschütz, who introduced me to the lab, guided me through my lab work and always had an open ear for every problem throughout the whole time. Her experience was a big help from the start until the end of my laboratory work.

I also want to thank my fellow Master's students, Kiki and Matteo, for their good company and always being there if I needed support.

The greatest thanks go to my family, my parents and my brother, who made my studies and my academical education possible in the first place. They always believed in me from the very start and gave me the feeling that I can achieve anything that I want in life. Furthermore, they were always there for me when I had stressful and hard times and motivated me to keep going.

Lastly, I want to thank my friends for making my time at university more pleasant and for always supporting me. But especially, I thank my boyfriend Christoph, who was the biggest mental support for me during my whole studies and in my life in general. I don't know how I would have done this without you.